HYDRATE PLUG DISSOCIATION IN PIPELINES BY PRESSURE REDUCTION: EXPERIMENT AND MODELING

~~by~~

Phaneendra Bollavaram

HYDRATE PLUG DISSOCIATION IN PIPELINES BY PRESSURE REDUCTION: EXPERIMENT AND MODELING

by

Phaneendra Bollavaram

A thesis submitted to the Faculty and the Board of Trustees of the Colorado School of Mines in partial fulfillment of the requirements for the degree of Doctor of Philosophy (Chemical Engineering and Petroleum Refining).

Golden, Colorado

Date: 08|22|02

Signed: Phani

Phaneendra Bollavaram

Approved: E Dendy Sloan Jr.

Dr. E. Dendy Sloan, Jr.
Thesis Advisor

Golden, Colorado

Date: 8|23|02

James F. Ely

Dr. James F. Ely
Professor and Head
Department of Chemical Engineering
And Petroleum Refining

ABSTRACT

The plugging of pipelines by natural gas hydrates has been recognized as a serious problem since their discovery in pipelines (Hammerschimdt 1934). Since that time, very little work has been conducted to determine the best methodology to remove the hydrate plugs. Most of the work in hydrates has focused on the prevention of hydrates (*"A gallon of prevention is better than a mile of cure"*, Sloan (2000), pg.1). However, hydrate plugs cannot always be prevented and many situations arise when it is required to remove the hydrate plugs. One of the most common options to remove the hydrates is by lowering the pressure. The knowledge base on depressurization is very scarce.

In this work, we concentrated on hydrate dissociation by the method of depressurization (two-sided and one-sided). Experiments focused on formation of hydrate plugs and subsequently their dissociation by both the methods to develop a database. The experiments lead to broadening our limited knowledge on hydrate dissociation by depressurization. The work was conducted with both structure I/structure II type of hydrates. The mechanism of hydrate dissociation (radial or axial) was studied in this work.

Laboratory and flow loop experiments suggest that the hydrate plug dissociates radially when depressurized from both ends. This is good news to flow assurance because it indicates that the plug length is not nearly important as the plug radius – as long as there has been insufficient time for the plug to anneal to a lower permeability.

Jager (2001) reported the hydrate structural transitions for a processed natural gas lean in heavy hydrocarbons. This work presents data showing that dissociation time for removal of a hydrate plug depends on the hydrate structure. In cases of large diameter pipelines, this difference can be as much as several days or weeks.

Work on hydrate dissociation modeling is very limited. Peters (1999) had modeled the two-sided hydrate dissociation as a radial moving boundary model. The model is capable of predicting the hydrate dissociation time and the total time for plug melting. This model was verified with the laboratory and flow loop experiments. A one-sided depressurization model was developed that predicts the time to re-start the flow. The re-start time depends on the downstream pressure, length, porosity and permeability of the hydrate plug. A safety model was developed that assesses the hydrate plug movement when subjected to pressure gradients. The safety model provides the user a safety optimum downstream pressure for one-sided depressurization.

The one-sided model was verified with laboratory and Tommeliten field plugs. The model predicted that the Tommeliten field plugs were re-started when the annulus spacing was 8% of pipeline radius. The safety model compared to the simulations of Xiao et al. (1998), and predicted higher, but comparable plug velocities.

TABLE OF CONTENTS

LIST OF TABLES

LIST OF FIGURES

ACKNOWLEDGEMENTS

This work would not have been possible with out the enormous help from many people. I would like to thank:

Dr. E. Dendy Sloan, Jr. (My Guru) for his inspiration, advice and never-ending support during my research work. His insight and enthusiasm for hydrate work will be cherished the rest of my life. His famous words "criticize by redesign" and "an individual being the best critic of his own work" has transformed us to being leaders.

The late, Dr. Sami Selim for being a constant boost of energy, be it chemical engineering or life. His absence is felt every single moment.

The members of my committee – Dr. Kidnay, Dr. Marr, Dr. Wang, Dr. Wendlandt, and David Peters, without their critique and help, this work would not have been possible.

Todd Bullerdick and Don Schroeder for helping me with the Marathon Oil Company flow loop experiments. I thank them for giving me industry's perspective of the hydrate problem.

Dr. Phil Notz and Jim Chitwood for making me feel at home during my visits to Houston for DeepStar meetings. The discussions on flow assurance and the needs of the industry helped in shaping this work.

Hydrate busters, Shiva Subramanian, Vu Thieu, Surya Devarakonda, Ramesh Kini, Zhongxin Huo, Marc Yager, Nathan Torres, Erik Freer, Keith Hester, Douwe Bruinsma, Jason Ivanic, Sung-Oh Yang, Mike Eaton, Dr. Kumar and Douglas Turner for their friendship and endless hours discussing the beauty (mystery) of hydrates.

My parents, and lovely sister and brother-in-law for being extremely patient and believing in me through the past 5 years. Words cannot express what they have gone through and their love for me.

My family in Boulder, Aunty, Arun, Subha, Usha, Jeff and Rama for cheering me up all the time, and being a constant support and critics of my life. Thanks to Arun for introducing me to the game of golf that taught me patience, perseverance and consistency.

My friends Sam, Sara, Sid, and Helen for their friendship and providing me with a new home in Boulder. Sid and Helen's kids – Ashwin, Nishant and Nalina for all the smiles and pleasant moments with their Phani Mamu.

My roommate, Ratan who has been of great support throughout the research effort. Thanks for being patient to my long conversations about hydrates. Saki, Atul and Sandy for their friendship and cheering me up during the tough times.

My friends from REC, Surathkal, for being there, and helping me achieve and dream the goals for the past 10 years of my life.

I would also like to thank the faculty and students of Chemical Engineering department at CSM for all the help and a pleasant working environment.

Guru Brahma, Guru Vishnu, Guru Deva, Guru Maheshwara;
Guru Shakshat, Para Brahma, Tasmai shree, Guru ve namah.

(Guru is the ultimate creator, savior, and destroyer.
Guru is ultimate God, and we bow with all our respect and belongings)

Dedicated to all my "Gurus", including my parents who have imparted unending knowledge to me.

CHAPTER 1

INTRODUCTION AND MOTIVATION

This chapter details: 1. an introduction to clathrate hydrates, 2. an introduction to the flow assurance problems by hydrate blockages, 3. why this research is helpful to the hydrate community, and 4. what to expect from the rest of the Chapters. Only a brief hydrate description is given in this Chapter. The reader is advised to refer the text by Sloan (1998) for complete description of clathrate hydrates.

1.1 Clathrate Hydrate

Gas hydrates belong to a class of compounds called clathrates. Hydrates are crystalline compounds similar to ice – with guest molecules like methane, ethane, propane, hydrogen sulfide etc. enclathrated ("trapped") inside cavities or cages formed by the hydrogen bounded framework of water molecules. The van der Waals forces between the guest and the water molecules of the cavity help in stabilizing the hydrate structures.

Davy (1811) first observed clathrate hydrates in the chlorine+water system. It wasn't until 1934, however, that clathrate hydrates were extensively studied. Hammerschmidt (1934) found that natural gas transport lines could be blocked by the formation of clathrate hydrates. This raised a lot of attention in the oil and gas industry, prompting more research to be performed on clathrate hydrates of natural gas.

There are three basic hydrate structures known to form from natural gases, structure I (sI), structure II (sII), and structure H (sH). The type of hydrate that forms depends on the size of the gas molecules included in the hydrate. As a rule of thumb, small molecules such as methane or ethane form sI hydrates as single guests, larger molecules such as propane and i-butane form sII hydrates. Larger molecules such as i-pentane form sH hydrates in the presence of a "help" molecule such as methane. The type of hydrate that forms depends on the composition, temperature, and pressure of the system.

Figure 1.1 shows how the several cages are arranged to give unit lattices of sI, sII and sH hydrates. The most commonly found hydrates in nature are sI, while those in pipelines are sII. This research mainly deals with both sI and sII hydrates.

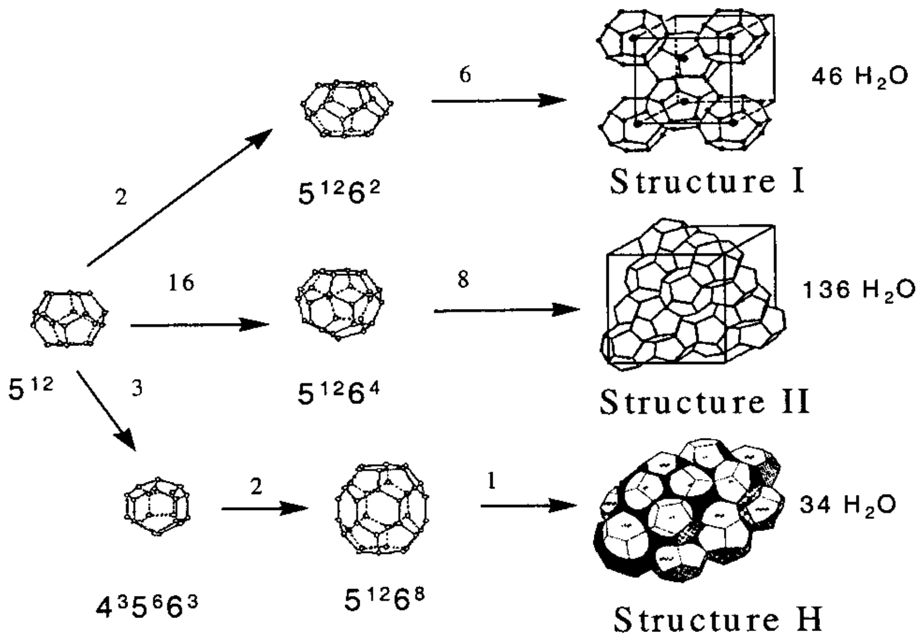

Figure 1.1: Crystal Lattices of sI (McMullan and Jeffrey, 1965), sII (Mak and McMullan, 1965), and sH Hydrates (Ripmeester et al., 1987)

1.2 Flow Assurance Problems with Hydrate Blockages

The major incentive for this research is the problem that hydrates pose for the gas and oil industry. These hydrates can form when small hydrocarbons and water come in contact at the right temperatures and pressures. Figure 1.2 shows a pipeline pressure and temperature conditions predicted with a multiphase program OLGA® or PIPEPHASE®, and those conditions superimposed on hydrate stability curves. At a short pipeline distance, say 7 miles, the fluid stream retains the high temperature from the hot reservoir. The ocean cools the fluid stream, and at 9 miles, the fluid enters the hydrate stability region. Injecting methanol is a preventive action to inhibit hydrates. Most of the time, methanol injection facilities are not available at the hydrate points, so injection is done at the wellhead.

Typically these conditions commonly exist in wells, valves, flow lines and meter discharges. In a pipeline, hydrates form at the hydrocarbon-water interface, and accumulate. Once the hydrates accumulate enough to plug the pipeline, they hinder flow through the pipeline. This is a major safety and economical concern to the industry.

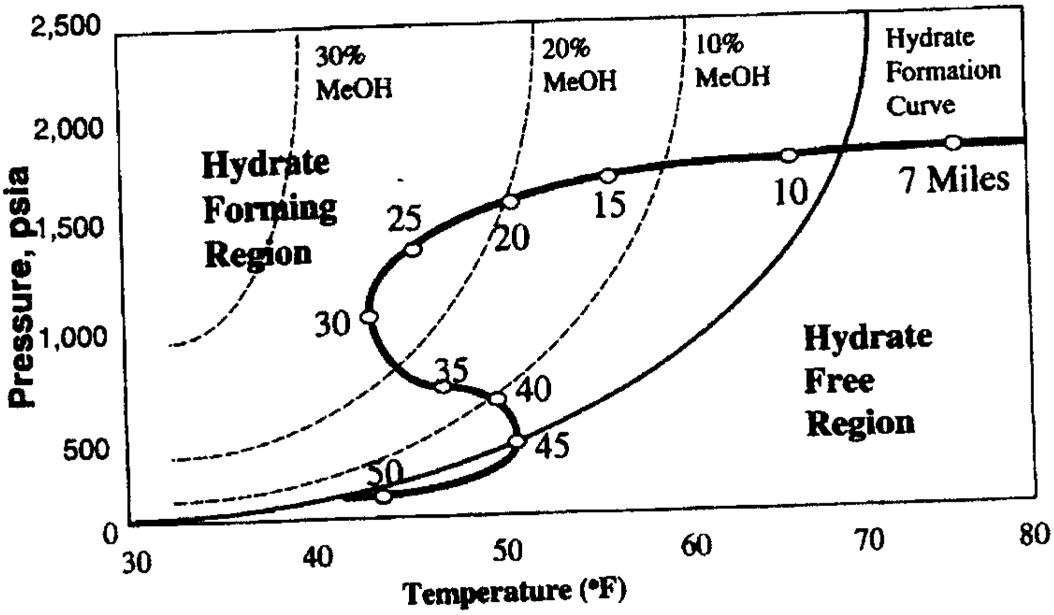

Figure 1.2: Pressure and Temperature Along Pipeline Distance (Notz, 1994)

Sloan (2000) has a detailed discussion on twenty-seven case studies regarding the formation and dissociation of hydrates. One such case study (1991 Chevron incident) involved one-sided depressurization of a hydrate plug formed in a sour-gas-flowline. Figure 1.3 shows the flow line profile buried under the ground. The foreman and an operator bled down the pressure in the distant end from the wellhead, and were standing near the line when the line failed, caused by a moving hydrate plug. A large piece of pipe struck the foreman. Figure 1.4 shows the damage caused due to the plug movement and the rupture of the pipeline.

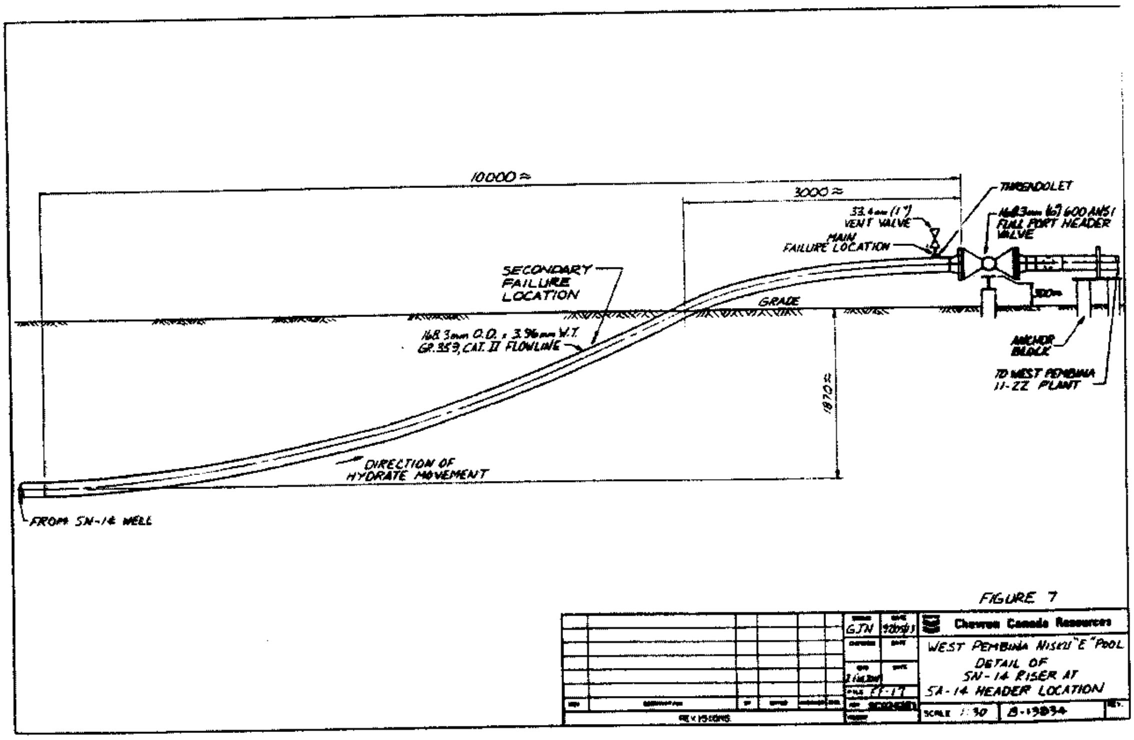

Figure 1.3: Chevron Hydrate Accident Flow Line Schematic (Fulton 2001)

Figure 1.4: Damage Caused Due to Plug Movement (1991 Chevron Accident, Fulton 2001)

Lysne (1995) lists three such incidents in which hydrate projectiles erupted form pipelines at elbows and caused loss of three lives and over $7 million (US) in capital costs. Concerns have been expressed (Campbell, 1991) about the effect of hydrates on foundations of platforms and pipelines, as well as offshore drilling.

The limited knowledge base on hydrate dissociation techniques resulted in three field trials. In 1994 Statoil purposely formed/removed over 17 hydrate plugs in a 6" gas/condensate line in the Tommeliten field of the North Sea (Austvik, 1997). Two of the hydrate plugs were removed through one-sided depressurization. Deepstar IIA report (A208-1, 1996) was compiled by Davalath (1996) to document 16 hydrate blockages. In February 1997 SwRI (Hatton et al. 1997) formed and dissociated hydrates in Kerr-McGee field line, resulting in three significant tests. Plugs were removed by one-sided depressurization and plug velocities as high as 82 m/s were reported. Lysne (1995) had conducted two-sided depressurization on hydrate plugs. He stated that dissociation takes place by radial mechanism.

Peters (1999) did two-sided experiments with methane hydrates and observed the radial dissociation process. He reported that the ideal scenario for dissociating the plug would be when the pressure is as low as possible, most likely, the atmospheric pressure. A radial dissociation model was proposed in his study. The model and experiments indicated that ice helps in the removal of hydrate. Since, the plug dissociates from the wall, any pressure gradient might move the plug and cause serious damage.

Kofoed (2001) proposed a new quasi steady-state model (QSS) based on the transient models of Kelkar et al. (1998) and Peters (1999). The proposed QSS model simplifies the transient system into sub-systems, where each sub-system is unique for the corresponding time-interval. The main objective of the work was to obtain analytical solution to the numerical problem proposed by Peters (1999). It was concluded that dissociation times predicted by the Cartesian transient model are only satisfactory for hydrate dissociation temperatures just above and below the freezing point of water. Most of the above knowledge base has been towards two-sided depressurization.

Frequently, the only viable technique available for industry to remove the hydrate plugs is by one-sided depressurization. Little is known in about hydrate plug dissociation by one-sided depressurization. A major incentive was for research to address this vital issue for the oil and gas industry. Peters et al. (2002) proposed a hydrate dissociation model based on facts, conjecture and field experience. The models attempts to include the effects of hydrate kinetics with those related to energy transfer and simulate the plug dissociation process in pipelines. The main objective of the model was to give an order of magnitude estimate of the time required to remove the hydrate plug.

Natural gas hydrates are found in deepwater areas where conventional oil and gas operations are conducted. The possibility of production of natural gas hydrates is very attractive, since it is estimated that natural gas in hydrates exceeds other fossil reserves by a factor of two (Kvenvolden, 1993). Larsen et al. (1998) state that of all the production techniques available for gas hydrates, pressure reduction is simple, as it does not involve chemicals or any injection equipment. Simple pressure reduction pipeline modeling and experiments can give useful insight on the upper bounds on gas production by pressure reduction.

1.3 How This Work Helps the Hydrate Community

This work involves addressing an important question for oil and gas production. If hydrates form, what is safe operation for plug remediation and re-start of the flow line? No quantitative tool is available for pressure reduction. Most of the plugs in the field are remediated by rules-of-thumb obtained by experience. This research provides the operators with a tool for plug remediation by pressure reduction. The following questions will be answered in this thesis:

1. Is there a safe operating pressure for depressurization of hydrate plugs?
2. What are the major variables that influence hydrate plug remediation, either by two-sided or one-sided pressure reduction?
3. How do we quantitatively remediate and design for hydrate plug depressurization?

Laurence J. Peter once said, "*All science is concerned with the relationship of cause and effect. Each scientific discovery increases man's ability to predict the* *consequences of his actions and thus his ability to control future events"* (Peter, 1993). Hopefully, this thesis is a step toward avoiding hydrate safety problems.

1.4 Outline of the Thesis

Chapter 2 details the experimental apparatus used in the research. A brief overview of the experimental procedures for formation and dissociation of hydrate plugs by both two-sided and one-sided depressurization is provided.

Chapter 3 gives a description of hydrate dissociation models developed previously, and the present one-sided depressurization model developed in this work. The safety simulator is also presented at the end of the chapter.

Chapter 4 provides the results from formation and dissociation of hydrate plugs in the lab. This dissociation was conducted by two-sided depressurization. The two-sided radial dissociation model is verified with the data obtained in the lab.

Chapter 5 gives the unusual phenomenon of hydrate structural transitions of a processed natural gas. The effects of these structural transitions on plug dissociation are predicted.

Chapter 6 deals with formation and dissociation of hydrate plugs on a flow loop. The capability of two-sided radial dissociation model is illustrated via the two tests on the flow loop.

Chapter 7 provides data for hydrate plugs dissociated by one-sided depressurization in the lab. The one-sided model developed in Chapter 3 is verified with the lab data. The limited data from Tommeliten field trials are compared with the one-sided model. Plug movement data from DeepStar Wyoming field trials are compared with the safety model.

Chapter 8 summarizes the conclusions from the thesis and presents guidelines and recommendations for future work in the field of hydrate plug dissociation.

CHAPTER 2

EXPERIMENTAL APPARATUS AND PROCEDURES

This chapter deals with an introduction to the experimental apparatus used in the research. A brief overview of the experimental procedures for two-sided and one-sided depressurization is provided.

The purpose of the experiment was to form hydrates from ice and to dissociate the hydrate plug. The experiments were conducted in an unstirred batch reactor under isobaric and isothermal conditions. The formation experiments were conducted under variable temperature and pressure. Experimental conditions were limited to pressures between 0 and 21 MPa and temperatures between 263.15 K and 278.15 K.

2.1 Experimental Equipment

Two different stainless steel cells were used in this study. A short cell built by Peters (1999) was used during the initial phase of this work. A schematic view of the short cell is shown in Figure 2.1. The main section of the apparatus was a 0.2 m long stainless steel cell. The cell had an internal diameter of 0.0476 m, a wall thickness of 0.003 m, and an internal volume of 0.00035 m^3. The short cell had a threaded end cap. A Rocket Seal® was used between the cap and cell to prevent any leaks through the system.

In the present work, a new long cell was built in order to study effects of length/diameter on plug dissociation times. Figure 2.2 shows the schematic of the long cell. The stainless steel cell is 0.92 m long, has an internal diameter of 0.0254 m and an internal volume of 0.00047 m^3. Similar to the short cell, the new long cell had a threaded end caps sealed by a rocket seal®.

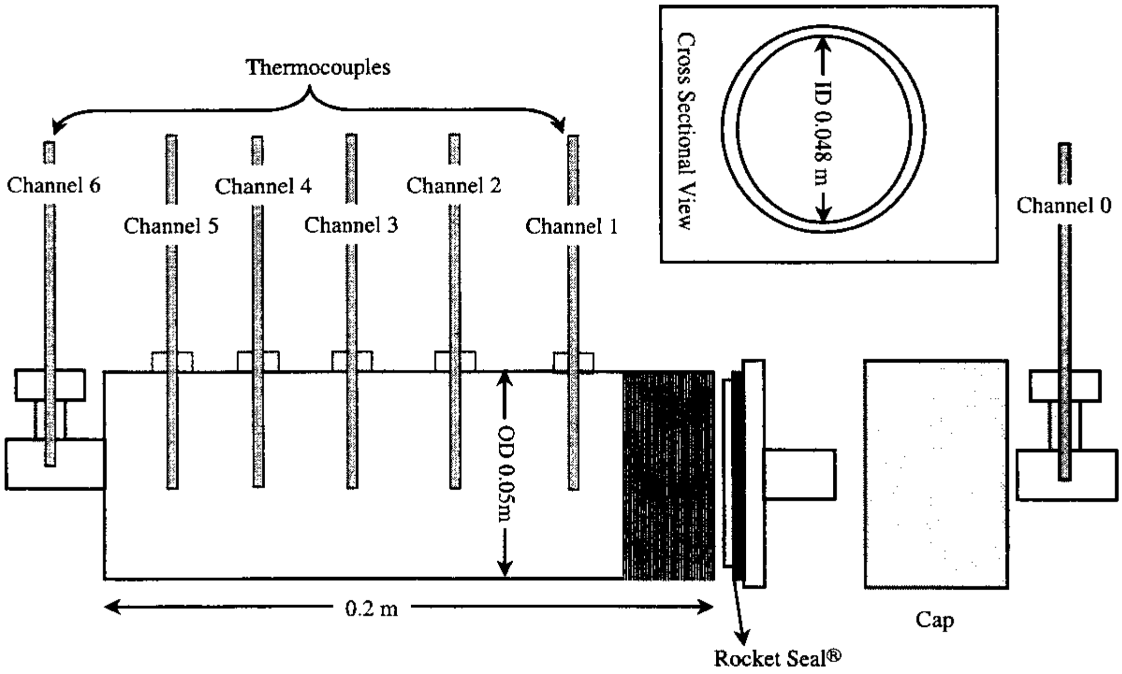

Figure 2.1: Schematic of the Short Cell (not to scale)

The main cell (short or long) was located in a temperature-controlled, ethylene glycol/water bath. The bath temperature was controlled with a Neslab immersion cooler model PBC-75II, and a 1000 Watt immersion heater controlled by a Precision Instrument Controller model 123 (Bayley Instrument Company). The voltage input to the heater was adjusted by the controller to maintain the desired set point. The fluctuations in bath temperature using this system were approximately $\pm$0.2 K. This small fluctuation did not affect the results of this work.

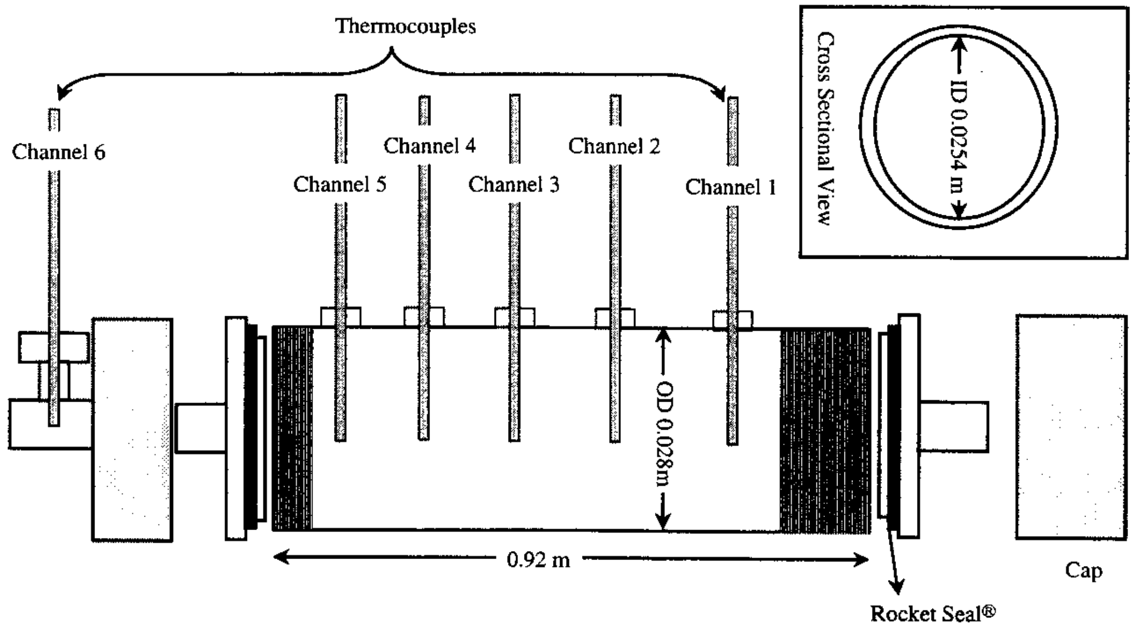

Figure 2.2: Schematic of the Long Cell (not to scale)

All other parts of the apparatus (Figure 2.3) were connected with 0.006 m stainless steel tubing connected with Swagelock fittings. An Omega/Ashcroft pressure transducer, with a pressure range between 0 and 34.4 MPa, was used to continuously monitor the pressure in the cell. The accuracy of pressure transducer was $\pm$ 0.17 MPa. The temperature inside the cell was determined with the use of five type T (Copper–Constantan) thermocouples. The location and numbers of the thermocouples are also detailed in Figure 2.2. The temperature of the gas just outside each end of the cell was also measured using type T thermocouples. The temperature of the bath was monitored using a platinum resistance temperature detector (RTD).

The pressure and all the temperature measurements were continuously measured using a Kiethley DAS 802 data acquisition card with an EXP-800 external board. Connected to the EXP-800 was a FWA-EXP, which measured the thermocouples, and an FWA-37U, which measured signals from the RTD and pressure transducer. Voltage readings from the EXP-800 were sent to a computer and recorded in a data file for later analysis.

The cell was attached to a gas supply through valves V_{i1} and V_{i2} (Figure 2.3). The methane gas used in all experiments was technical grade purity (99.96% purity). Before valve V_{i1} was a Ruska high-pressure pump capable of increasing the system pressure to 41.4 MPa. The valve upstream of the cell, V_{i2}, could be closed to prevent gas flowing through the cell. During the depressurization, valves V_{o1}, V_{o2}, V_{o3}, and V_{o4} could be opened to reduce the pressure in the cell at both ends of the plug.

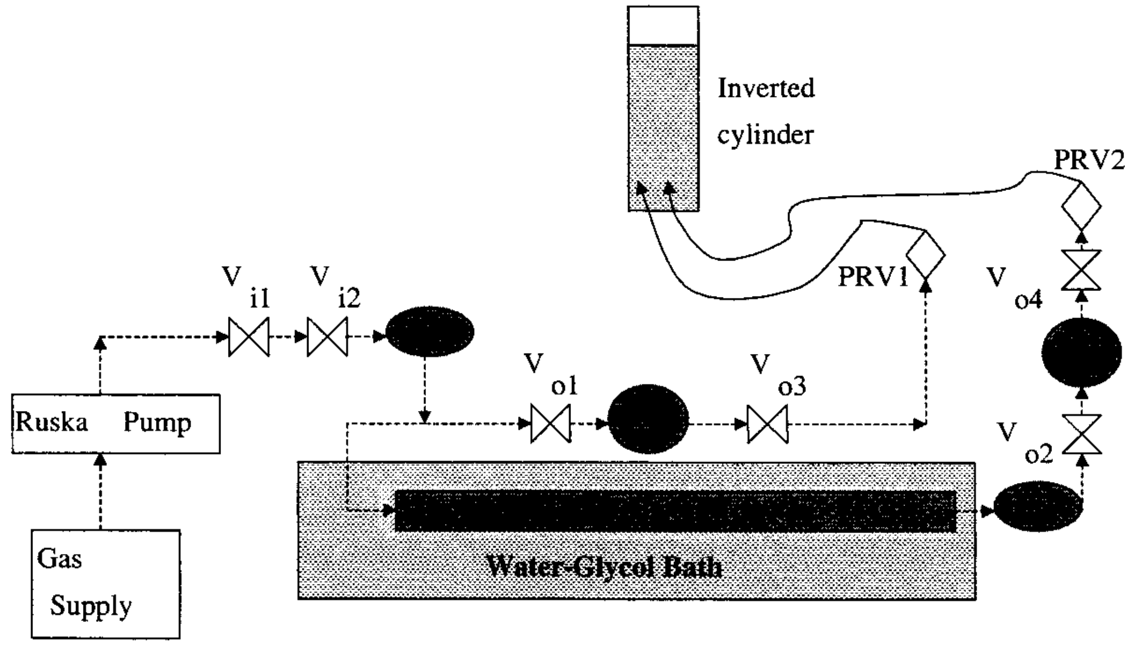

PRV - Pressure Relief Valve
PG - Pressure Gauge
PT - Pressure Transducer
V_{ix} - Inlet Valve
V_{ox} - Outlet Valve

Figure 2.3: Schematic Diagram of the Experimental Apparatus

The flow rate of gas during dissociation was measured using an inverted cylinder. The process of measuring flow rates was done using an inverted 1000 ml graduated cylinder, filled with water. The cylinder had graduation increments of 10 ml. The cylinder was inverted over a five-gallon bucket filled with water. The gas evolution during dissociation was fed into the inverted cylinder and gas flow rates measured. The volume of the water displaced as a function of time was used to calculate the flow rate.

2.2 Background on Hydrate Plug Formation

The process of making a large, reproducible sample of hydrates proved to be one of the most challenging parts of the research. Hydrate plugs in pipelines are typically formed from water. Problems with making reproducible hydrates with water were reported in the work of Austvik (1992) and Lysne (1995). Hwang et al. (1990) stated the following reasons for using ice as a precursor to hydrate formation than water

- Ice has a hydrogen-bonded structure that was similar to hydrates
- Melting ice resulted in residual structure helpful in forming hydrate cages
- Small ice particles increase the surface area for hydrate formation
- Ice has a higher thermal diffusivity than water, hence increased heat absorption from hydrate formation

Another reason for using ice, as a precursor was that hydrate formation was not observed below 273.15 K. Hence, this was used in detecting leaks prior to hydrate formation. The method of making hydrates that was the most reliable was adapted from the method used by Stern et al. (1996) and tested rigorously by Peters (1999). The idea behind this method, for the formation of hydrates, was to begin with small ice particles (<850 μm) surrounded by a hydrate forming gas. The temperature and pressure conditions were maintained in the hydrate region during the formation experiments.

Figure 2.4 shows a general schematic of the steps followed to form and then to dissociate a hydrate plug, superimposed on the hydrate pressure-temperature diagram.

1. Step 1: Ice preparation
2. Step 2: Loading cell with ice
3. Step 3: Ice conversion to hydrate
4. Step 4: Hydrate plug preparation, as a function of the depressurization technique
5. Step 5: Hydrate plug one-sided or two-sided depressurization

Each of these steps is vital for hydrate plug formation and dissociation. Steps 1 through 3 are common for both two-sided and one-sided depressurization experiments, while step 4 is an additional procedure for forming impermeable plugs that sustain a pressure differential, in order to accomplish one-sided depressurization.

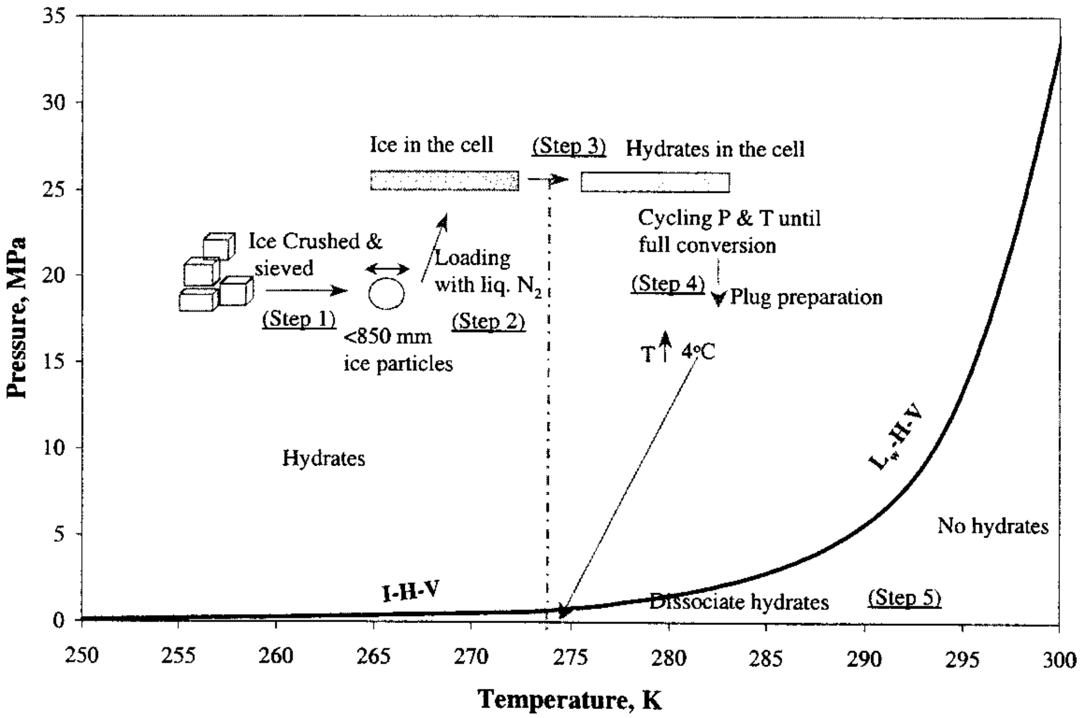

Figure 2.4: Schematic of hydrate formation and dissociation procedure

2.3 Hydrate Formation Procedure

2.3.1 Ice Preparation

The first step in hydrate formation was to prepare a homogeneous sample of ice particles. Initially, distilled water was frozen in a gallon size stainless steel container. The crushing process was begun as soon as the water was frozen. The next step was to break the ice particles into pieces that were small enough to go into a Hamilton Beach Scovill Model 936-2 blender. The blender was cooled with liquid nitrogen to prevent melting the ice during the crushing process.

After the ice was crushed, particles where separated by using a sieve with an opening of 833 μm. These particles were collected in a sieve with an opening of 250 μm to provide for the minimum particle size. The sieve was precooled with liquid nitrogen to prevent melting the ice. Once the desired separation was achieved, these fine ice particles were transferred in to an insulated container. The process was repeated until about 250 grams of fine ice particles were obtained.

The sieved ice particles were cooled with liquid nitrogen and loaded in the cell immediately in step 2. It was noted that within couple hours, these ice particles annealed in the refrigerator at 253.15 K. This crushing and sieving process was repeated prior to each experiment to ensure a uniform size and consistency in the results.

2.3.2 Loading Cell with Ice

The challenging part of hydrate formation procedure was to make sure that the cell was precooled prior to loading the ice. With the short cell, it was noted that the cooling process was not too difficult owing to the short length of the cell. The long cell required more effort, as it was difficult to fill the cell completely with liquid nitrogen. As soon as the cell was cooled below the ice point, the fine ice particles were quickly loaded in the cell. The packing was accomplished by vertically mounting the cell on an anvil. A thin stainless steel tube was used in packing the cell.

Once the cell was filled with ice, the end cap was screwed on to the cell. Leak-proof sealant was used to prevent any leaks through the end cap. The cell was then quickly moved to the temperature controlled water bath, which was cooled to 268.15 K to start step 3 of converting ice to hydrate.

The porosity of the ice was controlled by the amount of ice loaded in to the cell. Knowing the amount of ice before and after loading the cell, volume of ice in the cell was calculated. The fraction of void space (porosity) was calculated from the ratio of volume of void space to total volume of the cell. The porosity in these experiments varied from 0.3 to 0.6. For one-sided depressurization experiments, a conscious effort was made to load the cell with more ice, resulting in low porosity hydrate plugs. The effect of porosity on hydrate dissociation was studied in these experiments.

2.3.3 Ice Conversion to Hydrate

After the cell was moved to the temperature controlled water bath, the piping was connected. The bath temperature was maintained below the ice point for a couple of hours. As soon as the cell was moved to the bath, the cell was pressurized with a hydrate forming gas (methane or natural gas) using a Ruska pump to take advantage of the initial cold temperatures resulting from the use of liquid nitrogen. Typically, the cell was left below ice point for a couple of hours, to test for any leaks in the system. Hydrate formation was not observed during this time; hence, pressure readings could be used as a leak indicator.

Once the pressure stabilized in the cell, the bath temperature was increased to 273.45 – 273.65 K. It is hypothesized that, as the ice began to melt, a thin layer of water was formed around the periphery of the ice particle. The hydrate shell formed around the ice particle, and further growth occurred due to diffusion of gas through the fissures in the ice/hydrate particle. The drop in pressure indicated hydrate formation over a 24-hour period.

The process of cycling the temperature and re-pressurizing the cell with gas was conducted until no further drop in pressure was observed. The asymptotic pressure trace was used as an indication of full conversion, usually in 3 to 4 days. In most of the experiments, >96% conversion was achieved. The conversions were based on PVT calculations using Peng-Robinson equation of state, as detailed in Appendix A. The conversion numbers were confirmed by a mass balance with the gas evolved on hydrate dissociation.

A typical temperature-pressure trace for hydrate formation is shown in Figure 2.5. In this experiment, after 64 hours, the pressure in the cell was increased to 13.8 MPa. The pressure in the cell remained constant for couple hours indicating that most of the ice was converted into hydrates (~98% conversion in this case).

2.3.4 Hydrate Plug Preparation

After the ice was fully converted into hydrates, the next step was to prepare the plug for dissociation. In the case of two-sided dissociation, pressure was reduced from both ends of the plug. Pressure drop across the plug was of not much importance because plugs were porous and permeable to flow (Peters, 1999).

Plug remediation by one-sided depressurization involved maintaining a pressure drop across the plug. Another challenge to the research was to obtain an impermeable plug that would hold a pressure drop across its length. Two different strategies were thought to provide the desired impermeable plug:

1. change the characteristic of the initial plug (ice) and
2. change the characteristic of plug after ice-to-hydrate conversion.

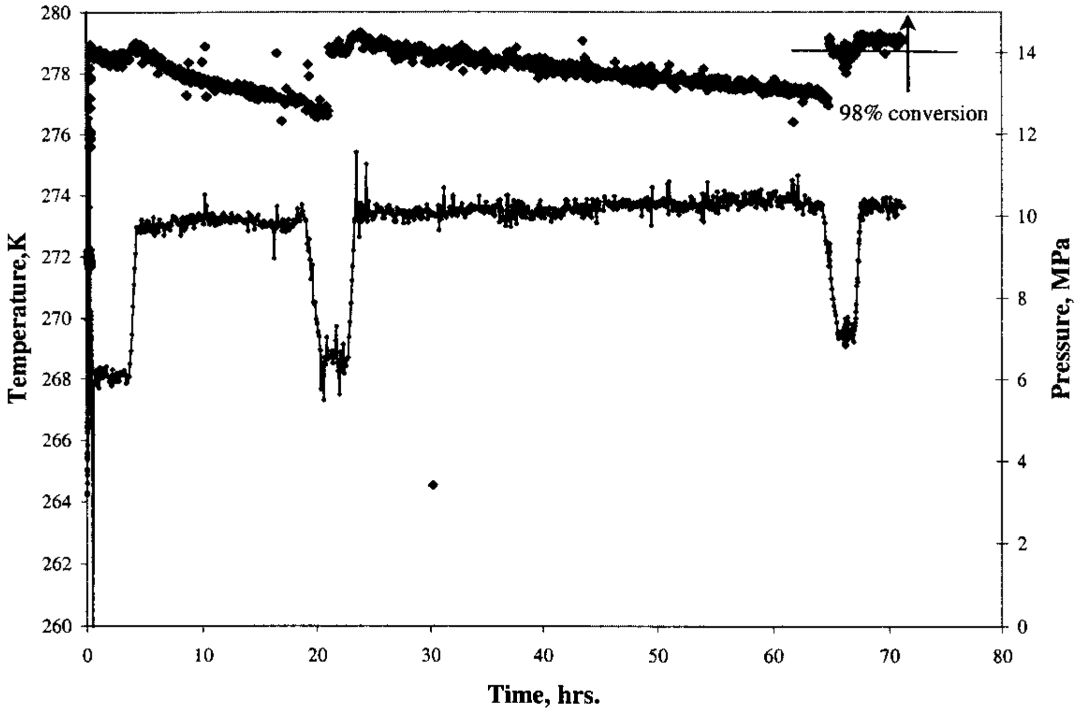

Figure 2.5: P –T trace During Hydrate Formation Experiment

<u>Change the characteristic of the initial plug prior to hydrate formation:</u>

After loading the cell with ice, the cell was kept below ice point (268.15 K) for 6-7 hours. The idea was to anneal the ice particles, and hence reduce the tortuosity or channels between the ice particles. The next step was to pressurize the cell with hydrate-forming gas. It was interesting to note that a pressure drop was observed indicating the changing matrix structure of the ice loaded in the cell. Hence, it was concluded that ice particles annealed with time.

The bath temperature was then raised to 273.65 K, to start converting the ice to hydrate. As the melting of ice occurred and hydrate formed, the pressure across the plug stabilized, indicating that the matrix structure had again changed. After complete conversion of ice to hydrate, pressure was reduced at the downstream end. It was observed that a pressure drop could not be achieved across the plug; it was too porous and permeable.

The above failure indicated that the rate of melting of ice plays an important role. Tortuosity is directly proportional to rate of melting of ice. Hence, the bath temperature was slowly raised to 273.35 K. The rate of hydrate formation was reduced, as observed from the slow rate of pressure decrease, indicating a slower melting of ice. This procedure of forming hydrates took longer, but the process did not result in an impermeable plug.

Another strategy was increasing the amount of ice loaded in the cell, in order to decrease porosity of the hydrate plug. A conscious effort to pack the cell with more ice, resulted in reducing the porosity from 0.4 to 0.25. However, reducing the porosity of the hydrate did not result in a pressure drop across the plug.

Hence, it was clear that changing the ice matrix and hydrate formation procedures was not helpful. The next logical step was to change the characteristics of plug formed after full conversion of ice to hydrate.

<u>Changing the characteristic of plug after ice-hydrate conversion:</u>

De Boer et al. (1985) showed experimentally that permeability of a hydrate plug decreases with time. The study involved forming propane hydrates in a vertical cylindrical glass tube (inner diameter 0.025 m, length 0.7m) and flowing propane through it. The idea behind the experiment was to form seals in the pore space, so as to obtain large pressure drops across the plug length. The experiment was conducted with propane gas saturated with water. As shown in Figure 2.6, the permeability of the plug decreased almost linearly with total amount of propane passed through the plug. De Boer et al. (1985) reported that the permeability reached a value of ~ 3μD and that the plug could withstand a pressure difference of 248.2 KPa.

This method of sealing the pore space, annealing the hydrates over time, was used. Several experiments were conducted by flowing saturated hydrate-forming gas into the long cell to form seals. Annealing did help in establishing a pressure drop across the plug. However, as the pressure was reduced from the downstream end of the plug, equilibration between upstream and downstream pressures was seen within 15 - 20 minutes. Sometimes, the pressure drop was established only for two stages of pressure reduction as shown in Figure 2.7. The plug would become permeable before the pressure downstream was dropped below the equilibrium pressure (P_{eq}) to dissociate the plug. Below equilibrium pressure, the plug would dissociate by two-sided dissociation, as the pressure communication was established across the plug length.

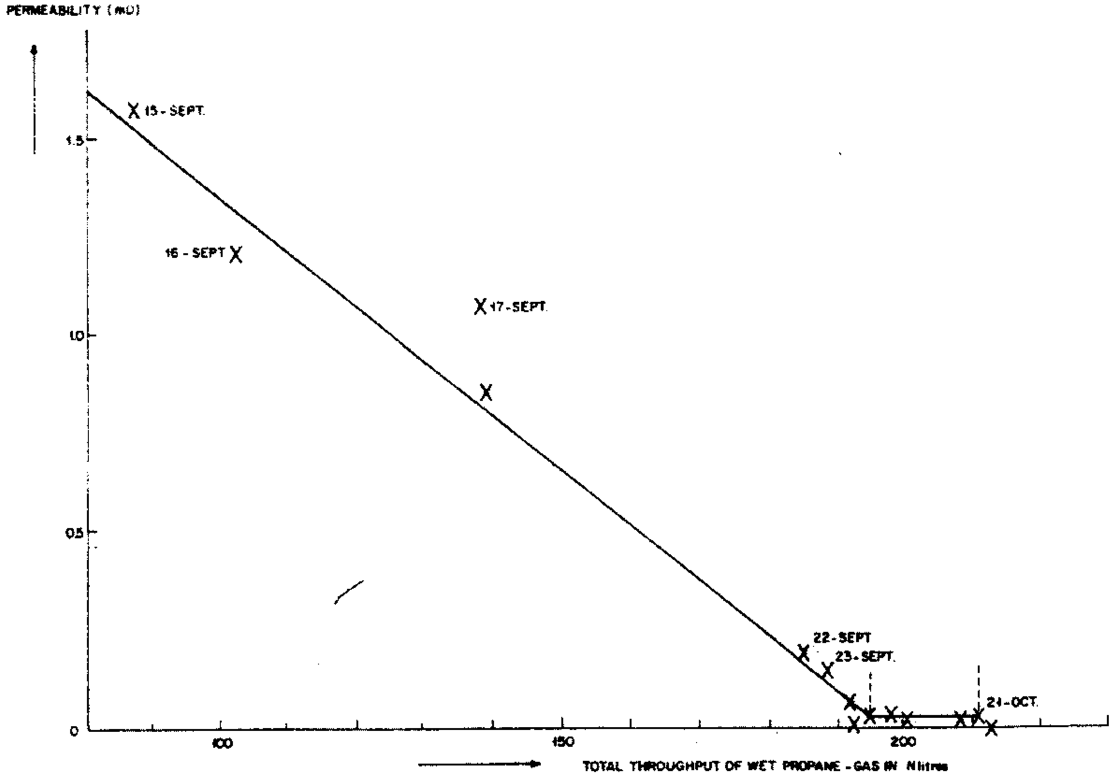

Figure 2.6: Permeability of Hydrate Plug Decreases with Time (De Boer et al., 1985)

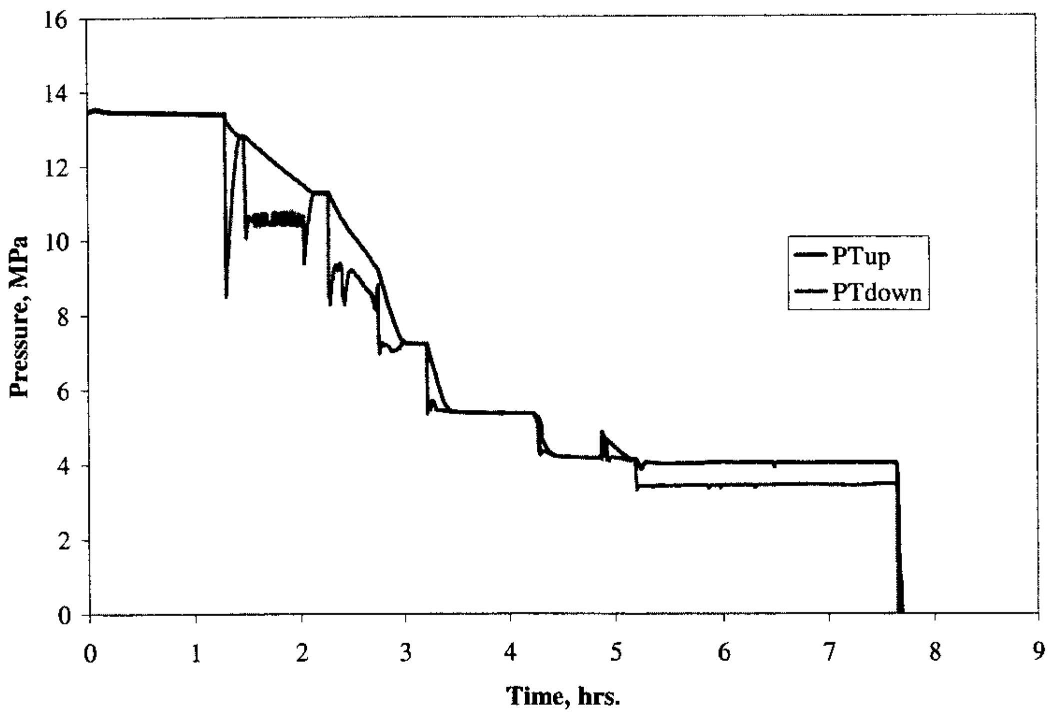

Figure 2.7: Pressure Communication when Plug was Permeable

Due to the limitations in packing ice into the cell, most of the experiments resulted in a pore space ≥25% in the hydrate plug. An additional step was needed to fill the pore space with some solid (as shown in Figure 2.8). Since heavy hydrocarbons like tetradecane or hexadecnae freeze around 277.15 K, they could be injected as a liquid into the hydrate plug before freezing, thereby reducing the pore space. This procedure resulted in decreased hydrate plug permeability.

The first step for pumping liquid heavy hydrocarbon was to raise the bath temperature above the freezing point of the heavy hydrocarbon (in case of tetradecane, 279.15 K). The pressure in the cell was maintained above the hydrate equilibrium pressure (4.9 MPa) at 279.15 K, to prevent any dissociation of the hydrate. A known amount of liquid heavy hydrocarbon was pumped using the Ruska pump from the upstream end of the plug. The bath temperature was then reduced to 277.15 K, a typical deep ocean temperature. The cell was left at these conditions for a day or two. The pressure was decreased from the downstream end to check for a pressure drop across the plug. If no pressure drop was observed, more heavy hydrocarbon was injected and the procedure repeated until the desired pressure drop was observed.

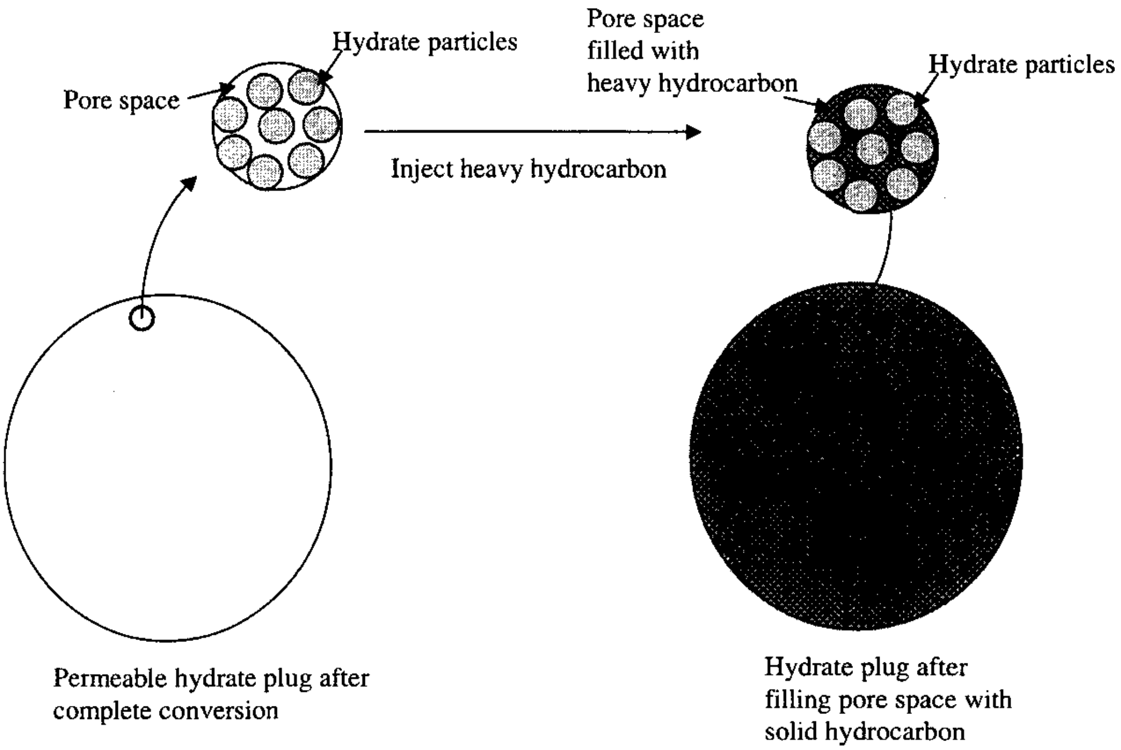

Figure 2.8: Conceptual picture of impermeable plug formation

Figure 2.9 shows the pressure profile after 150 ml of tetradecane was pumped into the cell to fill the pore space. In certain experiments a sufficient pressure drop was not observed; hence more tetradecane was injected to reduce the permeability of the hydrate plug. As seen from Figure 2.9; the pressure downstream was reduced slowly in 7 steps from 6.89 MPa to 2.41 MPa. The maximum and minimum pressure drops observed in this experiment were 1.72 and 0.172 MPa. The minimum pressure drop was obtained after the plug began dissociating below equilibrium pressure of 3.86 MPa (sI methane hydrate).

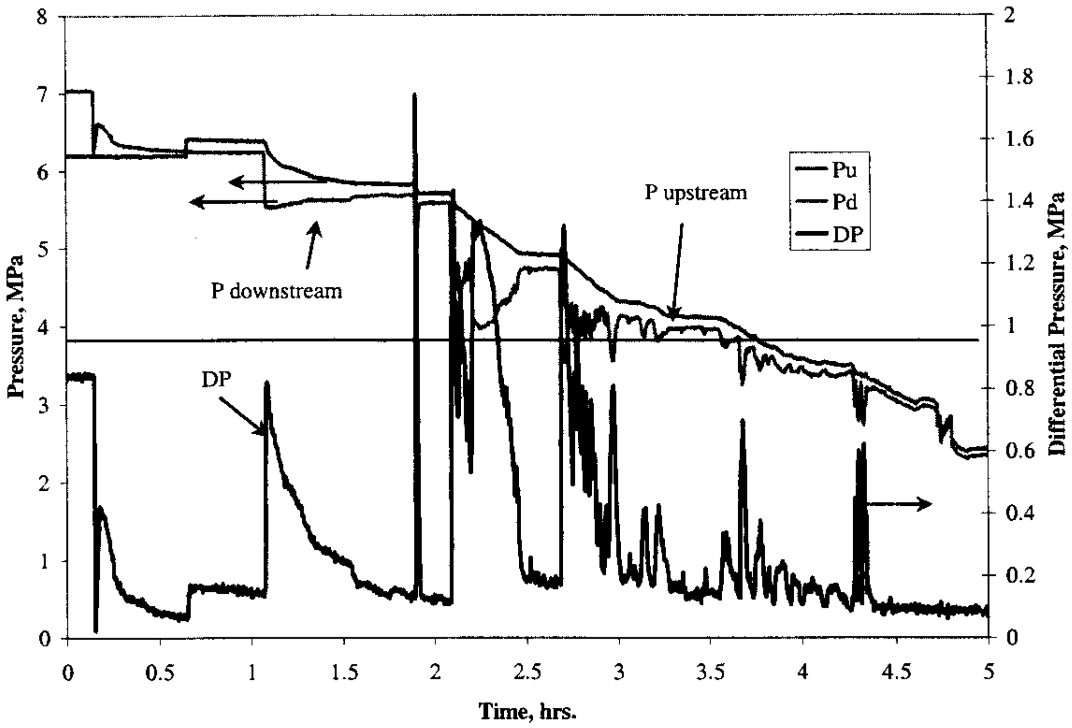

Figure 2.9: Pressure trace when Plug was Impermeable

2.4 Hydrate Dissociation Procedure

After the hydrate plug was formed, as described in the previous section, the dissociation procedure could begin. The temperature of the bath was raised to the desired temperature, typically the sea floor temperature of 277.15 K.

There were two different experiments conducted during this research. The dissociation process was based on whether one-sided or two-sided depressurization was required. Typically, the two-sided depressurization experiments involved reducing the pressure from both ends of the cell, as quickly as possible to atmospheric pressure. The one-sided depressurization experiments involved slow reduction of the pressure from downstream end of the plug below hydrate equilibrium pressure to dissociate the hydrate plug.

The two-sided depressurization procedure involved reducing the pressure by opening the outlet valves V_{o1}, V_{o2}, V_{o3} and V_{o4} (Figure 2.3) typically to atmospheric pressure, in less than a minute. As the pressure in the cell decreased below the equilibrium value, hydrates become unstable and dissociated. The resulting dissociated gas was monitored by using an inverted cylinder. The time when gas stopped evolving was an indication of the end of hydrate dissociation.

Figure 2.10 shows a plot of evolving flow rate versus time. The area under this curve could be integrated to obtain a plot of moles of gas evolved during dissociation as in Figure 2.11. In this case, the total moles of gas evolved during hydrate dissociation was 1.75 moles. As described in Section 2.3.3, gas consumed during formation could be calculated using Peng-Robinson equation of state. The calculated value for gas consumed during formation experiment was around 1.67 moles. These numbers were used to check for mass balance; in this case, a 5% error was reported.

During two-sided depressurization, gas evolution was measured from both ends of the plug. As time progressed, it was observed that gas evolved only from one side of the plug. This phenomenon indicated that gas takes the path of least resistance to flow even though both ends of cell were open. Most of the two-sided depressurization experiments showed this behavior.

One-sided depressurization involved reducing the pressure by opening the outlet valves V_{o3} and V_{o4} at the downstream end of the plug to a desired pressure. The pressure was reduced slowly using the pressure regulator valves. The downstream pressure was reduced below equilibrium pressure, at which point, the regulation valves was set to a constant pressure. Using an inverted cylinder, dissociated gas was monitored.

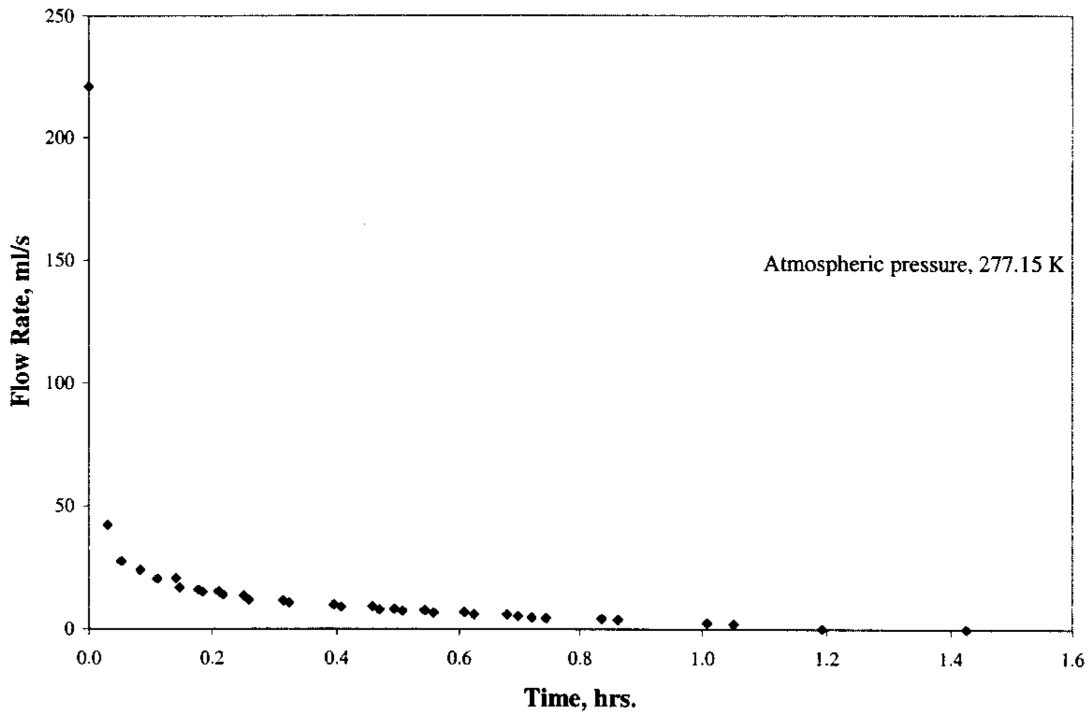

Figure 2.10: Flow rate of gas evolved during hydrate dissociation

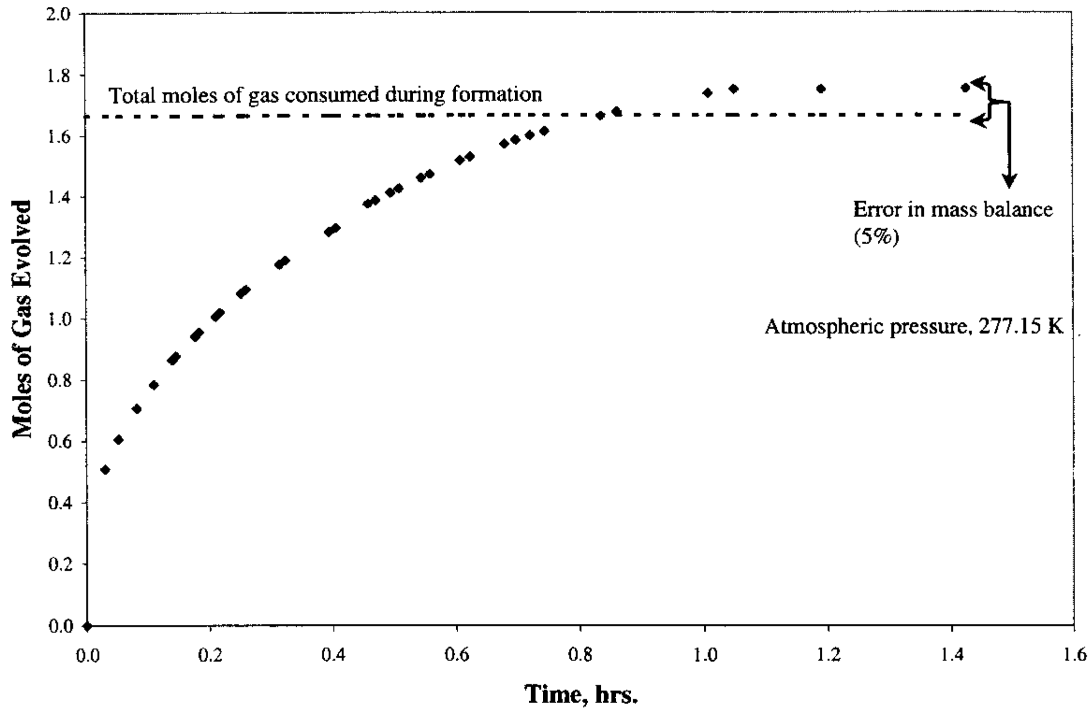

Figure 2.11: Gas Evolution During Dissociation Process

The time when total plug melts was obtained when no solids i.e., hydrate or ice was present. Figure 2.12 shows the temperature profiles when hydrate plug was depressurized from both ends. As seen from the figure, temperature in the cell remained at 273.15 K, indicating ice formation. The time when the last thermocouple indicates an increase in temperature above 273.15 K is reported as the total time for plug melting. From Figure 2.12, the ice melting time was 0.35 hours.

The goal of the one-sided experiments was twofold. The first goal was to obtain data at different pressures to compare with the mathematical model. The second goal was to reduce the pressure slowly until two-sided depressurization was observed.

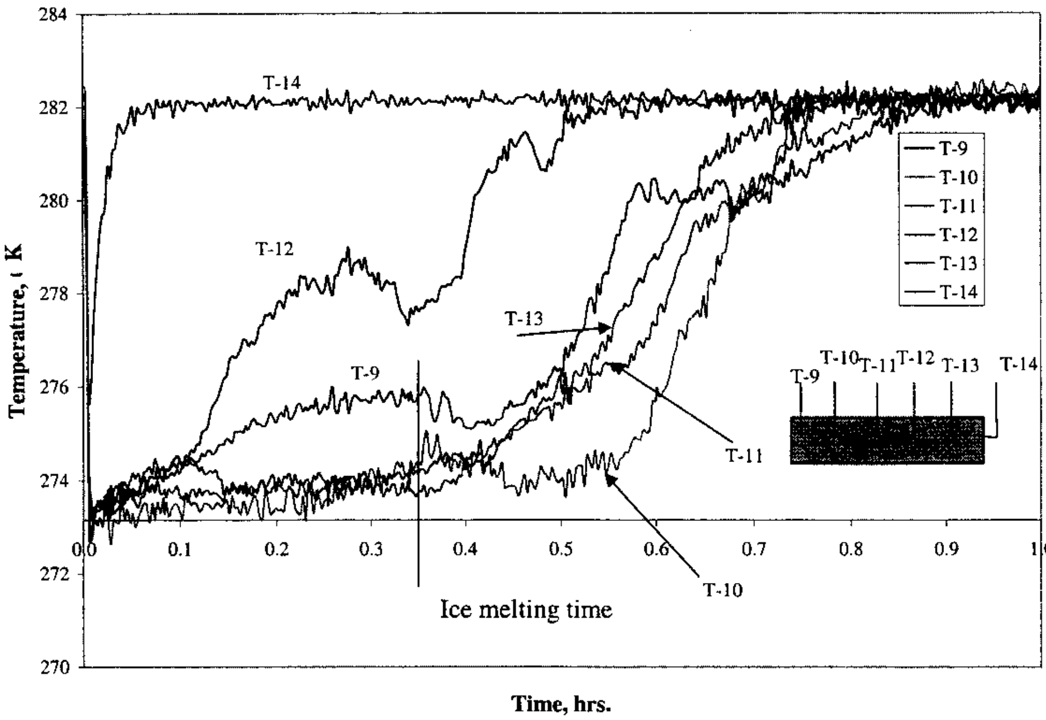

Figure 2.12: Ice Formation During Hydrate Plug Dissociation

2.5 Summary

A total of 40 plugs were formed. Some trials were unsuccessful, as outlined in the previous sections. Table 2.1 lists a summary of the 30 successful hydrate plugs that were formed and dissociated in the short and long cells. The lab experiments were conducted to study the effect of remediation strategy: two-sided and one-sided depressurization and the effect of hydrate structural transitions on remediation time. The information in Table 2.1 will be used when discussing the results in following Chapters.

Table 2.1: Summary of Experiments

Plug	Data File	Hydrate Structure	Dissociation Method	Mass Balance moles Consumed	Evolved	% Absolute Error	Dissociation Time, hrs. Hydrate	Ice
1	Hyddissqatar073099	sII	2SD	1.4	1.33	5.0	3.32	4.7
2	Hyddissqatar080699	sII	2SD	1.36	1.28	5.8	3.02	4.6
3	Hyddissqatar082899	sII	2SD	1.45	1.56	7.5	3.8	5.1
4	Hyddissqatar091399	sII	2SD	1.32	1.48	12.1	4.6	6.1
5	Hyddiss101899	sI	2SD	1.05	1.11	5.7	0.81	1.08
6	Hyddiss102899	sI	2SD	1.65	1.5	9.1	0.87	1.15
7	Hyddiss111599	sI	2SD	1.78	1.75	1.6	1.19	1.68
8	Hyddiss122799	sI	2SD	1.85	1.9	2.7	1.15	1.54
9	Hyddiss01202000	sI	2SD/axial	1.74	0.67	-	5.3	-
10	Hyddiss01272000	sI	2SD/axial	1.8	0.47	-	13.0	-
11	Hyddiss10162000	sII	ST/ 2SD	1.63	1.4	14.0	0.71	0.86
12	Hyddiss11132000	sII	ST / 2SD	0.9	0.82	8.8	0.51	0.57
13	Hyddiss11222000	sII	ST / 2SD	1.36	1.31	3.0	0.62	0.7
14	Hyddiss12042000	sII	ST / 2SD	1.39	1.32	5.1	0.61	0.75
15	Hyddiss12142000	sII	ST / 2SD	1.62	1.51	6.8	1.05	1.35
16	Hyddiss01032001	sI	ST / 2SD	1.57	1.44	8.3	0.72	0.93
17	Hyddiss01082001	sII	ST / 2SD	1.34	1.22	8.9	1.28	-
18	Hyddiss05192000	sI	1SD	1.9	1.96	3.15	2.13	2.21
19	Hyddiss06192000	sI	1SD	2.1	1.98	5.71	2.83	2.95
20	Hyddiss06262000	sI	1SD	2.2	2.15	2.3	2.36	2.49
21	Hyddiss09112000	sI	1SD	2.18	2.33	6.88	1.62	1.81
22	Hyddiss01172001	sII	1SD	1.4	1.32	5.71	3.5	3.56
23	Hyddiss07112001	sI	1SD	1.8	1.6	11.11	1.93	2.08
24	Hyddiss08122001	sI	1SD	2.09	1.91	8.61	2.61	2.76
25	Hyddiss10142001	sI	1SD	1.97	2.16	9.64	2.46	2.63
26	Hyddiss10262001	sI	1SD	1.93	1.77	8.29	1.85	2.03
27	Hyddiss12062001	sI	1SD	2.24	2.08	7.14	3.91	4.26
28	Hyddiss01062002	sII	1SD	2.2	2.1	4.54	2.73	2.92
29	Hyddiss01182002	sII	1SD	2.1	1.87	10.95	2.3	2.47
30	Hyddiss01262002	sII	1SD	2.28	1.79	21.5	3.87	4.12

2SD – Two-sided depressurization, ST – Structural Transitions, 1SD – One-sided depressurization. Plugs 1 – 4 conducted on short cell, while plugs 5 – 30 on long cell.

CHAPTER 3

PHYSICAL AND MATHEMATICAL MODEL

This chapter is intended to provide an overview of the physics of hydrate plug formation in real pipelines, the dissociation procedure followed, describing the physics of the problem, and the mathematical model for pressure reduction by one-sided depressurization. This chapter also provides the state of the art for hydrate depressurization models.

3.1 Hydrate Plug Formation and Dissociation in Pipelines

Hydrate blockages occur owing to abnormal operations such as well tests with water, dehydrator malfunction, startup, shut-in and loss of inhibitor injection. Hydrates can form with subcooling as low as 1 to 2 K, particularly in industrial systems where contaminants like sand, slag, etc. are present to aid in nucleation. All natural gas hydrates are formed from 85 mol% water and 15 mol% gas. It is a well-known fact that hydrates formation depends upon the system – gas or gas-condensate, static or dynamic.

Figure 3.1 shows a schematic of the case for hydrate formation along the wall periphery in a gas system. This slow buildup of hydrates along the wall may be characterized by the gradual increase in the pressure drop across the line, finally leading to a complete blockage.

Figure 3.2 shows a schematic of the case of hydrate formation as agglomerating particles in a condensate pipeline, resulting in a porous structure. Austvik et al. (2000) formed 44 hydrate plugs, and showed that 77% of the hydrate plugs were porous for the gas condensate system.

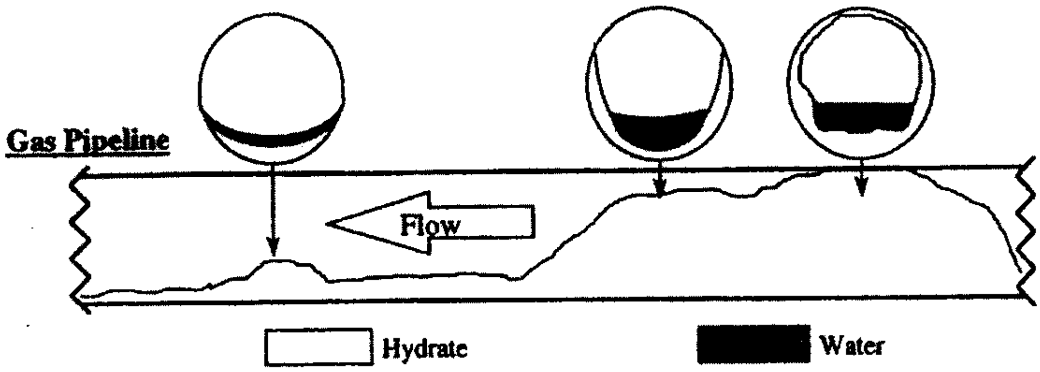

Figure 3.1: Hydrate Formation in Gas Pipeline (Lingelem et al. 1994)

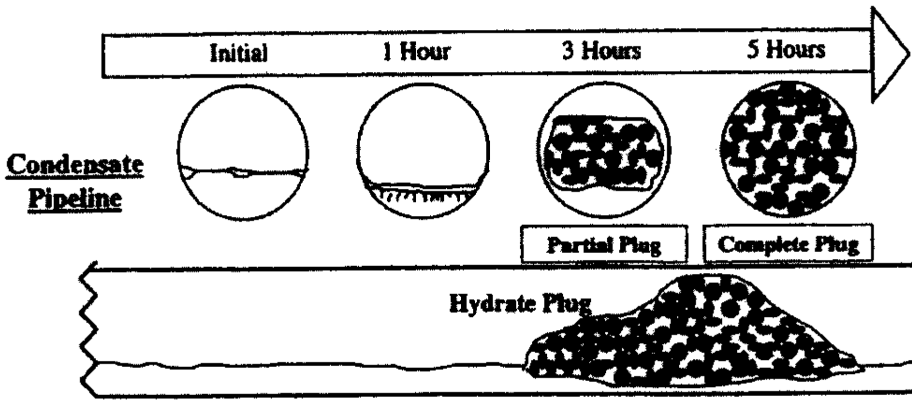

Figure 3.2: Hydrate Formation in Condensate Pipeline (Lingelem et al. 1994)

Figure 3.3 shows two types of pressure drop that might occur during hydrate formation. Figure 3.3a shows the gradual increase in pressure drop that would occur if hydrates formed from the walls. Figure 3.3b shows the more typical case of multiple spikes when small hydrate particles agglomerate to form a blockage.

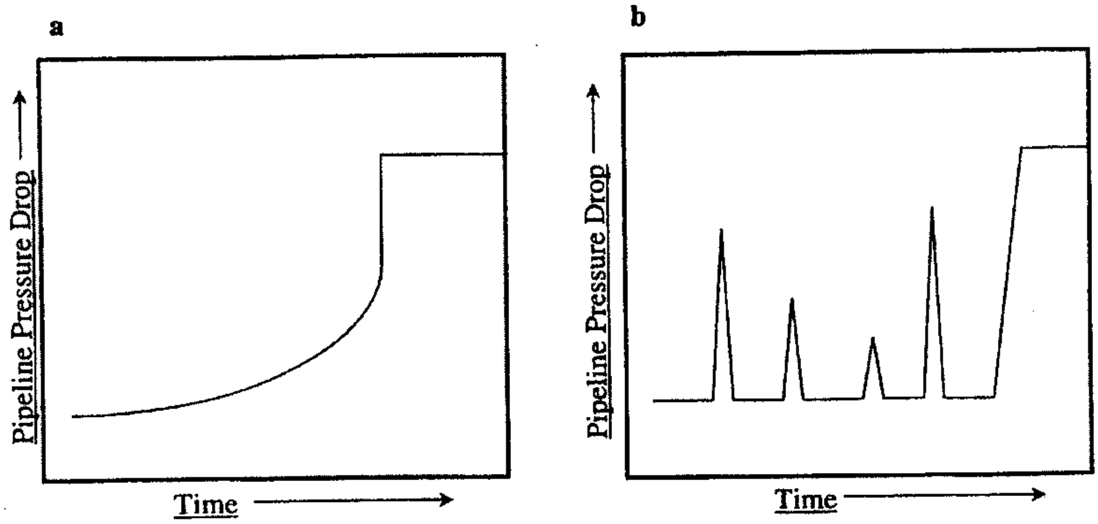

Figure 3.3: Pipeline Pressure Drops Caused by Hydrates: a) Hydrate build up on Walls and b) Hydrate Particle Agglomeration (Sloan, 2000)

In a controlled experiment, British Petroleum formed hydrates in a 14.5 in. ID, 13.7 mile long gas line in the southern North Sea. Corrigan *et al.* (1996) reported an increase in line pressure drop to 35 psi (0.24 MPa) at two days after the start of the test, as shown in Figure 3.4. A further rise in pressure drop to 49 psi (0.33 MPa) was observed for three days. High pressure drop and decreased gas flow indicated formation of hydrates. The plug was remediated by injecting methanol. A large slug of condensed phase, presumed to be hydrates, arrived at the slug catcher at the trial conclusion. Corrigan *et al.*, estimated about 50 metric tons of hydrate formation.

In January 1996, Statoil depressured a hydrate plug from one side in a 7.2 mile and 6 in. gas condensate pipeline in North Sea. Figure 3.5 shows the depressurization of the line, with upstream (subsea) pressure, downstream (topside) pressure and pressure drop. During dissociation, the pressure was decreased in steps, and a slow bleed through the plug was observed for 120 hours. Before 120 hours, the upstream pressure slowly decreased, but never decreased to the downstream pressure, indicating that the plug was not permeable to black oil. After 120 hours, the line pressure was maintained below

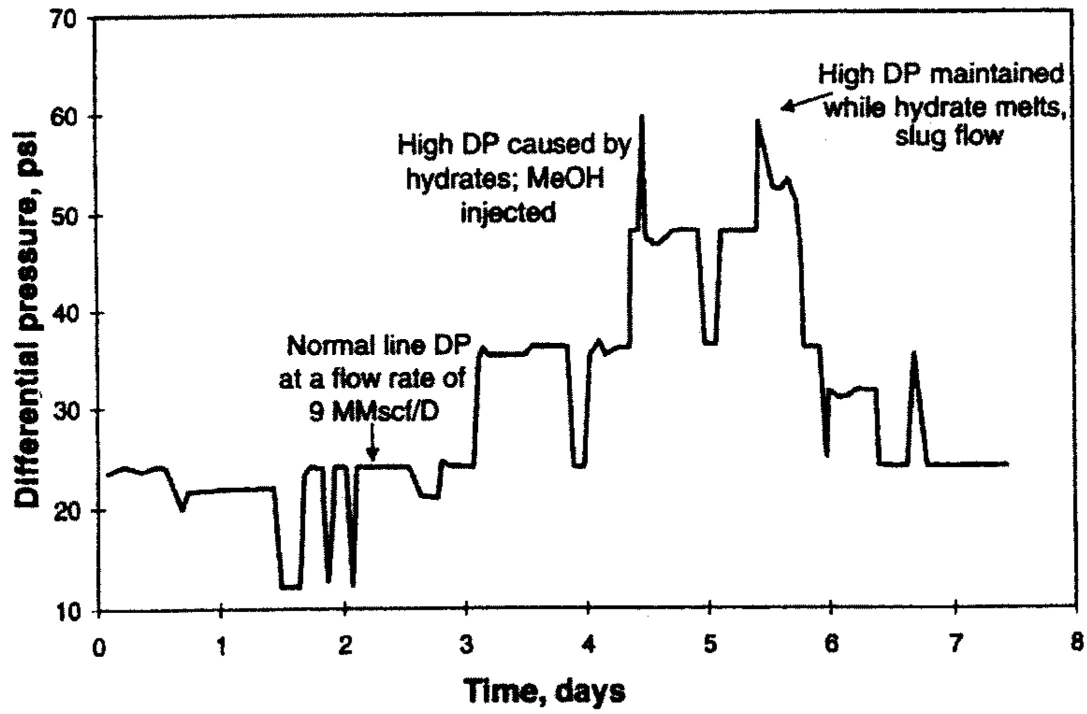

Figure 3.4: Differential Pressure Caused by Hydrate Blockage (Corrigan et al., 1996)

hydrate equilibrium pressure to dissociate the plug. At about 180 hours, a sudden decrease in upstream pressure and an increase in downstream pressure were observed. Finally, the pressure stabilized and plug dissociated from both ends. The pipeline was restarted with methanol injection at about 215 hours.

The number of state-of the-art hydrate studies in field pipelines is too small to determine the actual phenomenon for hydrate blockage formation. However, it is very clear that a wide range of hydrate porosities and permeabilities may be obtained. The porosity and permeability of the hydrate plug determines the remediation strategy.

The mechanism of dissociation depends on the porosity of the hydrate plug. For example, when a highly porous plug is depressurized from one side, gas flow through the plug can result in pressure equalization, resulting in two-sided dissociation. In the case of low porosity plugs, pressure transmission takes more time and hence, longer restarts as shown in Figure 3.5.

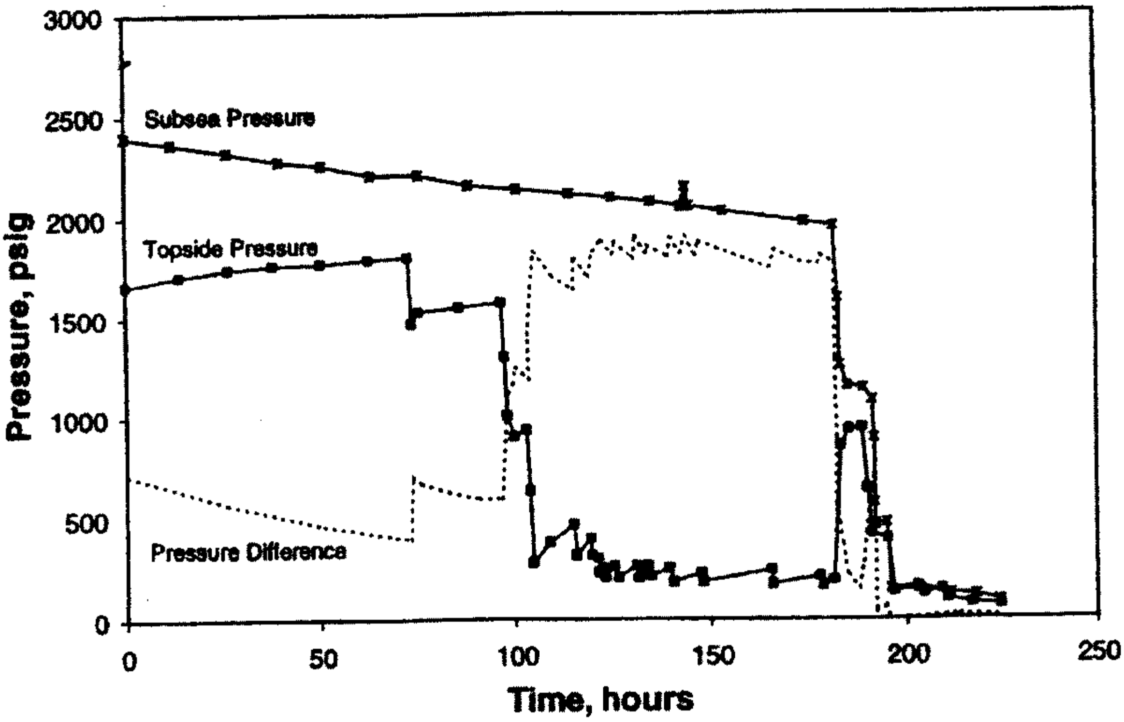

Figure 3.5: One-sided Depressurization for Low Porosity Plug (Gjertsen *et al.* 1997)

3.2 State-of-the-art in Hydrate Plug Depressurization Modeling

Modeling of hydrate dissociation has been studied by a few researchers around the world. Lysne et al. (1992) and Kelkar et al. (1998) developed the first models for hydrate dissociation. Both of these models make certain assumptions that limit the utility of their use. The two-sided radial dissociation model for hydrate dissociation developed by Peters et al. (1999) attempts to eliminate some of the assumptions so that the dissociation prediction program is of utility in predicting the time for hydrate dissociation in a pipeline. All these models were applicable only when a hydrate plug was depressurized from both ends. Kofoed (2001) generated a quasi-steady-state simplification of the rigorous method by Kelkar et al. (1998) and Peters (1999)

A brief description of the two-sided radial dissociation model is provided in this section. Peters (1999) model was used in comparing the results obtained for two-sided dissociation in this research. This model was extended to one-sided depressurization in this work.

3.2.1 Two-sided Radial Dissociation Model

The pressure is assumed to be step-changed to atmospheric pressure on either side of the plug. The resulting hydrate dissociation temperature is below that of the surroundings, causing heat to flow radially inward to melt the hydrates. Figure 3.6 shows a schematic of the hydrate dissociation model. Figure 3.6a shows an inner hydrate core surrounded by an ice layer, which is enclosed in a water layer adjacent to the pipe wall. Both the hydrate and ice layer shrink as a function of time until only water is present in the pipeline. Figure 3.6 represents the case when ice is formed during dissociation. The schematic for the case when no ice is present (when the hydrate dissociation temperature is above the ice point) is similar except the ice layer is of zero thickness.

The following assumptions were used in modeling two-sided dissociation:

1. Hydrate and ice are porous
2. Hydrate dissociation temperature is uniform
3. Radial dissociation dominates over axial dissociation
4. Dissociation is heat transfer controlled
5. Only heat conduction is important

Figure 3.6b shows a representation of the temperature profiles in the water, ice and hydrates layers. The temperature profiles are determined according to Fourier's law of heat conduction in cylindrical coordinates.

$$\frac{\partial T_W}{\partial t} = \alpha_w \left[\frac{1}{r}\frac{\partial T_W}{\partial r} + \frac{\partial^2 T_W}{\partial r^2} \right] \qquad r_{F1} < r < r_0 \qquad t > 0 \qquad \textbf{(3.1)}$$

$$\frac{\partial T_I}{\partial t} = \alpha_I \left[\frac{1}{r}\frac{\partial T_I}{\partial r} + \frac{\partial^2 T_I}{\partial r^2} \right] \qquad r_{F2} < r < r_{F1} \qquad t > 0 \qquad \textbf{(3.2)}$$

The boundry conditions for this system are:

$$T_W = T_0 \qquad r = r_0 \qquad t > 0 \qquad \textbf{(3.3)}$$

$$-k_W \frac{\partial T_W}{\partial r} = -k_I \frac{\partial T_I}{\partial r} + (1-\varepsilon)\rho_I \lambda_I \frac{dr_{F1}}{dt} \qquad r = r_{F1} \qquad t > 0 \qquad \textbf{(3.4)}$$

$$T_W = T_I = T_M \qquad r = r_{F1} \qquad t > 0 \qquad \textbf{(3.5)}$$

$$-k_I \frac{\partial T_I}{\partial r} = (1-\varepsilon)\rho_H \lambda_H \frac{dr_{F2}}{dt} \qquad r = r_{F2} \qquad t > 0 \qquad \textbf{(3.6)}$$

$$T_I = T_D \qquad r = r_{F2} \qquad t > 0 \qquad \textbf{(3.7)}$$

where r_o, r_{F1}, r_{F2} are shown in Figure 3.6, T_W, T_I, T_D, and T_M are the water, ice, hydrate dissociation and ice melting point temperatures, α_W and α_I are the thermal diffusivity of water and ice, ρ_W and ρ_I are the density of water and ice, k_W and k_I are the thermal conductivity of water and ice, λ_H is the latent heat of hydrate dissociation and ε is the porosity of the hydrate.

Boundary conditions 3.3, 3.5, and 3.7 are due to constant temperatures at the pipe wall, the water-ice interface, and the ice-hydrate interface, respectively. Boundary condition 3.4 indicates that the heat conducted through the water layer is equal to the heat conducted into the ice, as well as the heat to melt the ice. Boundary condition 3.6 equates the heat conducted through the ice layer to the heat to dissociate the hydrate. There was no analytical solution to the problem and hence a numerical finite difference scheme was used. Peters et al. (1999) give a detailed description of the numerical scheme.

The model solves for the time when the ice-hydrate interface ($r = r_{F2}$) and water-ice interface ($r = r_{F1}$) reaches the center of the pipeline indicating time for hydrate dissociation (t_{hyd}) and time for ice melting (t_{ice}) respectively. The input to the model includes radius of the pipeline, ambient and hydrate dissociation temperatures, as insulation layer is also considered in a subsequent version of Peters model.

a) Cross-sectional view of pipeline with all three phases present, heat flow radially into system

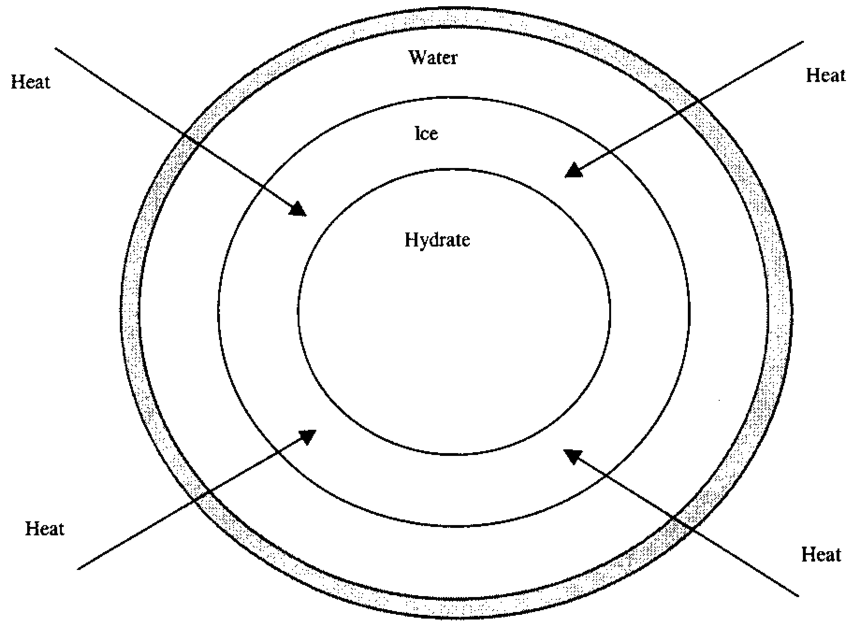

b) Temperature profiles in each phase and moving boundary motion

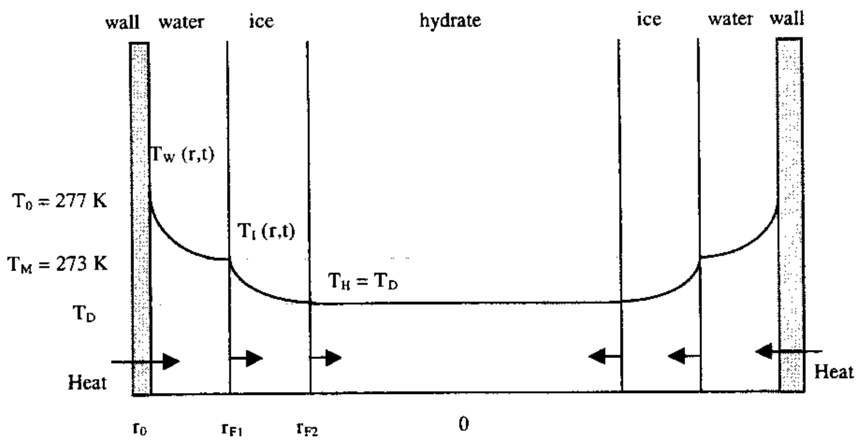

Figure 3.6: Schematic of radial two-sided dissociation when hydrate, water and ice are present (Peters 1999)

An important result to come from the dissociation experiments conducted by Peters (1999) was the verification of the assumption of radial dissociation. Figure 3.7 shows three different experiments, when the hydrate plug was dissociated from both ends, and the cell was opened to capture pictures of radial dissociation of hydrate plugs. This is an important observation, as it means that two-sided depressurization of high porosity plugs occurs radially, and length of the plug is not important. Pipe radii are never greater than 24 inches while hydrate plugs are sometimes as long as 2 miles (Lynch, 1996).

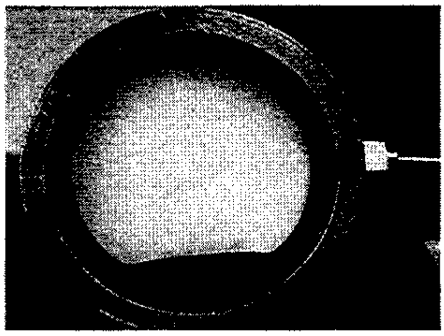

Plug after 1 hour

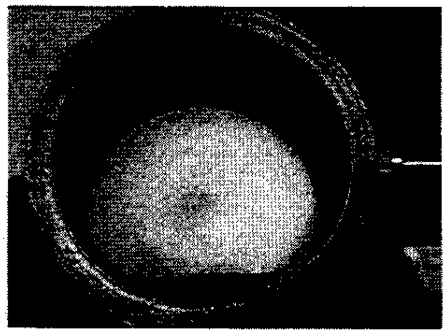

Plug after 2 hours

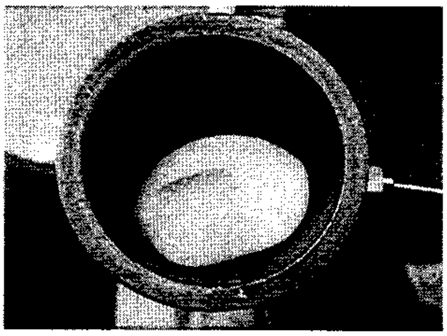

Plug after 3 hours

Figure 3.7: Radial Dissociation of Hydrate Plugs

3.3 Physical and Mathematical Description of the One-sided Model

This section outlines the physical description, general overview, modeling assumptions, and the mathematical description of the one-sided model.

3.3.1 Physical Description of the Model

Frequently in oil and gas pipelines, there is no access to both pipeline ends and so hydrate plugs are remediated by one-sided depressurization. During this procedure, the pressure at one end of the plug is reduced slowly below hydrate equilibrium pressure, at which point the hydrate is no longer stable and dissociates. The pressure is reduced in steps until flow of methanol is possible to help plug dissociation and flow.

Figure 3.8 shows a schematic view of the hydrate plug dissociation process by one-sided depressurization. In order for hydrate plug to melt, two criteria need to be met. The system conditions must be outside the hydrate stability region and a source of energy is required. Since hydrate plugs are long (typically, on the order of miles) pressure and temperature along the hydrate plug change. The pressure across the plug is dependent on one characteristic of the hydrate plug, i.e. permeability. Flow through the plug produces a pressure change. Since the pressure is not constant across the plug neither is the temperature, due to expansion and equilibrium considerations.

The source of energy to melt hydrates comes from the surroundings. The temperature gradient between the pipe wall and the center of hydrate plug results in conductive heat transfer. Since, the energy flux is maximum at the pipe wall, the hydrate plug dissociates radially, resulting in the bullet profile shown in Figure 3.8 (b).

Figure 3.8 shows a timewise sequence of hydrate plug dissociation by one-sided depressurization. Figure 3.8 (a) shows the hydrate plug after complete plugging of the pipeline. The low permeability of the hydrate causes a pressure gradient across the plug. This pressure drop can be as high as 1000 psig (6.89 MPa), as reported by Berge et al.

(1996). At this point of time, the plug adheres to the pipe wall and prevents any flow of gas/liquid through it.

Figure 3.8 (b) shows the schematic at time $t = t_1$ when the downstream pressure is reduced below the hydrate equilibrium pressure, P_{eq}. The hydrate dissociates wherever it is not thermodynamically stable. The dissociation is dominant in the radial direction, resulting in the bullet profile. As the downstream pressure is decreased further below the hydrate equilibrium pressure, the hydrate plug dissociates further across the length, as shown in Figure 3.8 (c) at time $t = t_2$. The hydrate temperature changes in accordance with the changing pressure across the plug.

Figure 3.8 (d) shows that during this dissociation process, the hydrate plug might detach from the plug wall and move due to the pressure differential across the plug. There are two forces that act on the hydrate plug: the adhesive force (F_{AD}) between the hydrate plug and pipe wall, and the pressure force (F_{DP}) caused due to the differential pressure across the plug length. When the pressure force exceeds the adhesive force, the resultant force is towards the downstream end. Hence, the plug detaches from the pipe wall, and the plug moves. Davalath (1996) reported plug velocities as high as 80 m/s during one-sided depressurization of hydrate plugs.

The adhesive force between the hydrate plug and pipe wall depends on the length of the undissociated part of hydrate plug, defined as the contact length (L_c), the radius of the pipeline, and adhesive strength between the pipe wall and hydrate plug. The pressure force depends on the differential pressure across the plug and cross sectional area of the pipeline. Further description of the strength model will be presented later in this Chapter.

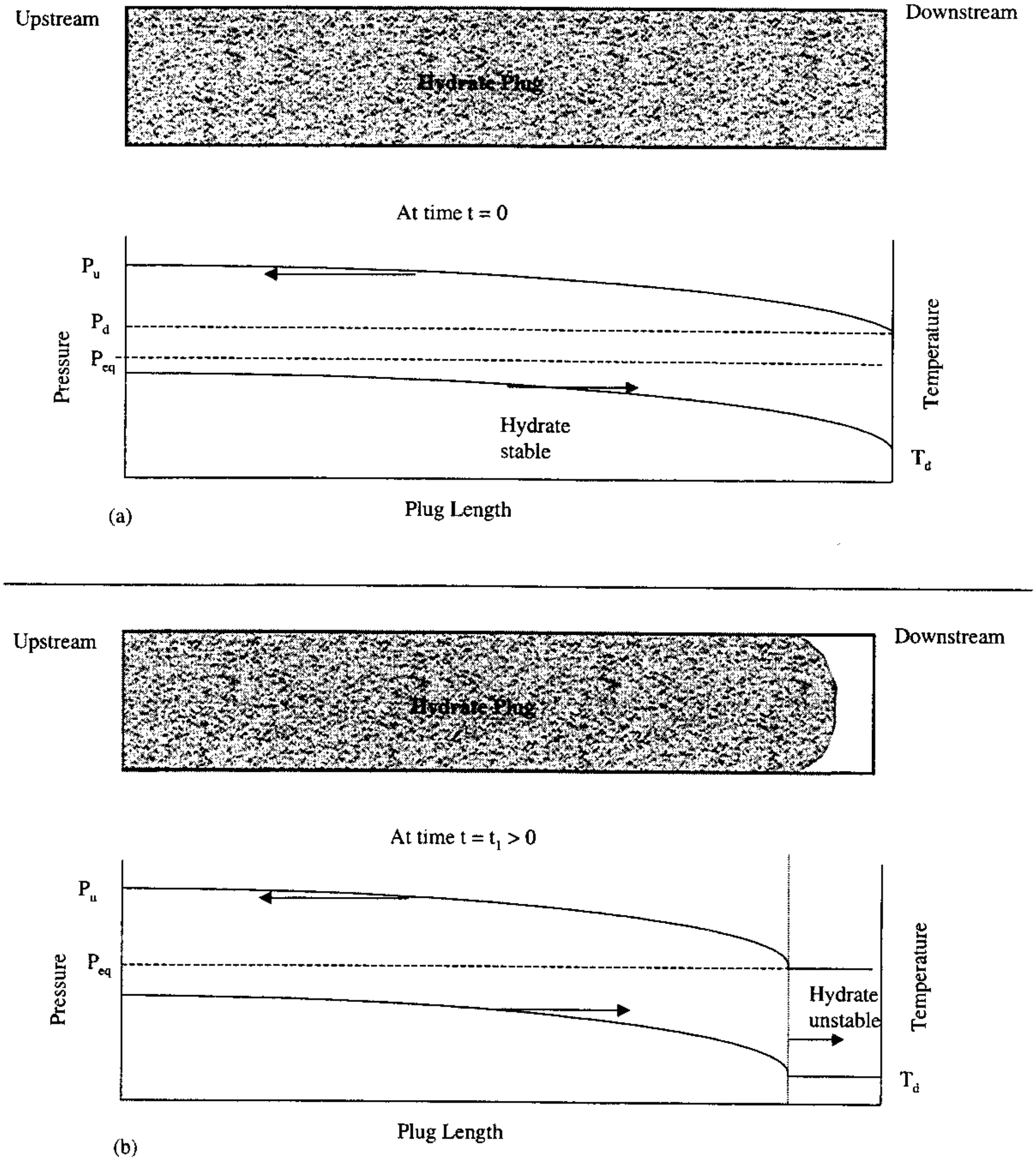

Figure 3.8: Schematic of one-sided depressurization. (a) Initial plug formed with a high-pressure drop across the length, shows pressure and temperature profile at time t = 0 before pressure is reduced, (b) Bullet shaped profile after pressure is reduced below hydrate equilibrium pressure P_{eq} at time $t = t_1$.

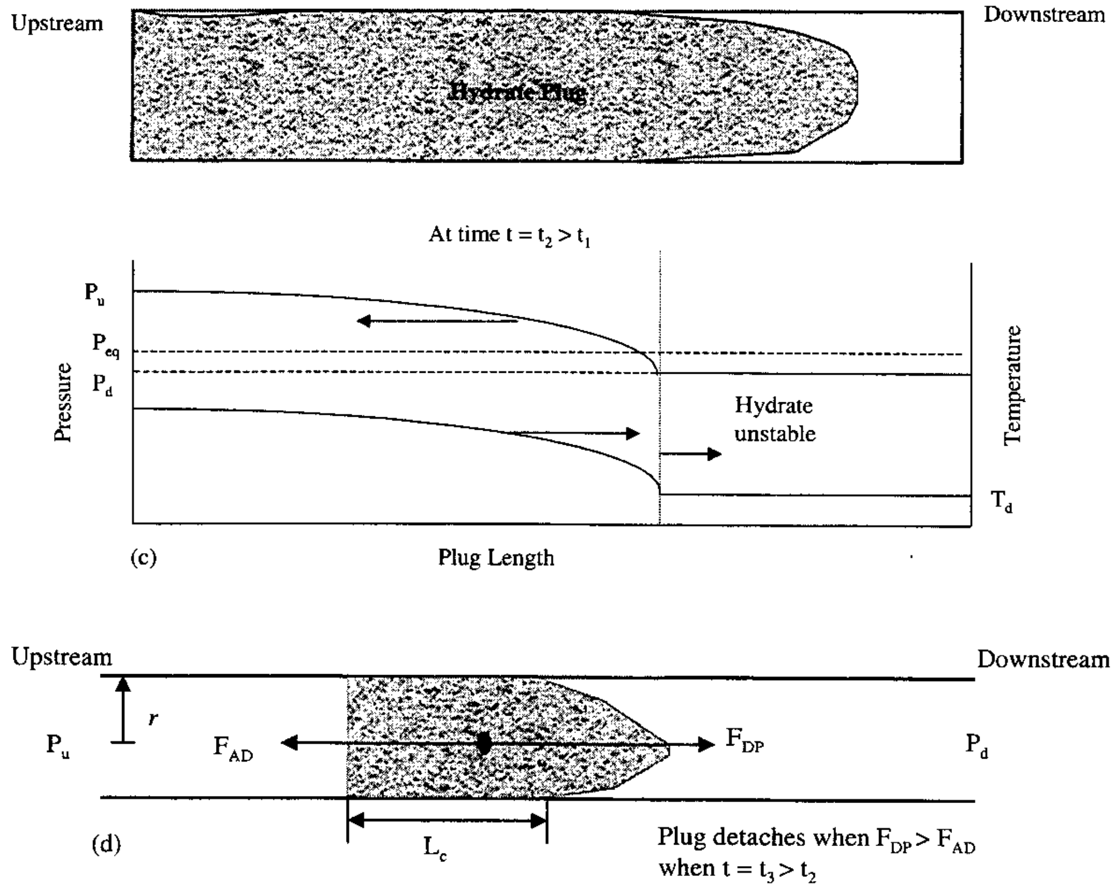

Figure 3.8: (c) Plug dissociation after time $t = t_2$, (d) Plug detaches at time $t = t_3$

A moving hydrate plug will compress the gas downstream of the plug. The compressed gas might increase the downstream pressure resulting in bursting of the pipeline. Sloan (2000, pg 1) reports instances of rupturing pipelines due to gas compression upon plug movement. Newton's laws of motion can be used to describe the moving hydrate plugs. The section on the safety simulator will detail the effect on downstream pressure of 1) differential pressure, 2) mass of the hydrate plug and 3) volumes of gas upstream and downstream of the plug. The goal of the safety model is to help an operator to determine the safe operating one-sided depressurization procedure.

3.3.2 General Overview of the Model

One objective of the research was to find an optimal way to depressurize a pipeline such that hydrate will dissociate the fastest and within safety limits. This objective was met by creating a computer model that simulates hydrate dissociation in a pipeline.

This section outlines the mathematics of one-sided dissociation, strength and safety models. The differential equations with relevant boundary conditions are provided. The solution scheme is described in the next section.

The mathematics consists of the following steps:

1. Calculate the pressure profile along the plug length
2. Calculate the flow of gas along the plug length
3. Calculate the temperature along the plug length
4. Divide the plug into small sections and calculate the radial dissociation of each section

3.3.3 Modeling Assumptions

As with any model, there are certain assumptions required to make the problem relatively easy to solve. The model assumptions are:

1. Typically the time taken to depressurize a pipeline is small compared to the time taken to dissociate the hydrate plug (Sloan 2000, p78). In the cited case study it took several days to depressurize the pipeline below hydrate equilibrium pressure, and 23 days for the hydrate to dissociate. This is the general case, even when the pipeline is depressurized slowly to prevent movement of the hydrate plug. One of the assumptions in the model was to neglect the initial time during the depressurization procedure. Only the time for hydrate dissociation and ice melting

is modeled. In any case, no hydrate dissociation occurs until the pipeline pressure is below the hydrate equilibrium pressure, typically less than 1.37 MPa.

2. Heat conduction is the only source of energy for the hydrate to dissociate in the radial direction. Heat transfer by convection in the radial direction is neglected. A calculation of Peclet Number, defined as the ratio of convective to conductive heat transfer, shows that for impermeable hydrate plugs (k = 0.01 – 1 mD), the Peclet Number ranges from 0.1 – 0.001. Hence, convection is negligible compared to conduction in the radial direction. The calculations of Peclet Number are shown in Appendix B.
3. The permeability of hydrate plugs has not been measured so far, and it is assumed to be similar to that of carbonate sediments. Bear (1972, pg. 136) and Muskat (1937, pg. 113) outline that permeability of carbonate stones ranges from 0.1 – 0.01 mD.
4. The Peclet Number in the axial direction for plugs with permeability (k = 0.01 – 1 mD) ranges from 1 – 100. Hence, heat transfer by both convection and conduction are considered while modeling in the axial direction.
5. It is assumed that the response time for heat transfer between gas and hydrate is much shorter than the response time for gas flow through the long plug. The shorter response time may be safely neglected and the gas and hydrate temperature assumed equal. That is, local thermal equilibrium exists between the gas and hydrate.
6. The lowest temperature in the hydrate during the dissociation process is assumed to be at 272.15 K. All the experiments on hydrate plug dissociation by Lysne (1995), Peters (1999), Fidel-Dufour (2002) and this work, showed that upon rapid depressurization to dissociate the hydrate plug, the lowest temperature measured in the hydrate plug was around 272.15 K. However, the model does not limit the user from inputing lower temperature limits less than 272.15 K. It is believed (Peters, 1999) that ice freezing buffers lower temperatures less than 272.15 K.

7. Frictional losses due to plug movement have been neglected in the safety model. It stands to reason that the frictional losses are negligible. The safety model is modeled as a worst-case scenario situation. The pipeline has been assumed to be void of any liquids. Xiao et al. (1998) used OLGA®, a transient multiphase flow simulator to conclude that the presence of liquid (oil or condensate) and hydrate debris in pipelines can slow down the plug movement. However, to reduce the peak velocity, the liquid must be injected close to the plug initial location. This will be rather difficult to achieve in the field, and for all practical purposes, liquid does not affect the plug velocity.
8. Radiation was neglected while modeling the heat transfer effects in porous medium.

3.3.4 Mathematics of the Model

In formulating a model for gas flow in the porous medium (hydrate), it is desired that the model be sufficiently detailed that to predict the flow salient features, yet be sufficiently simple that the results can be broadly applicable. As described in Section 3.3.2 the first three of four steps involve modeling the pressure, velocity and temperature of the gas in the hydrate plug. The final fourth step uses the radial dissociation method established in the two-sided dissociation model.

The schematic diagram of the problem described above is represented in Figure 3.9. A uniform pressure equal to the upstream pressure is maintained in the plug at the upstream boundary so that there is always a pressure gradient between the upstream and downstream sides of the plug, thus sustaining the vapor flow. The downstream pressure governs the pressure at the right hand side of the boundary during the depressurization. In essence this is a forced convection flow through a porous medium. The problem is analyzed for the case in which the two horizontal walls are maintained at constant temperature.

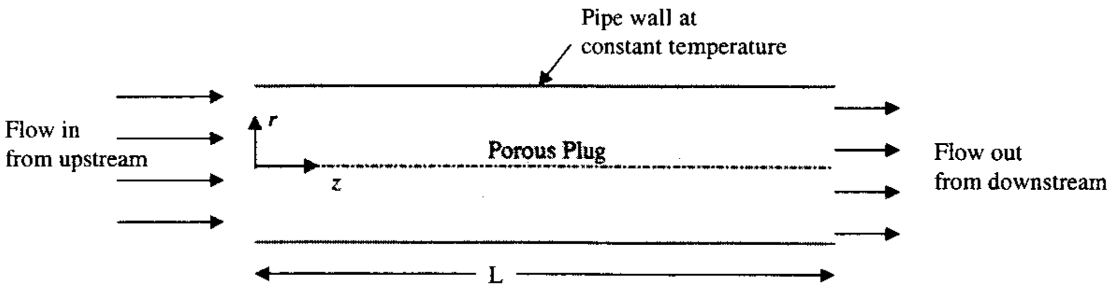

Figure 3.9: Schematic Diagram of Flow Through the Plug

The basic relations governing the flow of gas in porous media are the continuity equation, the momentum equation, and the equation of state. The continuity equation for the steady state flow of a compressible fluid in a porous media is easily obtained by performing a mass balance on an infinitesimal element (Kidder, 1958). The relation reduces to

$$\frac{d}{dz}(\rho v_z) = 0 \tag{3.8}$$

where ρ is the gas density, v_z us the velocity of gas, and z is the position coordinate in the direction of flow.

The momentum equation will be replaced by a constitutive equation, Darcy's law (Muskat, 1937)

$$v_z = -\frac{\kappa}{\mu}\frac{dP}{dz} \tag{3.9}$$

where κ is the permeability of the medium, μ is the fluid viscosity, and P is the fluid pressure. The permeability and viscosity are assumed constant.

The gas is assumed to obey the perfect gas equation of state

$$P = \rho RT \tag{3.10}$$

where T is the absolute temperature, and R is the gas constant. The compressibility of the gas was modeled as a function of pressure at the surrounding temperature. The details are given in Appendix C, and show that the predictions with perfect gas are within 2% of that obtained by assuming real gas.

Holding the temperature constant and eliminating the velocity and density by substituting Equations 3.9 and 3.10 into Equation 3.8, an equation with pressure as the sole dependent variable results.

$$\frac{d}{dz}\left(P\frac{dP}{dz}\right) = 0 \tag{3.11}$$

The appropriate boundary conditions are

$$P = P_u \qquad z = 0 \tag{3.12}$$

$$P = P_d \qquad z = L_c \tag{3.13}$$

where P_u and P_d are the upstream and downstream pressures, and L_c is the contact length as described in Figure 3.8. Initially, the contact length is set as the plug length. As the dissociation occurs, the contact length changes, depending on the amount of radial dissociation.

The velocity of gas through the plug may be obtained from Darcy's law, given by Equation 3.9. To obtain the velocity distribution, Equation 3.11 is solved with the boundary conditions given by Equations 3.12 and 3.13.

The next step involves the development of the temperature distribution in the hydrate plug. The mathematical equation is obtained by analyzing the energy in the hydrate plug with forced convective flow. The energy transport in porous media takes place by the three modes: conduction, convection and radiation.

We start with a simple situation in which the medium is isotropic, and where radiative effects, viscous dissipation and the work done by pressure changes are negligible. Taking averages over an elemental volume of the medium, energy transport for the solid hydrate phase is given by Neild (1992, pg. 21),

$$(1-\varepsilon)k_h \frac{\partial^2 T_h}{\partial z^2} + (1-\varepsilon)q_h''' = 0 \tag{3.14}$$

and, for the fluid phase,

$$(\rho C_p)_f v_z \frac{\partial T_f}{\partial z} = \varepsilon k_f \frac{\partial^2 T_f}{\partial z^2} + \varepsilon q_f''' \tag{3.15}$$

Here the subscripts h and f refer to the hydrate and fluid phases, C_p is the specific heat at constant pressure of the fluid, k is the thermal conductivity, and q''' is the heat production per unit volume.

In Equation 3.14, the first term on the left hand side represents the net rate of heat conduction into a unit volume of the hydrate. The conductive heat transfer rate in Equation 3.15 is given by the first term on the right hand side, while the first term on the left hand side of Equation 3.15 represents the rate of change of energy in the elemental volume due to the convection of fluid.

Setting the assumption that local thermal equilibrium exists between the hydrate and fluid phase, so that $T_h = T_f$ and adding Equations 3.14 and 3.15 we have

$$(\rho C_p)_f v_z \frac{\partial T_h}{\partial z} = k_h \frac{\partial^2 T_h}{\partial z^2} + q_m''' \tag{3.16}$$

where q_m''' is the overall heat production per unit volume of the medium. Since, there is no chemical reaction in the hydrate, this term can be neglected. If the work done by pressure change is not negligible then a term $-\beta T_h(\partial P/\partial z)v_z$ should be added to the left-hand side of Equation 3.16 resulting in,

$$(\rho C_p)_f v_z \frac{\partial T_h}{\partial z} - \beta T_h v_z \frac{\partial P}{\partial z} = k_h \frac{\partial^2 T_h}{\partial z^2} \tag{3.17}$$

where β is the coefficient of volumetric thermal expansion, defined by

$$\beta = -\frac{1}{\rho}\left(\frac{\partial \rho}{\partial T}\right)_P \tag{3.18}$$

Appendix D gives a brief description of obtaining the coefficient of volumetric thermal expansion using an equation of state.

Equation 3.17 governs the mathematical equation for the temperature distribution in the z-direction. The appropriate boundary conditions are

$$T_h = T_u \qquad z = 0 \tag{3.19}$$

$$T_h = T_d \qquad z = L_c \tag{3.20}$$

The boundary condition given by Equation 3.19 represents the temperatures at the upstream end of the plug and Equation 3.20 represents the hydrate dissociation temperature. Dividing the plug into small sections and obtaining the hydrate temperature at each section, is fed to the radial dissociation model as the dissociation temperature (T_D) in Equation 3.7.

3.4 Solution Scheme

This section describes the solution to the mathematical problem. Analytical solutions for pressure and velocity distributions were obtained, while the temperature distribution required a finite difference solution. Simplifying the temperature differential equation given by Equation 3.17 by neglecting the work done by pressure resulted in

$$(\rho C_p)_f v_z \frac{\partial T_h}{\partial z} = k_h \frac{\partial^2 T_h}{\partial z^2} \tag{3.21}$$

Equation 3.21 was solved analytically with boundary conditions given in Equations 3.19 and 3.20. The finite difference scheme was then verified with the analytical solution.

3.4.1 Solution to the Pressure Equation

The solution to Equation 3.11 is facilitated by the introduction of the following dimensionless quantities,

$$\phi = \frac{(P - P_d)}{(P_u - P_d)} \tag{3.22}$$

$$N = \frac{P_u}{P_d} \tag{3.23}$$

$$\eta = \frac{z}{L_c} \tag{3.24}$$

where ϕ is the dimensionless pressure, η is the dimensionless distance along plug length, and N is the pressure ratio.

Equation 3.11 and the appropriate boundary conditions given by Equation 3.12 and 3.13 change to

$$\frac{d^2}{dz^2}\left(\phi^2 + \frac{2\phi}{N-1}\right) = 0 \tag{3.25}$$

$$\phi = 1 \qquad \eta = 0 \tag{3.26}$$

$$\phi = 0 \qquad \eta = 1 \tag{3.27}$$

Morrison (1972) gives the analytical solution to this problem.

$$\phi = \frac{\left\{\sqrt{N^2 - (N^2 - 1)\eta}\right\} - 1}{N - 1} \tag{3.28}$$

The pressure distribution is a strong function of the pressure ratio N. Figure 3.10 shows the solution for a particular case when the pressure ratio changes from N = 2.2 to 20. As the pressure ratio increases, the distribution becomes more non-linear or curved in nature.

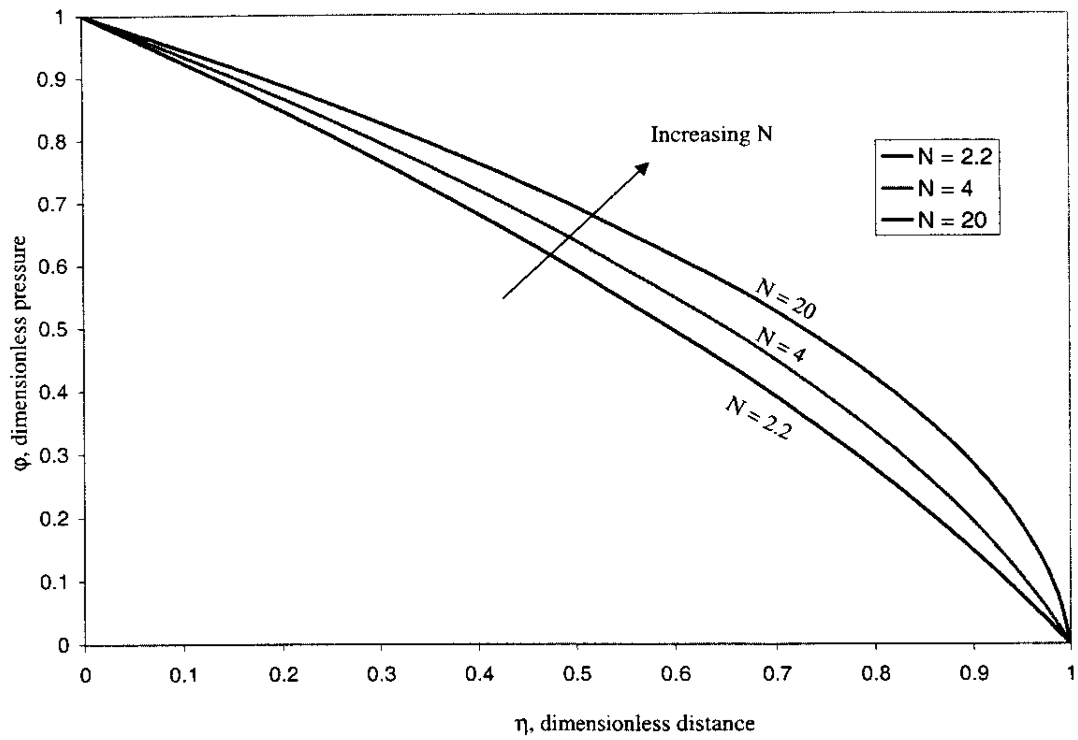

Figure 3.10: Dimensionless Pressure Distribution as a Function of Pressure Ratio, N

3.4.2 Solution to the Velocity Equation

Darcy's law as described in Equation 3.9 gives the fluid velocity. To calculate the velocity, the pressure gradient across the plug length should be calculated. The pressure gradient along the z-direction (in dimensionless variables) is obtained by differentiating Equation 3.28

$$\frac{d\phi}{d\eta} = \frac{-(N+1)}{2\sqrt{N^2-(N^2-1)\eta}} \tag{3.29}$$

Using Equation 3.29, the solution to the velocity profile is

$$v_z = \frac{\kappa\, P_d}{2\mu\, L_c} \frac{(N^2-1)}{\sqrt{N^2-(N^2-1)\eta}} \tag{3.30}$$

The velocity profile depends on the plug permeability, fluid viscosity, downstream pressure, contact length and pressure ratio. The dimensionless velocity, $v_z^{\sim}$ may be described by the following equation

$$v_z^{\sim} = \frac{(N^2-1)}{\sqrt{N^2-(N^2-1)\eta}} \tag{3.31}$$

where $v_z^{\sim} = 2v_z\mu L_c/(\kappa P_d)$.

Figure 3.11 shows the dimensionless velocity distribution along the plug length. The graph is a semi logarithmic plot. Again, it can be seen that velocity is a strong function of pressure ratio.

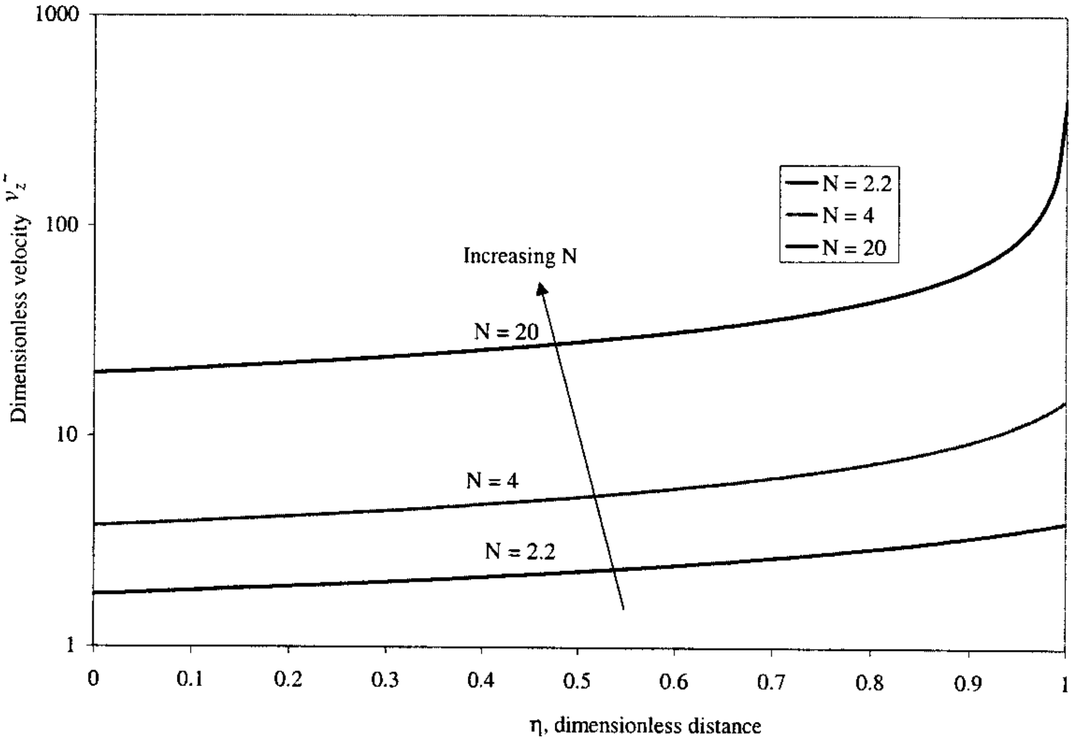

Figure 3.11: Dimensionless velocity as a Function of Pressure Ratio N

3.4.3 Solution Scheme for Temperature Distribution

Non-dimensionalizing the temperature in Equation 3.17 is accomplished by using the term

$$\theta = \frac{T_h - T_d}{T_u - T_d} \tag{3.32}$$

Equation 3.17 transforms into a nonlinear, second order, non-homogeneous ordinary differential equation.

$$\frac{d^2\theta}{d\eta^2} - F_t\, f(\eta)\frac{d\theta}{d\eta} - F_t\, \beta\, P_d\, g(\eta)\theta = F_t\, \beta\, P_d\, R_T g(\eta) \tag{3.33}$$

where the coefficients are given as

$$F_t = \frac{\kappa\, P_d}{\mu \alpha_m} \tag{3.34}$$

$$f(\eta) = \frac{N^2 - 1}{\sqrt{N^2 - (N^2 - 1)\eta}} \tag{3.35}$$

$$g(\eta) = \frac{(N^2 - 1)^2}{N^2 - (N^2 - 1)\eta} = \left[f(\eta)\right]^2 \tag{3.36}$$

$$R_t = \frac{T_d}{T_u - T_d} \tag{3.37}$$

where α_m is the thermal diffusivity equal to $k_h/(\rho C_p)_f$. The subscripts h and f represents the hydrate and fluid. The appropriate boundary conditions are

$$\theta = 1 \qquad \eta = 0 \tag{3.38}$$

$$\theta = 0 \qquad \eta = 1 \tag{3.39}$$

The solution to the above problem can only be obtained with a finite difference solution. Typically solutions to convective-diffusion equations involve two different schemes, owing to the dominance of convection over diffusion in the physics. Therefore, two different schemes were used in obtaining the solution: classical center difference scheme and upwind-differencing scheme.

Pozrikidis (1998, pg. 571) notes that the classical center difference scheme is conditionally stable for pure unsteady diffusion, and unconditionally unstable for pure linear convection. Using the classical second-order finite difference approximation for the first and second derivative:

$$\frac{d\theta}{d\eta} = \frac{\mathrm{W}_{i+1} - \mathrm{W}_{i-1}}{2\,\Delta x} \tag{3.40}$$

$$\frac{d^2\theta}{d\eta^2} = \frac{\mathrm{W}_{i+1} - 2\,\mathrm{W}_i + \mathrm{W}_{i-1}}{\Delta x^2} \tag{3.41}$$

where W_i, represents the dimensionless temperature at grid point i, and Δx is the finite difference grid step size.

Substituting the derivative approximations into the discrete form of the original ODE given by Equation 3.33, results in

$$\left(\frac{1}{\Delta x^2} - \frac{\mathrm{A1}}{2\,\Delta x}\right)\mathrm{W}_{i-1} - \left(\frac{2}{\Delta x^2} + \mathrm{A2}\right)\mathrm{W}_i + \left(\frac{1}{\Delta x^2} + \frac{\mathrm{A1}}{2\,\Delta x}\right)\mathrm{W}_{i+1} = \mathrm{A3} \tag{3.42}$$

where the corresponding coefficients are given by

$$\mathrm{A1} = F_t\, f(x_i),\;\; \mathrm{A2} = F_t\, \beta\, P_d\, g(x_i),\;\; \mathrm{A3} = \mathrm{A2}\, R_t \tag{3.43}$$

The solution to the finite difference scheme is obtained from setting up a tridiagonal matrix and solving for the dimensionless temperatures by using the Thomas algorithm outlined in Hoffman (2001, pg. 473). Figure 3.12 shows the results from the finite difference solver for total of 40 grid points. The solution is dependent on the variables such as upstream and downstream pressure and temperatures, and permeability of the plug. The solution scheme fails when the permeability of the plug is high at 0.8 mD. This is the point when the coefficient of W_{i-1} in Equation 3.42 becomes negative, the second-order finite difference becomes unstable, leading to large errors in calculating the temperatures, as shown by the spike in temperature at 0.8 mD in Figure 3.12.

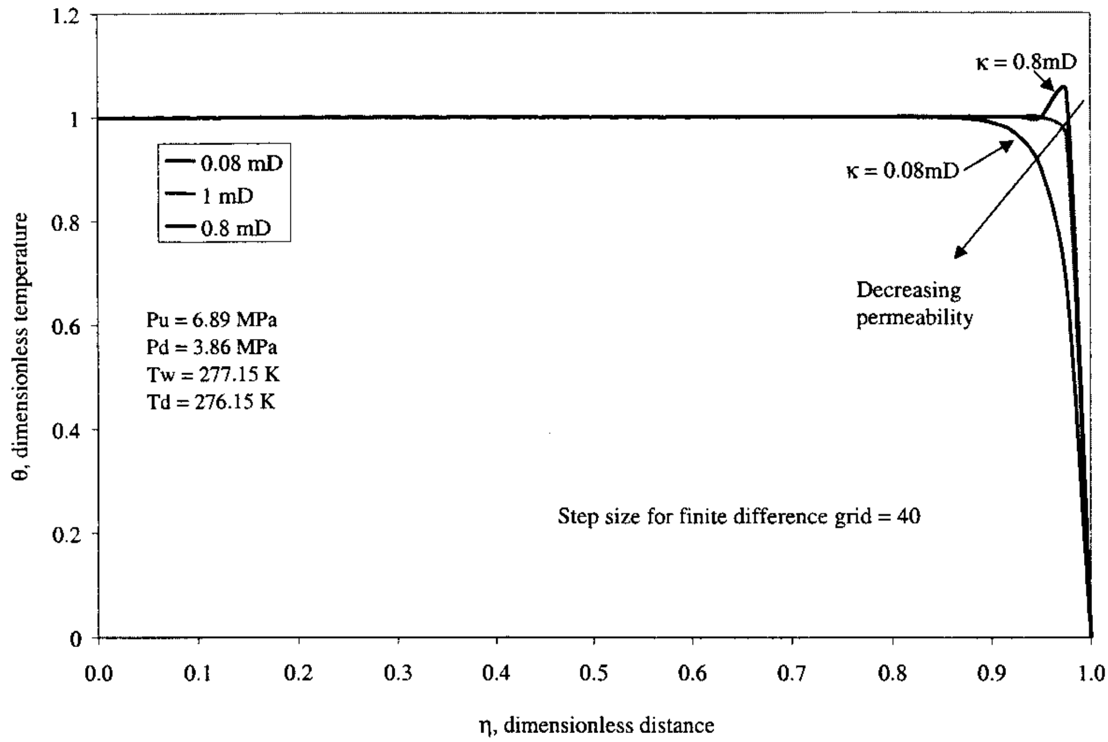

Figure 3.12: Second-order Finite Difference Solution for Temperature Distribution

Leonard (1979) proposed to eliminate the errors caused when convection becomes dominant by using a upwinding difference scheme. This scheme uses a backward difference for the first spatial derivative, and a centered difference for the second spatial derivative is used and are given by:

$$\frac{d\theta}{d\eta} = \frac{\mathrm{W}_i - \mathrm{W}_{i-1}}{\Delta x} \tag{3.44}$$

$$\frac{d^2\theta}{d\eta^2} = \frac{\mathrm{W}_{i+1} - 2\,\mathrm{W}_i + \mathrm{W}_{i-1}}{\Delta x^2} \tag{3.45}$$

Substituting the derivative approximations into the discrete form of the original ODE given by Equation 3.33, results in

$$\left(\frac{A1}{\Delta x}-\frac{1}{\Delta x^2}\right)W_{i-1}-\left(\frac{2}{\Delta x^2}+\frac{A1}{\Delta x}+A2\right)W_i+\left(\frac{1}{\Delta x^2}\right)W_{i+1}=A3 \qquad (3.46)$$

where the coefficients are given by Equation 3.43.

The solution to the upwinding difference scheme is obtained by setting up a tridiagonal matrix and solving for the dimensionless temperatures as described above. Figure 3.13 shows the results from the finite difference solver for a total of 40 grid points. Figure 3.13 compares the solutions from the two schemes outlined in this section. Clearly, when convection becomes dominant, the second order finite difference scheme shows a spike in temperature. The upwinding scheme is more stable (shown in Figure 3.13) than the second-order finite difference scheme.

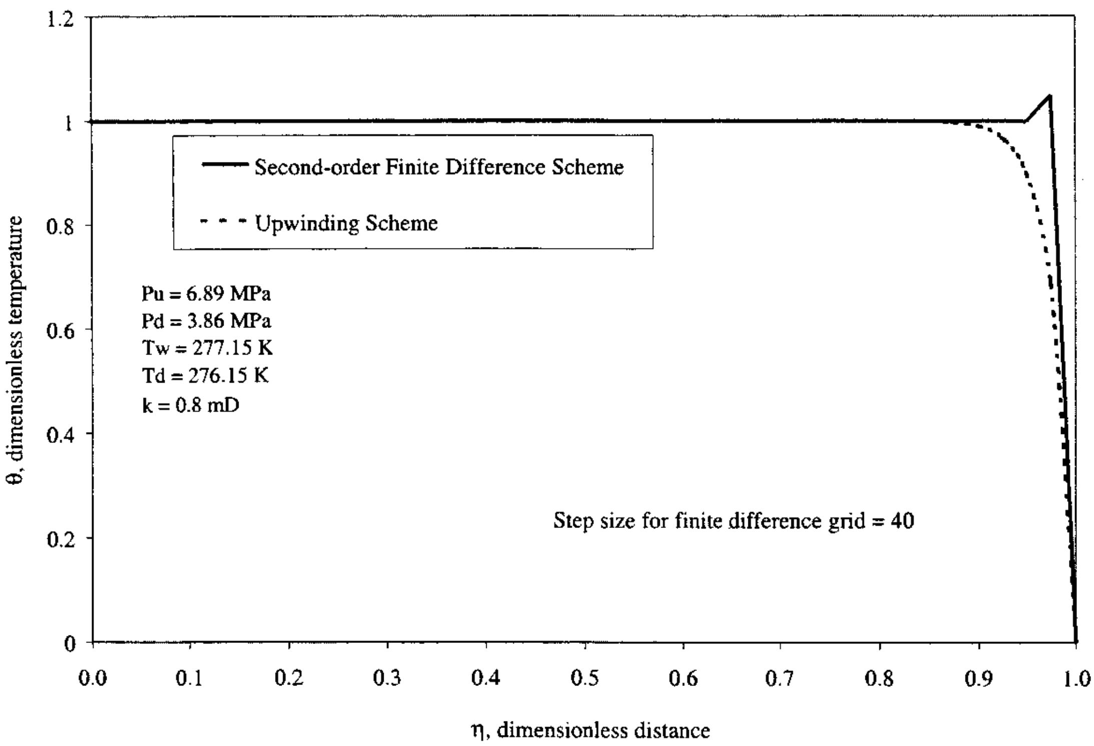

Figure 3.13: Comparison of Upwinding and Second-order Finite Difference Schemes

To verify the finite difference scheme, it was necessary to obtain an analytical solution to a simplified form of Equation 3.18. As described in Section 3.4, the work done by pressure can be neglected to obtain Equation 3.21. This equation is nondimensionalized by using Equation 3.32 and 3.30 to obtain

$$\frac{d^2\theta}{d\eta^2} = F_t\, f(\eta)\frac{d\theta}{d\eta} \tag{3.47}$$

Equations 3.38 and 3.39 give the appropriate boundary conditions. A analytical solution can be obtained for this problem. A detailed solution is given in Appendix E. The solution is given as

$$\theta = \frac{A(a,\eta=1,F_t^{'}) - A(a,\eta,F_t^{'})}{A(a,\eta=1,F_t^{'}) - A(a,\eta=0,F_t^{'})} \tag{3.48}$$

where

$$A(a,\eta,F_t^{'}) = e^{-\frac{2F_t^{'}}{a}\sqrt{1-a\eta}}\left(\sqrt{1-a\eta} + \frac{a}{2F_t^{'}}\right) \tag{3.49}$$

The variables $F_t^{'}$ and a are given by

$$a = \frac{(N^2-1)}{N^2}, \quad F_t^{'} = F_t\left(\frac{N^2-1}{N}\right) \tag{3.50}$$

The finite difference scheme was compared with the analytical solution to check for the optimal grid spacing to be used in the model. Figure 3.14 shows the comparison between the finite difference scheme and analytical solution for one case when N = 2.2, and κ = 0.01 mD. It can be seen that for a total of 50 grid points the finite difference scheme works much better than for fewer (10) grid points.

The most important part of numerical techniques is the analysis of the errors. The results from the model are presented in Figure 3.15 for three different cases. The maximum error as a function of the number of grid points for N = 2.2, 4, and 20 is plotted in Figure 3.15. It can be seen that when the total number of grid points used is 50, the maximum error is <0.01, while the average error is <0.0008. The same magnitude of error was observed for other cases, and can be taken as the general error for the finite difference scheme.

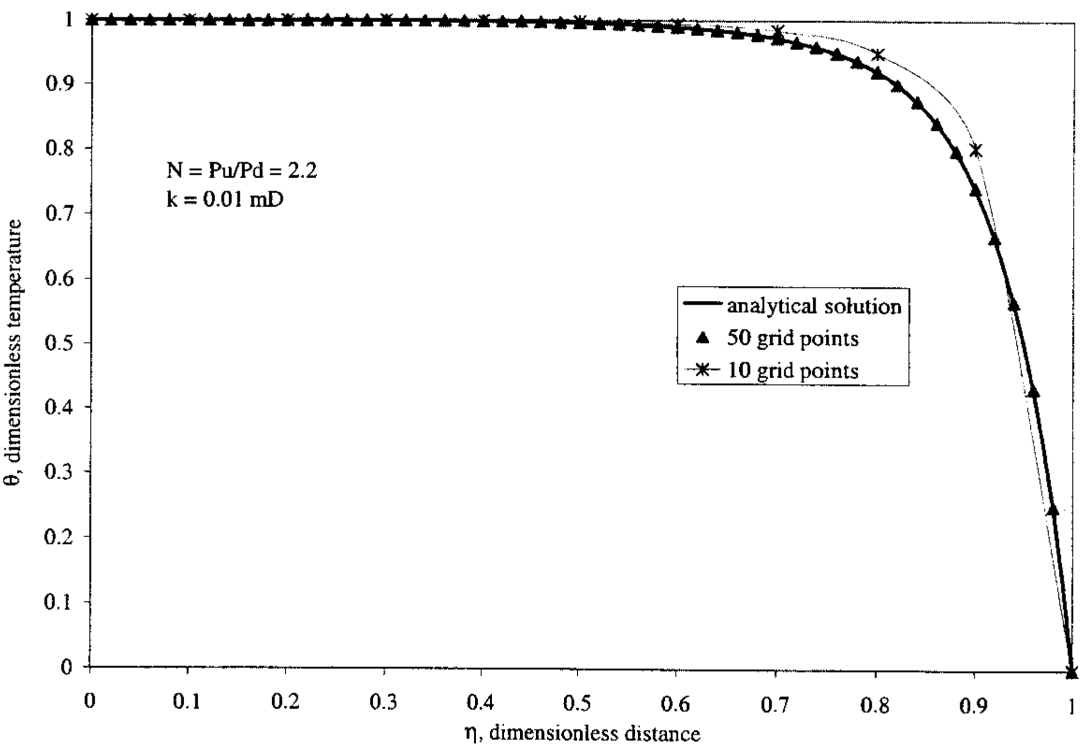

Figure 3.14: Comparison of Finite Difference to Analytical Solution

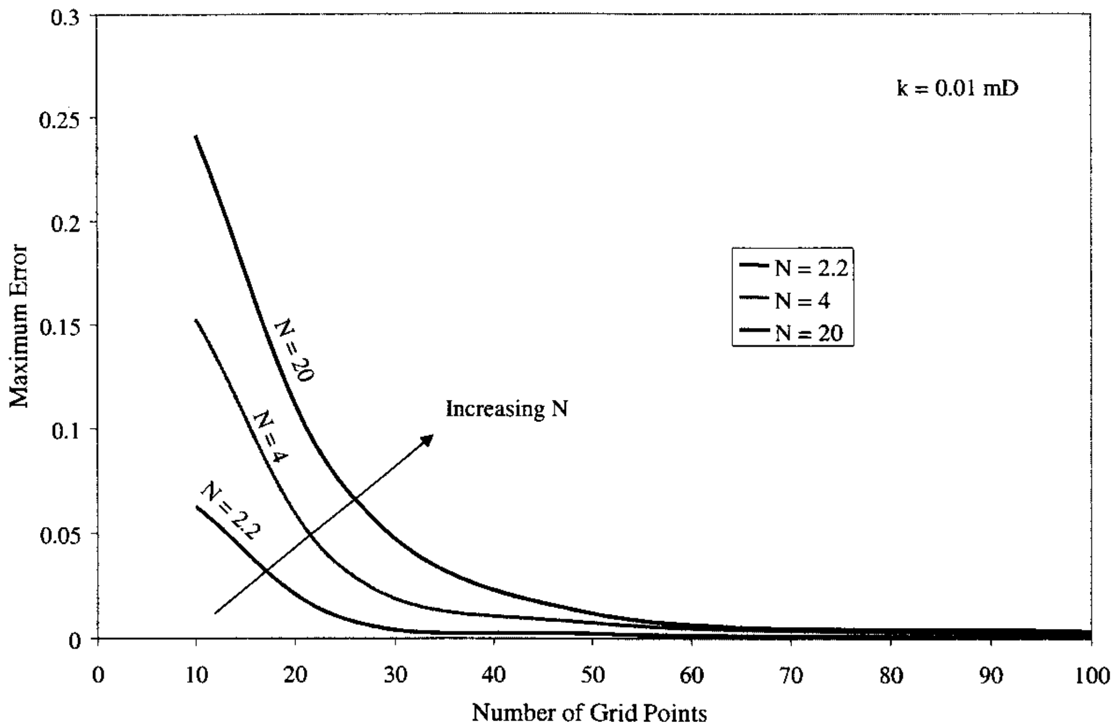

Figure 3.15: Error Analysis for the Finite Difference Scheme

3.5 Algorithm for the plug model

The steps are as follows to provide a computational algorithm for the plug model.

1. Solve the pressure profile through the hydrate plug
   - INPUT: Upstream pressure (P_u), downstream pressure (P_d), length
   - RELEVANT EQUATIONS: Equations 3.25 – 3.28
   - OUTPUT: *P(z)*
2. Solve the velocity distribution through the hydrate plug
   - INPUT: Upstream pressure (P_u), downstream pressure (P_d), length, permeability of the hydrate plug
   - RELEVANT EQUATIONS: Equations 3.30

- OUTPUT: $v_z(z)$

3. Solve the temperature profile in the hydrate phase
   - INPUT: $P(z)$, $v_z(z)$, upstream and downstream temperatures, length
   - RELEVANT EQUATIONS: Equations 3.42, 3.43, 3.46
   - OUTPUT: $T_H(z)$
4. Solve for the annulus between hydrate and pipe wall as a function of time
   - Divide the plug into 40 sections
   - INPUT: $T_H(z)$ at each section to be used in Equation 3.7 as T_d
   - RELEVANT EQUATIONS: Equations 3.1 – 3.7. At each plug section $T_H(z)$ is known, the annulus is solved at this position. This gives the annulus spacing along the length of the plug as a function of time. Calculations repeated by changing the length when assumed annulus spacing is obtained.
   - OUTPUT: Ice/hydrate and ice/water moving fronts as a function of time, temperature if ice and water as a function of time, and time when methanol may be injected.

3.6 Adhesive Strength Model to Determine when the Plug will Move

Figure 3.16 shows a schematic of the strength model. As described in Section 3.3.1, two forces exist at the hydrate plug and pipe wall interface. The first is the force of adhesion (F_{AD}) between the hydrate plug and the pipe wall (typically carbon steel), second is the force due to pressure gradient (F_{DP}) across the plug. The plug adhesion to the pipe wall prevents the plug movement. Once, the pressure force becomes strong, the plug detaches and moves as a projectile.

The adhesive force depends on the weight of the plug and the adhesive strength of hydrate to pipe wall. Bondarev et al. (1996) measured the adhesive strength of ice and hydrate on various substrates (pipe walls) like steel, duralumin, and polytetafluroethylene

(PTFE) at low temperatures ranging from 255.15 K to 271.15 K. Measurements indicated that adhesive strength depends on the type of hydrate (i.e. natural gas or tetrahydrofuran), temperature, and pipe wall. No measurements have been reported for adhesive strength of hydrates at 277.15 K. Hence, an extrapolated value (τ_H = 0.07 Mpa) has been used in this work.

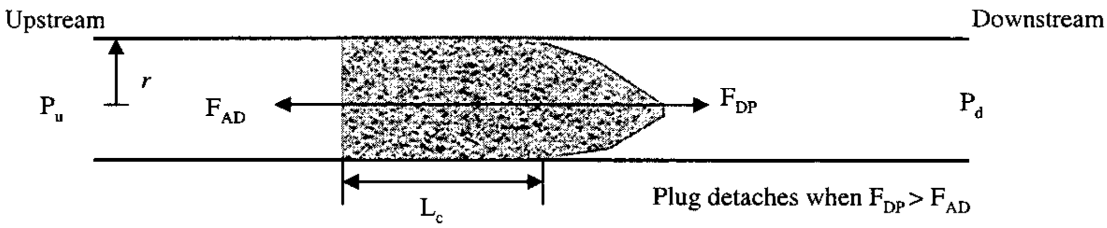

Figure 3.16: Schematic for Strength Model

The adhesive force is given by the following equation:

$$F_{AD} = \tau_h (2\pi r L_c) \tag{3.51}$$

where τ_h is the adhesive strength of hydrate with respect to pipe wall, r is the radius of the pipeline, and L_c is the contact length or undissociated part of the hydrate plug, obtained as a function of time from the one-sided dissociation model.

The pressure force depends on the pressure drop across the plug and the cross sectional area of the pipeline and is given by

$$F_{DP} = (P_u - P_d)\pi r^2 \tag{3.52}$$

Equating the two forces and calculating the contact length L_c

$$L_c = \frac{(P_u - P_d)\, r}{2\tau_h} \tag{3.53}$$

Figure 3.17 shows the effect of pipeline diameter on contact length L_c for different pressure drops across the plug. The adhesive strength of the hydrate with respect to steel at 271.15 K was measured to be 0.4 MPa (Bondarev et al. 1996). This value was used for the calculations in Figure 3.17. If pressure drop across the plug is 5.5 MPa, the diameter of the pipeline is 0.61 m, then the plug will detach when the plug length reduces to 2.1 m.

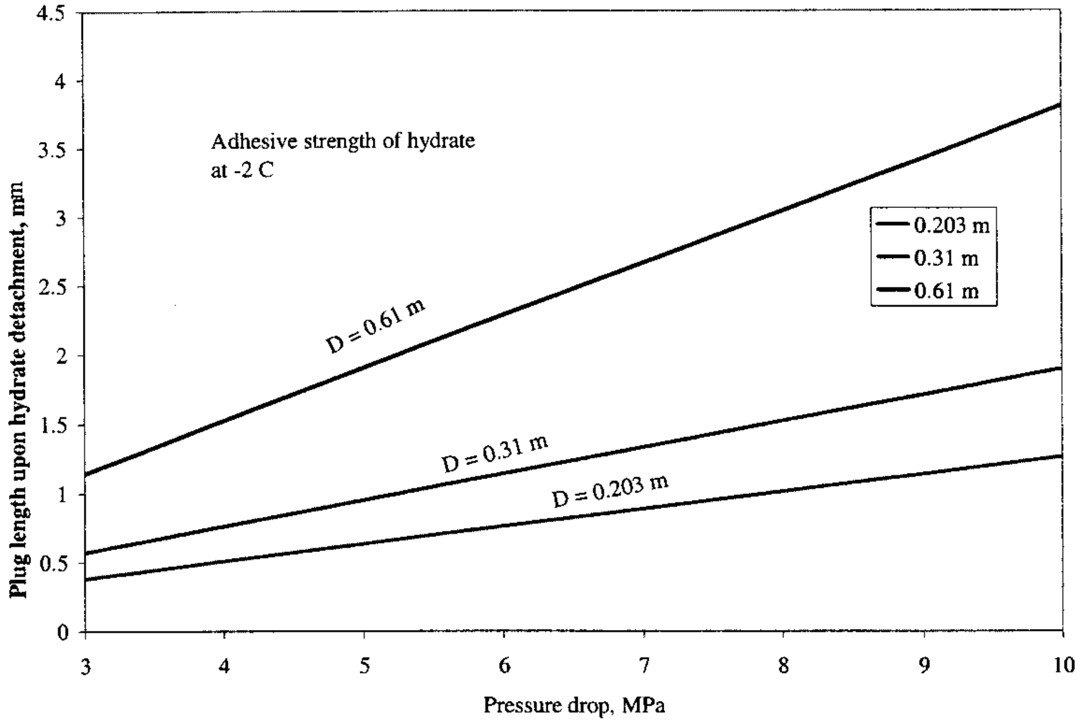

Figure 3.17: Contact Length upon Detachment as a Function of Pressure Drop for Various Pipeline Diameters at 271.15 K

Typically, in deep ocean pipelines, the temperature of the surrounding is usually around 277.15 K, and as described previously, adhesive strength of hydrate depends on temperature. Figure 3.17 re-plotted to show the effect on contact length of hydrate with the extrapolated value. As seen from the Figure 3.18, for a pressure drop of 5.5 MPa, 0.61 m pipeline diameter, the plug will detach from the pipe wall when the length reduces to 12.2 m. Compared to the previous case in Figure 3.17, there is a six-fold increase in the contact length. Hence, the plug detaches sooner as the temperature is increased.

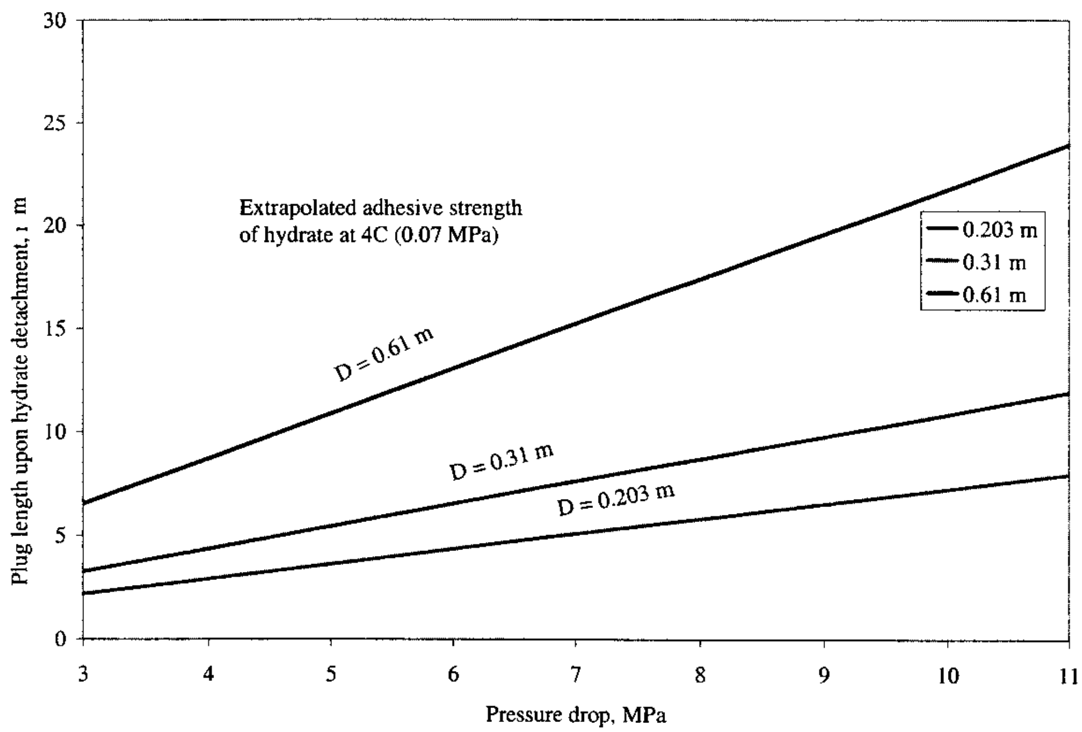

Figure 3.18: Contact Length upon Detachment as a Function of Pressure Drop for Various Pipeline Diameters at 277.15 K

3.7 Safety Simulator

The main goal of the safety simulator is to find an optimal downstream pressure for an operator to prevent any damage to the pipeline due to moving plugs. The driving force for moving plugs comes from the pressure gradient between the upstream and downstream ends of the plug. As soon as a hydrate blockage is formed in a pipeline, the well is shut off, and plug is located.

Sloan (2000, pg.46) describes two successful methodologies to locate a hydrate blockage that are performed on the platform side of the plug:

1. pressure reduction to locate relative volumes on either side of plug ends,

2. backpressurization to locate downstream end of plug

Pressure reduction is a strategy suitable for permeable plugs, and is done by decreasing the pressure downstream and monitoring the rate of upstream and downstream pressure change with time. One such study is outlined in Sloan (2000, pg. 46). In January 1996, a hydrate blockage occurred in a 6 inch, 1 mile long line in the North Sea Gullfaks field. The normal operating pressure was around 2400 psia (16.54 MPa). With the well shut in, the downstream pressure was rapidly reduced to 1670 psia (11.51 MPa), and then shut in. Figure 3.19 shows the pressure response upstream (subsea) and downstream (topside) across the plug. Over a 25 hour period, the downstream pressure increased by 73 psi (0.5 MPa) while the upstream pressure decreased by the same amount. Hence, it was concluded that there were equal volumes upstream and downstream of the plug as shown in Figure 3.20. The disadvantage is that this method does not allow determination of length of the plug or the proximity of the plug end to the platform.

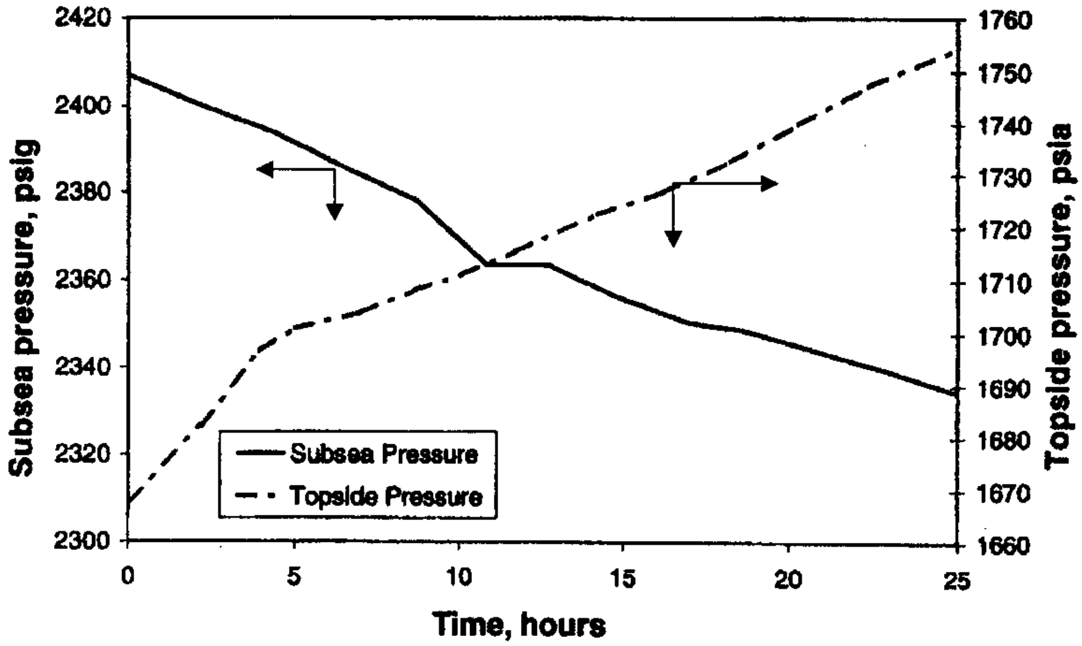

Figure 3.19: Pressure Reduction to Estimate Plug Location (Gjertsen, 1997)

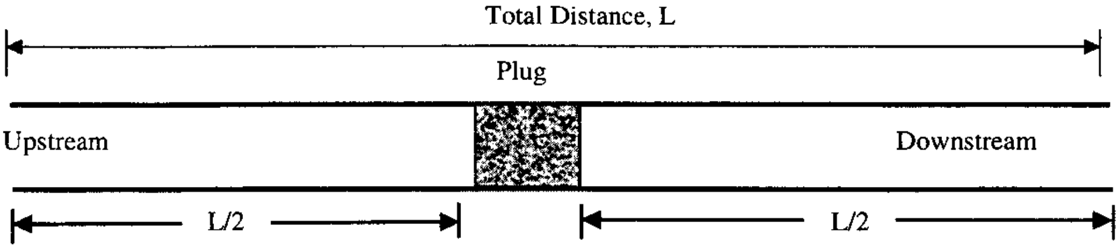

Figure 3.20: Hydrate Location in a Pipeline

Backpressurization is a means to measure the pressure increase when a known amount of gas is injected by a piston compressor from the platform. At constant volume at the downstream side of the plug, the pressure increase rate is proportional to the rate of gas input, hence determining the volume and pipeline length ($V/(\Pi D^2/4)$) between the blockage and the injection point. This method may result in plug compaction due to a "snow plow" effect caused by gas injection from the platform, decreasing the plug permeability. Thus it is not usually used in the industry.

Figure 3.21 shows a schematic of the safety simulator. The driving force for the plug movement is based on the pressure drop across the plug. Interaction between the pipe wall or fluid with the hydrate plug are neglected. The force balance gives,

$$F_{DP} = (P_u(t) - P_d(t))\,\pi r^2 \tag{3.54}$$

where $P_u(t)$ and $P_d(t)$ are the upstream and downstream pressures at time t, and r is the radius of the pipeline. As shown in Figure 3.21, the plug moves a distance dx in a step time dt. The distance dx is given by

$$dx = v\,dt + \frac{1}{2}\,a\,dt^2 \tag{3.55}$$

where a is the acceleration of the plug in time dt given by the expression

$$a = \frac{F_{DP}}{m} \tag{3.56}$$

where m is the mass of the plug, assumed to be constant, i.e. hydrate formation or dissociation is neglected during plug movement. Velocity v, is given by the expression

$$v = u + a\,dt \tag{3.57}$$

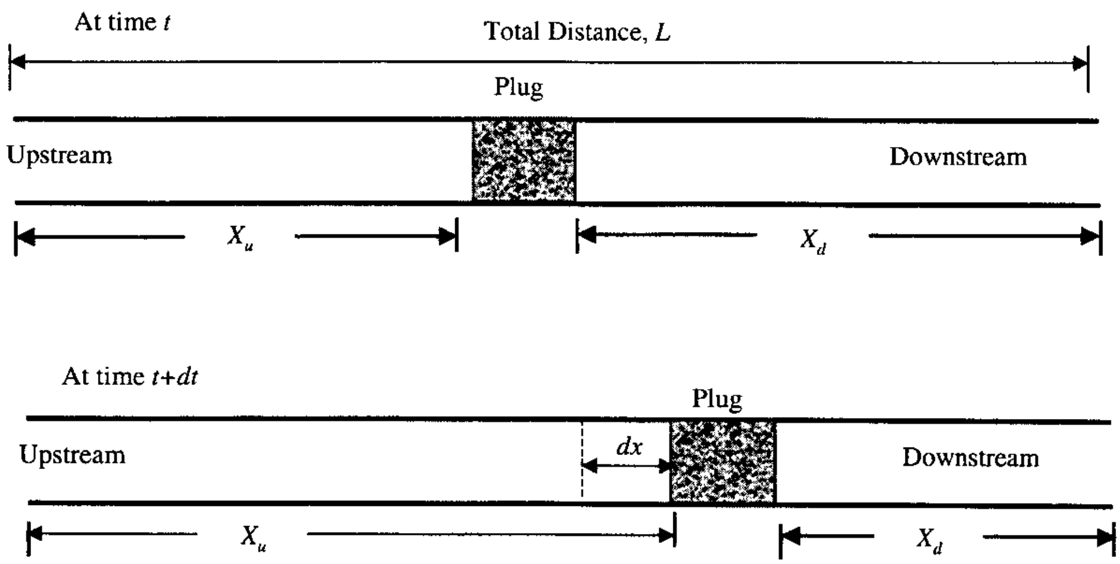

Figure 3.21: Schematic of the Safety Simulator

where u is the initial velocity of the plug at the previous time step. At the start of the simulator ($t = 0$), the initial velocity is assumed to be zero. As the plug moves the distance dx, it compresses the gas downstream of the plug. This compression results in a decrease in downstream volume and an equal increase in upstream volume. This incremental volume (Δv) is known by using the incremental distance dx.

With the knowledge of the amount of volume on either side of the plug after the plug moves in time dt, the new downstream and upstream pressures can be calculated using an equation of state. This new pressure drop acts as the driving force for the plug movement in the next time interval $t+dt$. The new driving force is calculated by using Equation 3.54. The procedure repeated for a selected time interval.

The time step is very crucial in determining the upstream and downstream pressures. A fixed time step of 0.001 second was selected to model the rapid transients, after running the model with other time steps of 0.005 second and 0.01 second. The time step 0.001 second was chosen, as it would give a better time resolution for simulations.

Figure 3.22 shows the results for two different simulations run by Xiao et al. (1998). The simulations were performed for two different pressure drops of 1150 psi (7.92 MPa) and 575 psi (3.96 MPa), the upstream distance was 7500 ft (2286 m), downstream distance was 16000 ft (4877 m), and the pipe diameter was 4 inches (0.1m). The upstream pressure was varied from 1200 psia (8.27 MPa) to 625 psia (4.3 MPa), keeping the downstream pressure constant at 50 psia (0.344 MPa). Figure 3.33 shows the results obtained from the safety simulator (this work). The predictions match fairly well between the simulations from this work and that of Xiao et al. The rate of change in pressure in our simulations was faster compared to that of Xiao et al.. The reason for this difference is the fact that, Xiao et al. considered friction effects while modeling the simulations. The difference in results will be presented in detail in Section 7.4.

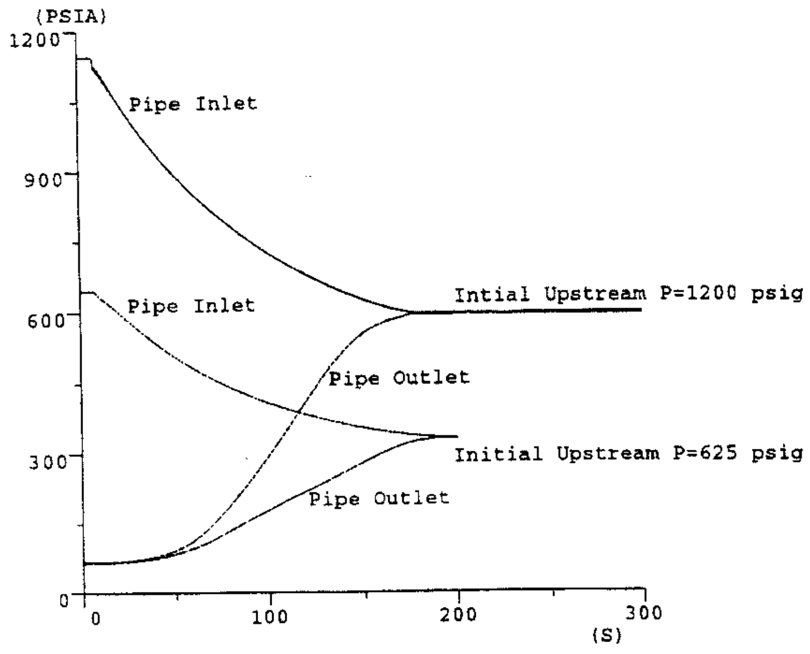

Figure 3.22: Simulation Results Showing Effect of Upstream Pressure (Xiao et al.)

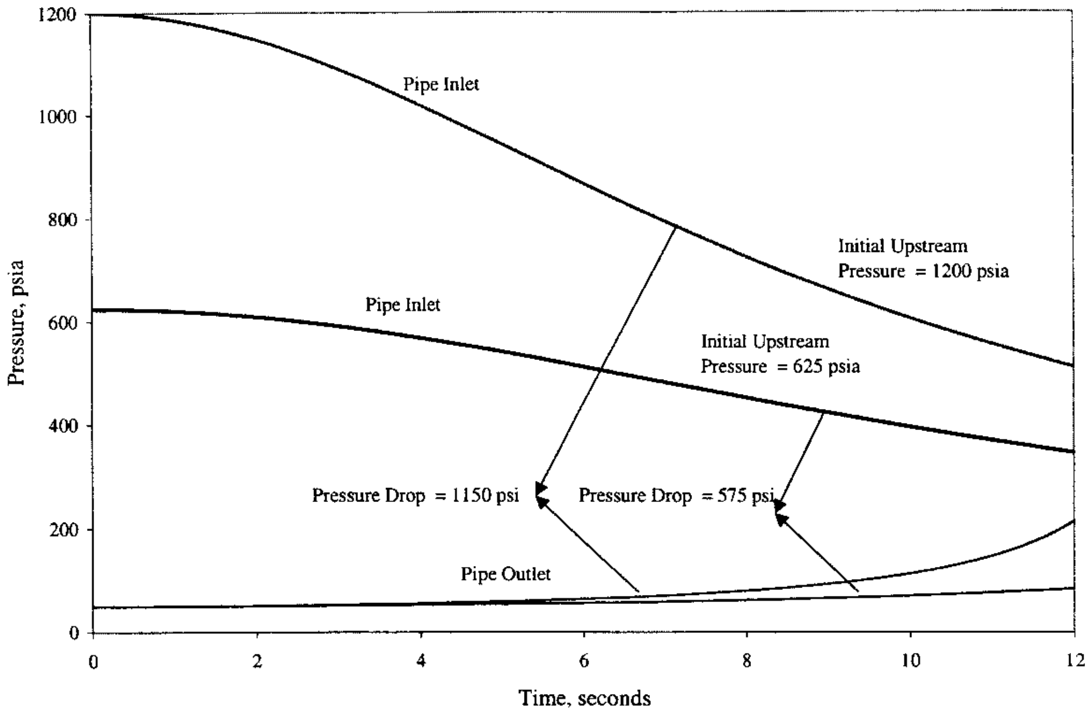

Figure 3.23: Simulation Results Showing Effect of Upstream Pressure (this work)

CHAPTER 4

RESULTS FROM TWO-SIDED DISSOCIATION

This chapter deals with the experimental results for plugs 1 – 10. All these plugs were dissociated by two-sided depressurization. The results were compared with predictions of the two-sided radial dissociation model. The goal of these experiments was to verify the radial dissociation model and its applicability in the long cell (L/D = 36).

4.1 Dissociation Studies with sII hydrates

The commonly found pipeline hydrates are sII. These hydrates are formed in the pipelines from mixed gases. In this particular study, a pseudo-gas mixture was used. The gas mixture was originally designed to have the same equilibrium conditions as a natural gas sample from a gas field in Qatar. The gas was prepared by Scott Specialty Gases, and had the following composition:

Table 4.1: Composition of Pseudo-Qatar Gas Mixture

Component	Mole Percent
Methane	83.8
Ethane	7.01
Propane	1.6
Iso-Butane	0.05
n-Butane	0.02
n-Pentane	0.02
n-Hexane	0.003
n-Heptane	0.003
Nitrogen	4.85
Carbon Dioxide	1.84

Peters (1999) conducted experiments with the pseudo-Qatar gas mixture. He observed very low temperatures (~ 238.15 K), but no reasons were mentioned. The present work attempted to decipher the dissociation of sII hydrates under these conditions. Experiments were conducted with the short cell with a formation procedure similar to that used to form methane hydrates. Four plugs (1-4) were formed and dissociated by two-sided depressurization.

Figure 4.1 shows the temperature profiles during the dissociation process for plug 1. The cell was depressurized from both ends rapidly. Very low temperatures (~238.15 K) were observed. This was quite contrary to the results obtained for methane hydrates. In all the experiments that were conducted by Peters (1999) and in this research with methane hydrates, the lowest temperature that was observed when the plug was depressurized from both ends rapidly to atmospheric pressure was 272.15 K, due to ice formation buffering the low hydrate dissociation temperature at one atmosphere.

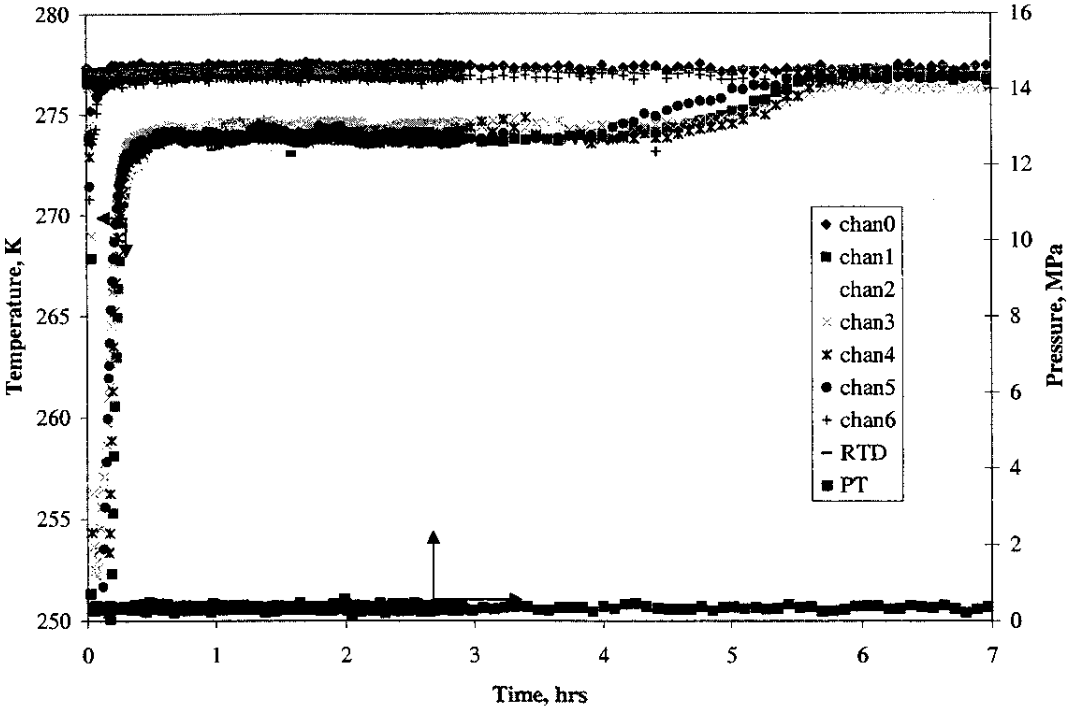

Figure 4.1: Depressurization of sII Hydrate Plug 1 Resulting in Low Temperatures

Figure 4.2 (Plug 3) shows the case when the system was depressurized in steps from 13.78 →12.82 → 8.61 → 5.72 MPa → atmospheric pressure. The same phenomenon of low temperatures was observed during the depressurization process.

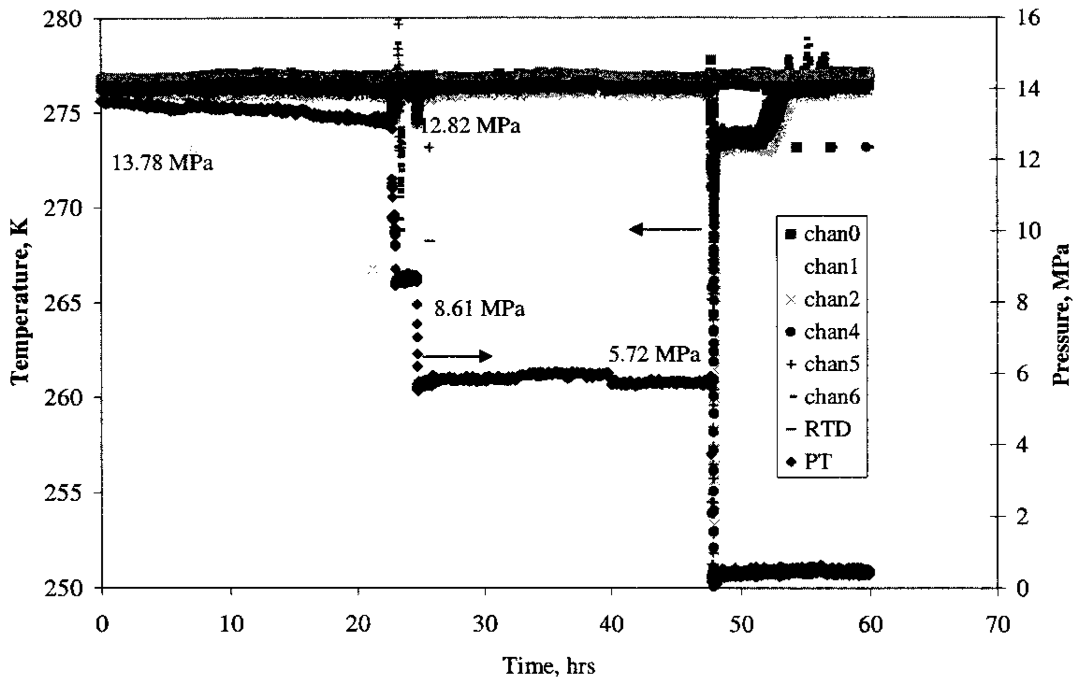

Figure 4.2: Depressurization of Plug 3 Resulting in Low Temperatures

Subsequently, plug 4 was depressurized in steps further below 5.72 MPa. Figure 4.3 shows the trial when the system was depressurized from 2.41 MPa. The step changes were made from 14.82 → 11.56 → 8.82 → 6.61 → 5.17 → 3.62 → 2.41 MPa → atmospheric pressure. In this case, no large drop in temperatures was observed as shown in Figure 4.3.

Table 4.2 shows the summary of plugs 1-4. This table shows the mass balance between gas consumed during formation and dissociation.

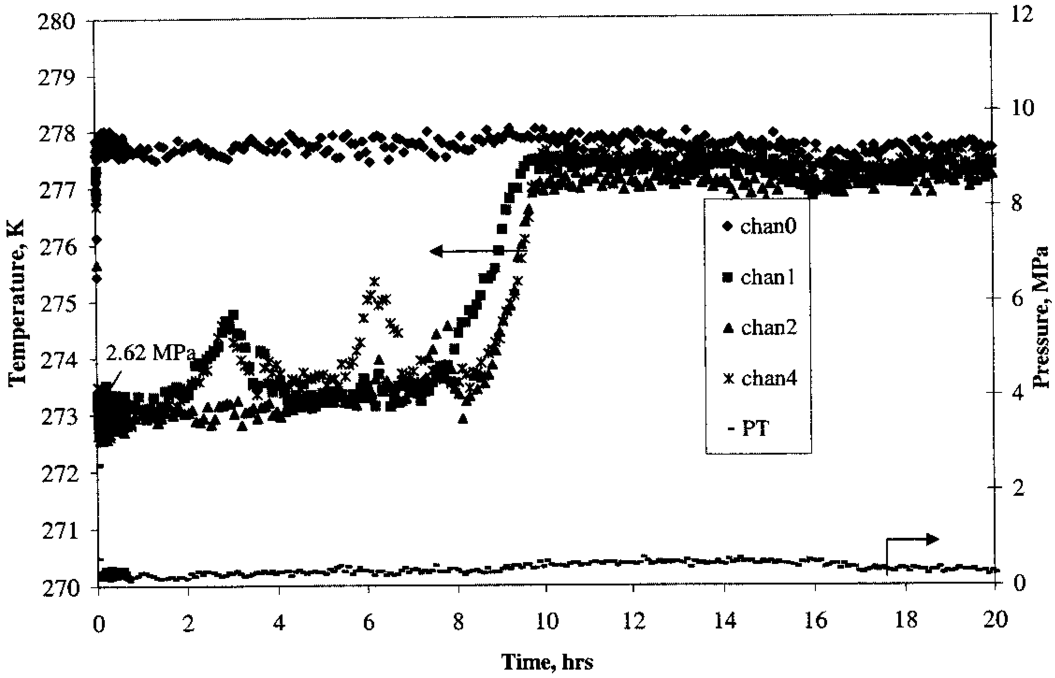

Figure 4.3: Slow Depressurization to Prevent Low Temperatures for Plug 4

Table 4.2: Summary of Hydrate Formation for Plugs 1 – 4

Plug #	Moles of Gas Consumed	Moles of Gas Evolved	Mass Balance % Error
1	1.4	1.33	5.0
2	1.36	1.28	5.8
3	1.45	1.56	7.5
4	1.32	1.48	12.1

A closer look at the thermodynamic phase diagram for the Qatar gas gives a better interpretation of the results. Figure 4.4 shows the hydrate equilibrium curve, vapor –

liquid equilibrium (VLE), Joule – Thomson (J-T) constant enthalpy curve for Qatar gas mixture. All the predictions in Figure 4.4 were obtained from the CSMGem program (Ballard, 2002). When the system was depressurized from 13.78 MPa to atmospheric pressure, as in the case for plug 1, the depressurization results in Joule-Thomson expansion into the VLE envelope, so that some of the higher components like n-hexane, i-butane and n-heptane liquefy. The endothermic process of liquefaction and subsequent vaporization of the heavy components, results in lowering the system temperature.

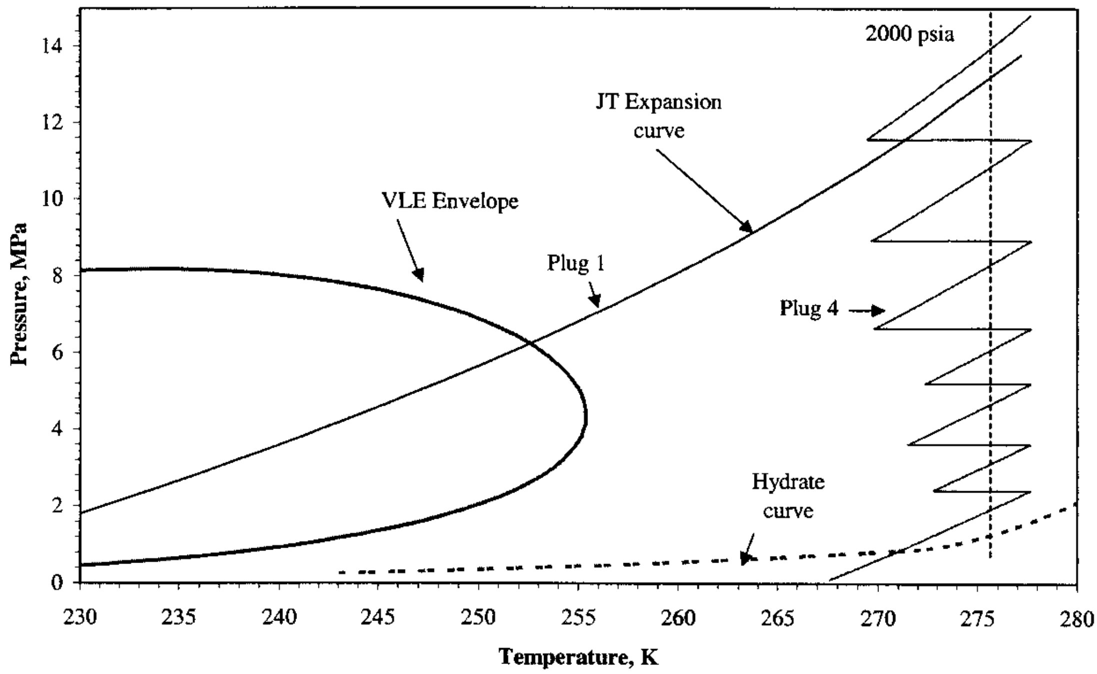

Figure 4.4: Thermodynamic Phase Diagram for Qatar Gas Mixture

Figure 4.4 shows the path followed when plug 4 was subjected to step-wise depressurization. Reducing the pressure in steps to atmospheric pressure does not result in liquefaction of the heavy components.

This study shows that when natural gas hydrates are subjected to J-T expansion, which is very common in the industry, liquefaction of higher components is possible. This scenario might pose a problem during plug remediation operations.

Results from plugs 1-4 were compared with the two-sided radial dissociation model. Table 4.3 shows the summary of comparison between data and model. The time for hydrate dissociation was obtained when gas stopped evolving, while total plug melting time was obtained when the temperature in the cell increased above ~ 273.15 K.

The dissociation temperature was obtained by averaging the temperatures in the cell. While doing so, the initial low temperatures were neglected to define the dissociation temperatures for plugs 1 – 3.

Table 4.3: Comparison of Two-sided Dissociation Model with Experiments

Plug#	Hydrate Porosity	Ambient Temperature, K	Dissociation Temperature, K	Experiment, hrs.		Model, hrs.		% Absolute Error	
				Hydrate	Total	Hydrate	Total	Hydrate	Total
1	0.45	277.15	272.15	3.32	4.7	3.52	5.5	6.0	17.0
2	0.53	277.35	272.35	3.02	4.6	3.41	4.8	12.9	4.3
3	0.42	277.45	272.35	3.8	5.1	4.17	5.77	9.7	13.1
4	0.44	277.65	272.65	4.6	6.1	5.06	5.98	10.0	1.9

From the table, the model over-predicted the times for hydrate and total plug melting time with respect to the experiments. The main reason for the over-prediction is that the hydrate dissociation temperature used in the modeling was 273.15 K. The low temperatures observed during dissociation were momentary compared to the total dissociation time; hence the dissociation temperature was obtained by averaging the measurements after the liquefaction was completed. The hydrate porosity was not varied while using the model; no fitted parameters were used in Table 4.3. The average absolute error between model and experiment for hydrate dissociation time was 9.6%, while for the total plug melting time was 9.1%.

4.2 Two-Sided Dissociation Studies with Long Cell

The goal of the following experiments (plugs 5-8) was to twofold. The first was to form and dissociate hydrate plugs in the long cell by two-sided depressurization. The second goal was to verify the radial two-sided model with longer plugs, which have a length to diameter ratio (L/D) of 36.

The procedure for forming hydrates was similar to that for the short cell. In the long cell, more ice was loaded in order to get the same porosities as for the short cell plugs. Using methane gas, sI hydrate plugs were formed. Table 4.4 shows the mass balance summary for plugs 5–8. This table shows the amount of methane used during formation, methane evolved during dissociation and the mass balance for each plug.

Table 4.4: Hydrate Formation Summary for Plugs 5 – 8

Plug #	Moles of Gas Consumed	Moles of Gas Evolved	Mass Balance % Error
5	1.05	1.11	-5.7
6	1.65	1.5	9.1
7	1.78	1.75	1.6
8	1.85	1.9	-2.7

Once the hydrate plug was formed, it was dissociated by reducing the pressure on both ends. Figure 4.5 shows the temperature profiles during the dissociation process for plug 5 as a typical case. As shown in the figure, temperature in the cell stayed close to

273.15 K, indicating that ice was formed during the rapid two-sided depressurization. The time when gas stops evolving is reported as the time taken for hydrate dissociation (t_{hyd}). The time when the last thermocouple in the cell indicates a temperature greater than 273.15 K is the reported time for plug melting (t_{ice}). This represents when the pipeline can be restarted, with both the ice and hydrate plug removed. In one of the experiments, the cell was opened when the last thermocouple showed a reading greater than 273.15 K. There was no ice or hydrate observed when the cell was opened, indicating that the pipe was safe to operate at this time. In another experiment the cell was opened when gas stopped evolving, but the temperature was still around 273.15 K, it was observed that ice existed in this case.

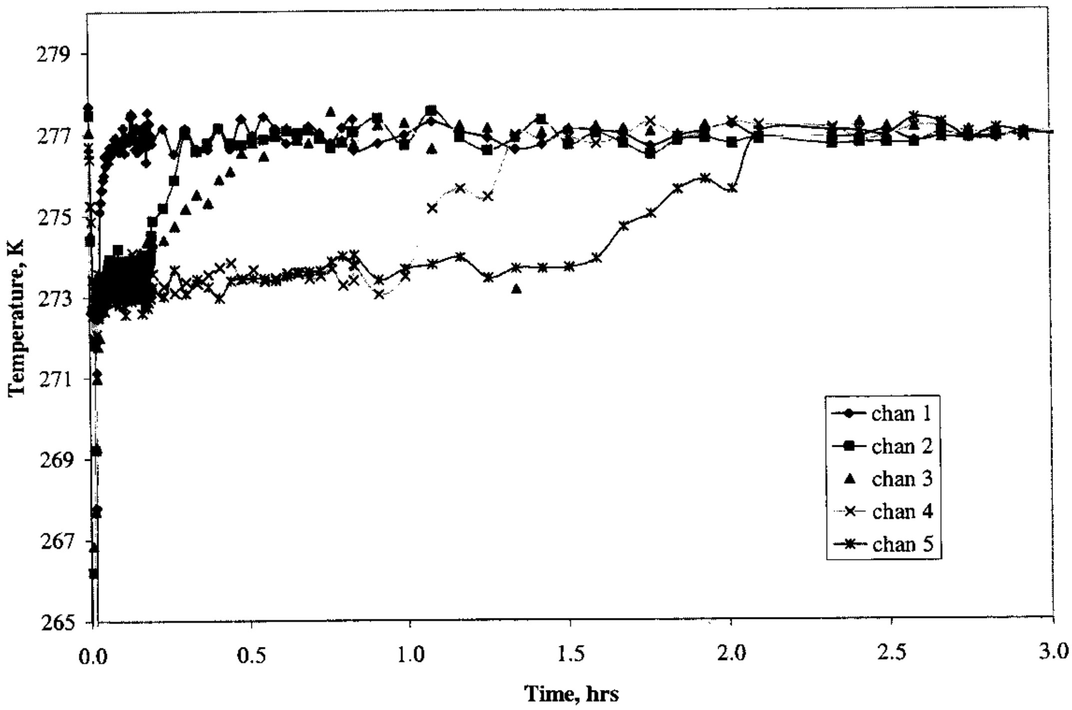

Figure 4.5: Temperature Profiles During Dissociation of Plug 8

Figure 4.6 shows the gas consumed during the formation process, experimental gas evolution and predicted gas evolution as a function of time for plug 5. The prediction was based on the radial dissociation model with a porosity of 0.69. The porosity was based on the amount of ice added while loading the cell. Clearly the model predicts the experimental results to a high accuracy. The error (experiments and modeling) in mass balances and time for hydrate and plug dissociation are represented in Figure 4.7 for four trials.

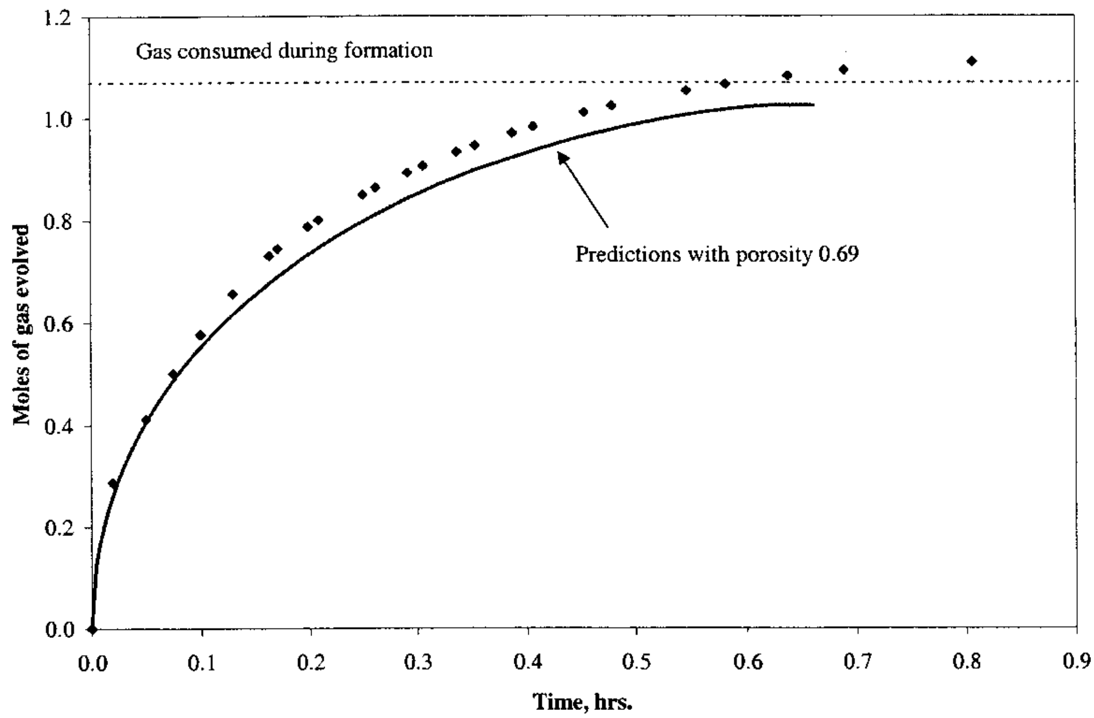

Figure 4.6: Comparison of gas evolved experimental to prediction

The results from the radial experiments indicate that with an increase in the L/D ratio, the hydrate dissociation will typically occur radially in a pipeline. The L/D ratios reported for hydrate plugs in normal pipeline ranges from 100 – 1000. The findings are very important for the industry as the length of the plug is shown to be unimportant, and length is one of the difficult parameters to obtain in the field. The time for hydrate dissociation can be predicted from the pipeline radius.

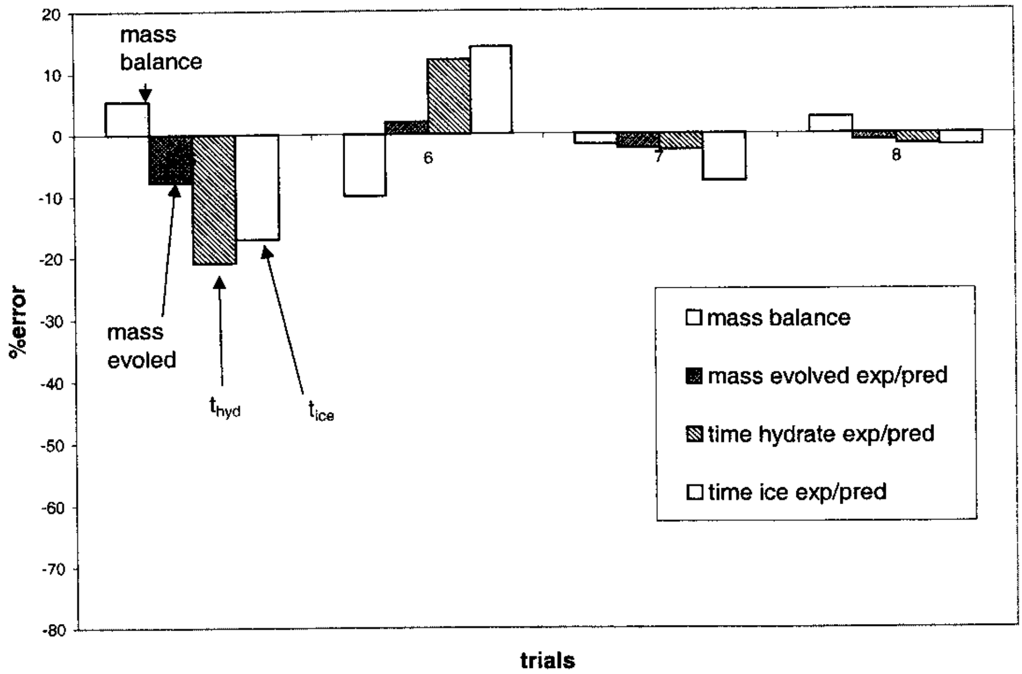

Figure 4.7: Summary for Plugs 5 – 8

Table 4.5 summarizes the comparison between model and experiments for plug 5 – 8. From the table, the model over-predicted the times for hydrate and total plug melting time with respect to the experiments. The hydrate porosity was not varied while using the model; hence no fitted parameters were used in Table 4.5. The average absolute error between model and experiment for hydrate dissociation time was 8.9% and that for total plug melting time was 10.1%.

Another important observation regarding the heterogeneity of the hydrate plug can be addressed. The temperature profiles from Figure 4.5 clearly indicates that the hydrate plug is not homogeneous. This varying porosity across the length of the plug can

Table 4.5: Comparison of Two-sided Dissociation Model with Data (Plug 5-8)

Plug#	Hydrate Porosity	Ambient Temperature, K	Dissociation Temperature, K	Experiment, hrs.		Model, hrs.		% Absolute Error	
				Hydrate	Total	Hydrate	Total	Hydrate	Total
5	0.69	277.15	272.65	0.81	1.08	0.67	0.92	17.2	14.8
6	0.54	277.05	272.75	0.87	1.15	0.99	1.34	13.7	16.5
7	0.46	277.35	272.65	1.19	1.68	1.16	1.56	2.5	7.1
8	0.45	277.15	272.55	1.15	1.54	1.13	1.51	1.7	1.9

be attributed to non-uniform packing of ice while loading the cell. The porosity that was used in the prediction was an average porosity. This implies that average porosity is sufficient to predict the time for hydrate dissociation. We may also assume that there were multiple plugs in the cell, which occurs in the actual pipeline situations; thus indicates another advantage of the model.

4.3 Forced Axial Dissociation

The question regarding the dissociation mechanism has been under debate for some time. This question, whether the dissociation of plugs in pipeline is radial (heat conduction) or axial (thermodynamic considerations), has been addressed by the following experiments.

Experiments to quantify the importance of axial dissociation were conducted by attempting to force the dissociation process to occur axially. The pipe wall temperature was set below at 272.15 K, as the hydrate dissociation temperature was around 272.15 K. Eliminating any temperature gradient across the pipe wall and bulk hydrate temperature ensured no radial dissociation.

Two plugs (9 and 10) were formed and dissociated to measure the extent of axial dissociation during two-sided depressurization. Plug 9 was depressured and gas evolution measured during dissociation. For about 5 hours, gas evolution was observed to be slow; thereafter the cell was opened for visual observations. Figure 4.8 shows the plug when the cell was opened. The end of the plug was observed to be ice, while sampling the plug across the length indicated more hydrates, than ice. This observation indicates that axial dissociation was small, as confirmed from the gas evolution rates. The protrusion in Figure 4.8 might have been caused due to the plug extension by pressure into a hole in the end cap.

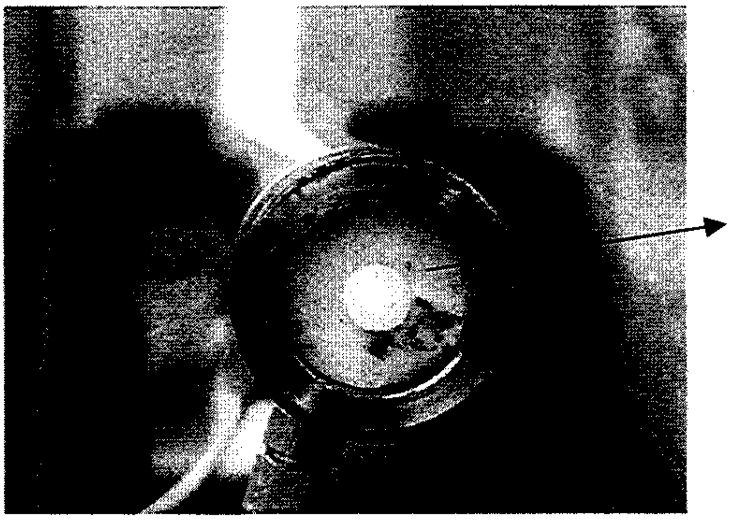

Figure 4.8: Picture of Hydrate Plug when Radial Dissociation was Suppressed

Figure 4.9 shows the temperature profiles, and gas consumed during formation and gas evolved during the dissociation process as a function of time for plug 10. The gas evolution is very slow (only 0.49 moles of gas evolved in 13 hours), indicating that the axial dissociation is not the dominating factor in dissociation of hydrate plugs.

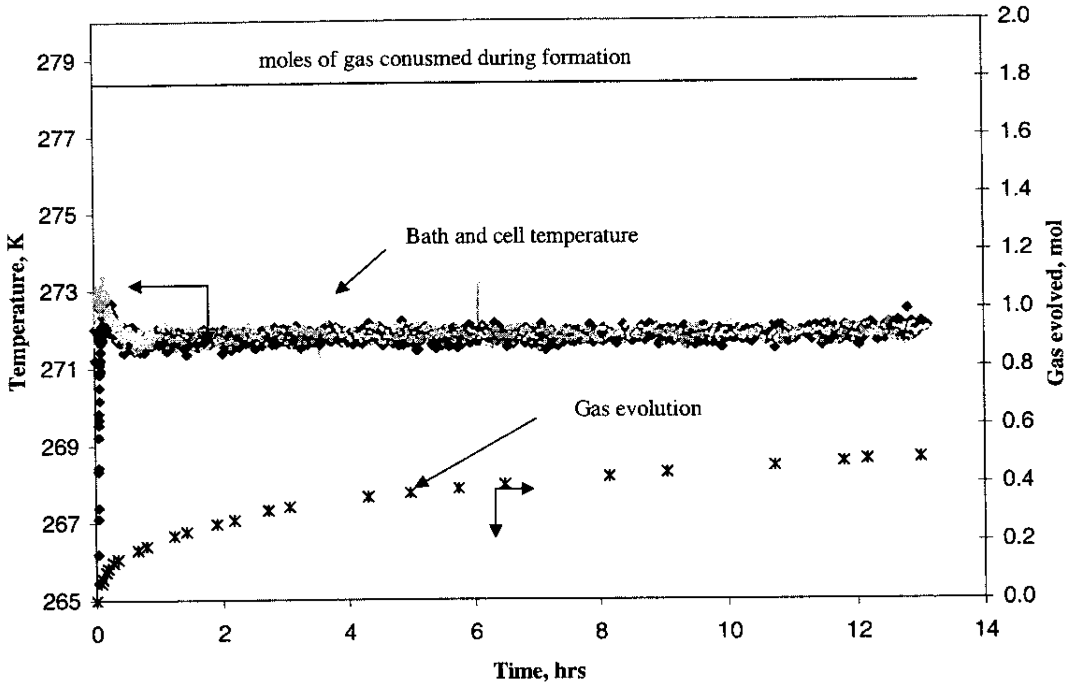

Figure 4.9: Forced Axial Dissociation Experiment for Plug 10

Figure 4.10 compares radial and axial dissociation rates. The gas evolution by axial dissociation is small (<10%) compared to radial dissociation. The results from these experiments also indicate that hydrate dissociation occurs radially in a pipeline. Hence, heat conduction from the pipe wall to the bulk of the hydrate is very important because it determines the time taken for hydrate removal in pipelines.

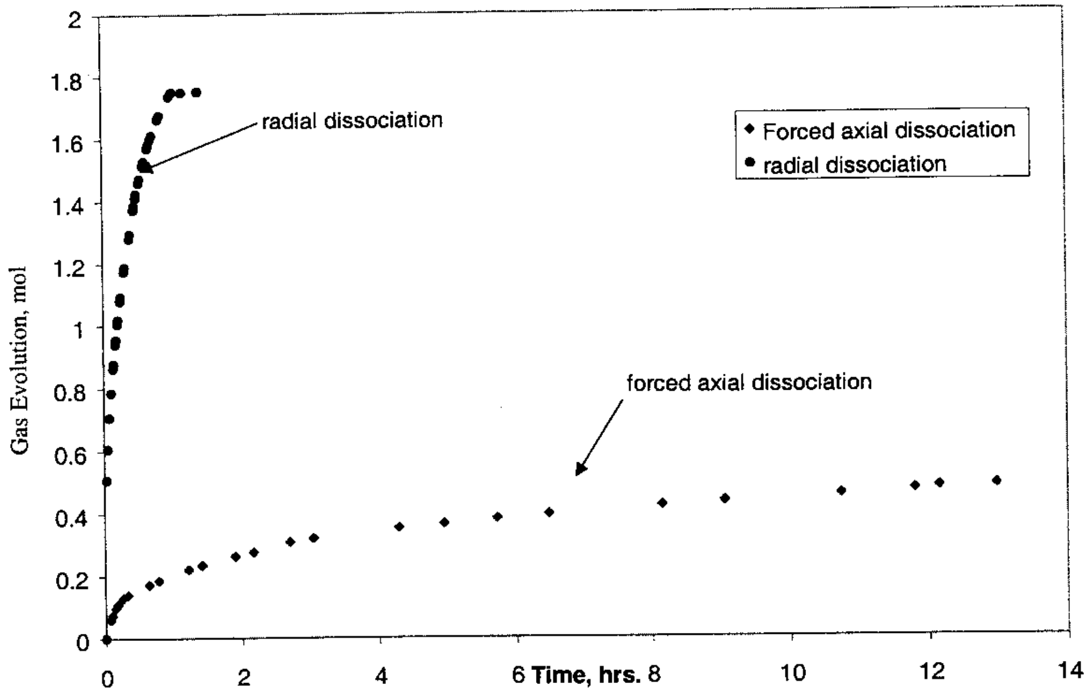

Figure 4.10: Comparison of Radial and Axial Dissociation Rates

4.4 Conclusions

Rapid depressurization of hydrate plugs formed from gas mixtures with heavy components such as butanes, pentanes and hexanes, show low hydrate temperatures. These temperatures result from first liquefaction, then vaporization of the heavy hydrocarbons during dissociation. However, these low temperatures do not exist for long due to heat transfer from the pipe wall to the center of the hydrate plug. This short time phenomenon does not prevent hydrate plug remediation.

The radial two-sided model was verified with data obtained from the long cell. The model predicts the dissociation time for hydrate and ice melting upon rapid depressurization to atmospheric pressure without any fitting parameters. This is good news to a flow assurance operator, as only plug radius is important for two-sided depressurization of porous plugs. The time for remediation by two-sided depressurization is independent of the plug length.

The data obtained by suppressing the radial dissociation to obtain the axial dissociation rate, supports the concept that dissociation of hydrate plugs occurs radially. The data also support the anomalous self-preservation effect of methane hydrates (Stern et al. 2001) below the ice point. This may be explained by the fact that heat transfer is very limited below the ice point, thus preventing the dissociation of hydrate plugs. Yakushev and Istomin (1992), Gudmundsson et al. (1996), Stern et al. (2001) and Shirota et al. (2002) studied this low dissociation below ice point as a potential solution to stranded natural gas storage and transportation.

CHAPTER 5

STRUCTURAL TRANSITIONS AND PLUG DISSOCIATION

5.1 BACKGROUND AND THERMODYNAMICS OF HYDRATE FORMATION

Hydrate plugs in field pipelines have been reported with permeabilities ranging from high to zero. Hydrate plugs with a finite permeability prohibit high flow rates but allow pressure equalization across the plug via low flow rates through the plug. With sufficient time, plugs with sufficiently high permeability can be depressurized on both sides by reducing the pressure (to near atmospheric pressure) on one side. In addition, it may be possible to depressurize (to near atmospheric pressure) both sides of non-permeable hydrate plugs that form due to off-specification gas or due to small seawater leaks that are stopped prior to significant flooding. Plug dissociation by depressurization (on both sides) of porous plugs differs from dissociation of non-porous plugs that cannot be depressurized on one side. In fact, a highly porous plug always dissociates from both sides (never one side) as shown in our experiments and model.

In this work, hydrates were formed in a laboratory pipe with an internal diameter of 0.0254 m and an L/D ratio of 36. The experiments were performed with the processed natural gas (PNG) composition shown in Table 5.1 at pipeline pressures. A PNG is one in which almost all non-combustible and non-methane components are removed. Hydrate plug dissociation measurements were made with two-sided and one-sided depressurization at two pressures (1) most often to atmospheric pressure, representing complete dissociation, and (2) for test 7, a pressure was maintained to cause the dissociation temperature to be between 273.15 K and 282.15 K.

Table 5.1: Composition of Processed Natural Gas used in the Long Cell Experiments

Component	Gas Mole Fraction
C1	0.974788
C2	0.009310
C3	0.001310
IC4	0.000161
NC4	0.000271
IC5	0.000239
NC5	0.000242
NC6	0.000286
C7+	0.000163
N2	0.009230
CO2	0.004000
Total	1.000000

In the presence of free water, the line pressure, temperature, and gas composition govern the type of hydrate structure. This is important, both for hydrate formation and dissociation in the processed natural pipeline because the hydrate structure changes from sII hydrate at low temperature and pressures (bypass and startup conditions) to sI hydrate at higher pressures of the design conditions. The amount of methanol required to inhibit hydrates depends on the hydrate structure. Similarly, hydrate plug removal time is a function of hydrate structure.

As shown in Figure 5.1, Multiflash® predicted formation of sII hydrates at the three phase (V-L_w-H) boundary below 288.15 K, 12.5 MPa, with sI hydrates above that point. In this figure, the negative sloping line, which intersects this point, divides the two-phase region (V-H) into sI (above the negative sloping line) and sII (below). Also shown in Figure 5.1 are pipelines P-T simulations from OLGA® at low pressure (startup conditions) and high pressure (design conditions) for the pipeline.

Figure 5.1 indicates that when the processed natural gas pipeline operates in the hydrate region at design operating conditions (between about 285.15K, 27.57 MPa and 268.15 K, 17.5 MPa) the hydrate formed will be structure I. However at some startup or bypass pressure and temperature conditions, (at the lower P and T profile shown in Figure 5.1, structure II hydrates may form. The figure also shows the Raman data obtained by Jager (2001) in the low and high pressure region of the phase diagram.

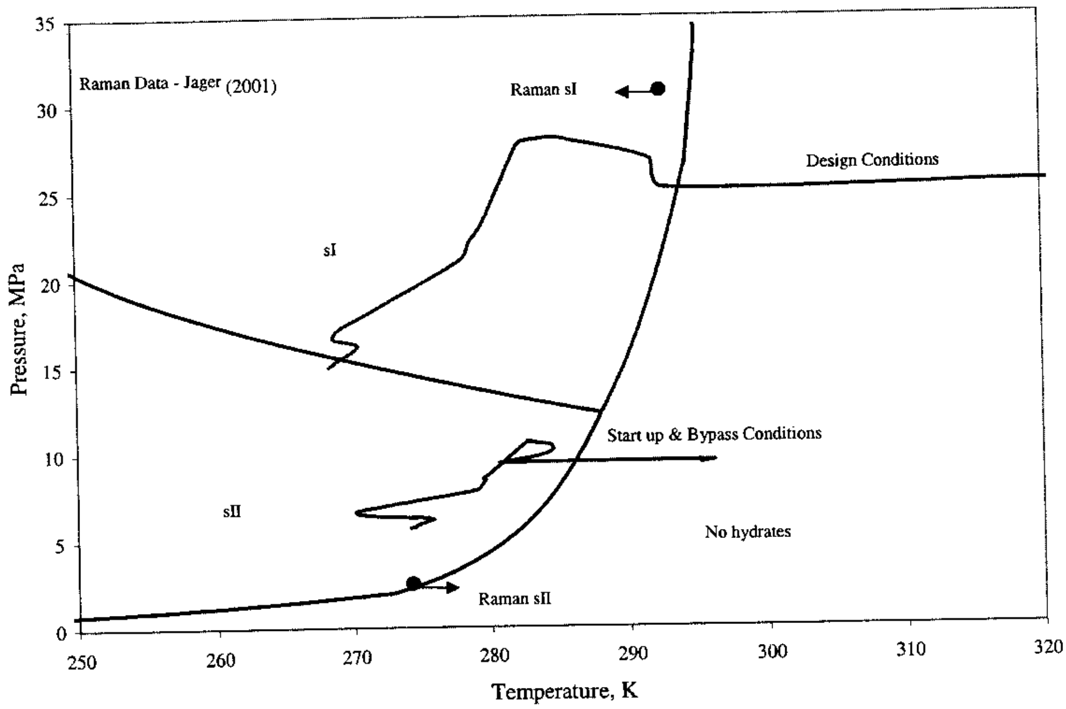

Figure 5.1. Processed Natural Gas P-T Pipeline Profiles and Hydrate Boundaries

5.2 EXPERIMENTAL RESULTS

Figure 5.2 shows the apparatus pressure and bath temperature profiles during the hydrate formation process for sII hydrates. Ninety hours were required for full conversion of ice to hydrates as seen from the asymptotic pressure profile. Following the conversion, the temperature of the pipe was increased to 282.15 K, and dissociation of the hydrate plug was begun by depressurizing both sides of the plug. As the hydrate began to dissociate, gas evolution was measured using water displacement from an inverted graduated cylinder.

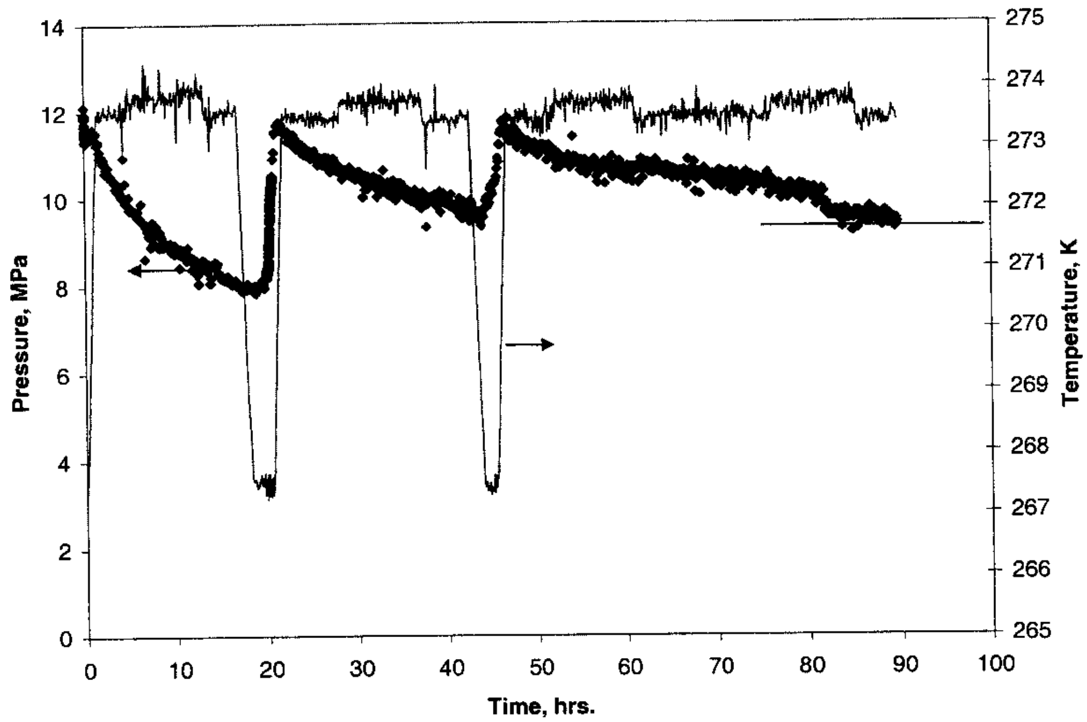

Figure 5.2: Pressure-Temperature Profiles During Hydrate Formation

Figure 5.3 shows temperature profiles (along the apparatus) during the dissociation process. As gas evolved upon hydrate dissociation, the temperatures stayed close to 273.15 K. This indicates that ice was formed during hydrate dissociation, even when the bath temperature was 282.15 K. The ice subsequently melted as the temperature rose above 273.15 K, at which time all solids associated with the plug were melted.

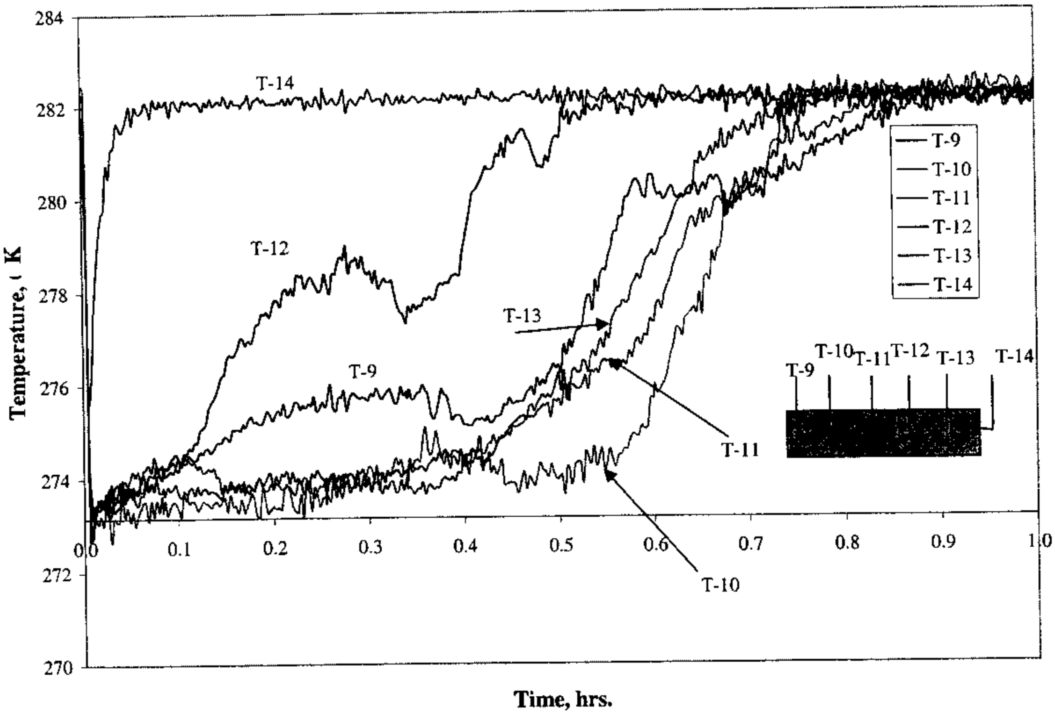

Figure 5.3: Temperature Profiles During Two-sided Dissociation

These data and those of 13 similar runs confirm that the hydrate dissociation resulted in ice in the short term, and subsequently the ice melted to water. Because water is the phase with the highest thermal conductivity, hydrates drew their heat of dissociation from liquid water in contact with the hydrate, causing a conversion of that water to ice. The heat of fusion of hydrates and ice caused the pipe temperature to remain stable around 273.15 K until all ice melted. Once all the ice melted at a thermocouple, the temperature at that thermocouple increased above 273.15 K. Of course the operator may wish to take action before all the solids are melted (e.g. to flow methanol around the plugs).

With complete depressurization, our lab experiments (and the Marathon Oil loop tests detailed in Chapter 6) showed ice formation in every case. The water-to-ice fusion supplies the heat of hydrate dissociation; when the ice subsequently melts, initially the heat of ice fusion buffers the hydrate dissociation temperature at about the ice point (272.15 to 273.15 K). This process (with ice as an intermediate phase) results in a shorter melting time in the apparatus than the process in which the apparatus is depressurized to a pressure higher than atmospheric to prevent ice formation.

Counter-intuitively, plugs 11 and 17 and the computer model (see experimental summary Table 5.2 below) all indicate that complete line depressurization with ice formation provides the most rapid plug removal. Plugs melt more rapidly with ice formation for two reasons:

1. the thermal diffusivity (thermal conductivity divided by volumetric heat capacity) of ice is an order of magnitude higher than that of hydrates
2. a higher temperature gradient (when ice is formed) provides a more rapid driving force for radial heat transfer to the plug.

To illustrate this counter-intuitive phenomenon of ice aiding plug dissociation, two experiments were conducted for two sII hydrate plugs (11 & 17): with and without formation of ice during dissociation. Figure 5.4 shows the gas evolution rate for these two kinds of experiments. The rates for hydrate dissociation are significantly different, requiring 1.28 hours for melting the plug by slowly reducing the pressure by avoiding ice formation during dissociation, while the time on rapid depressurization leading to subsequent ice formation was 0.71 hours.

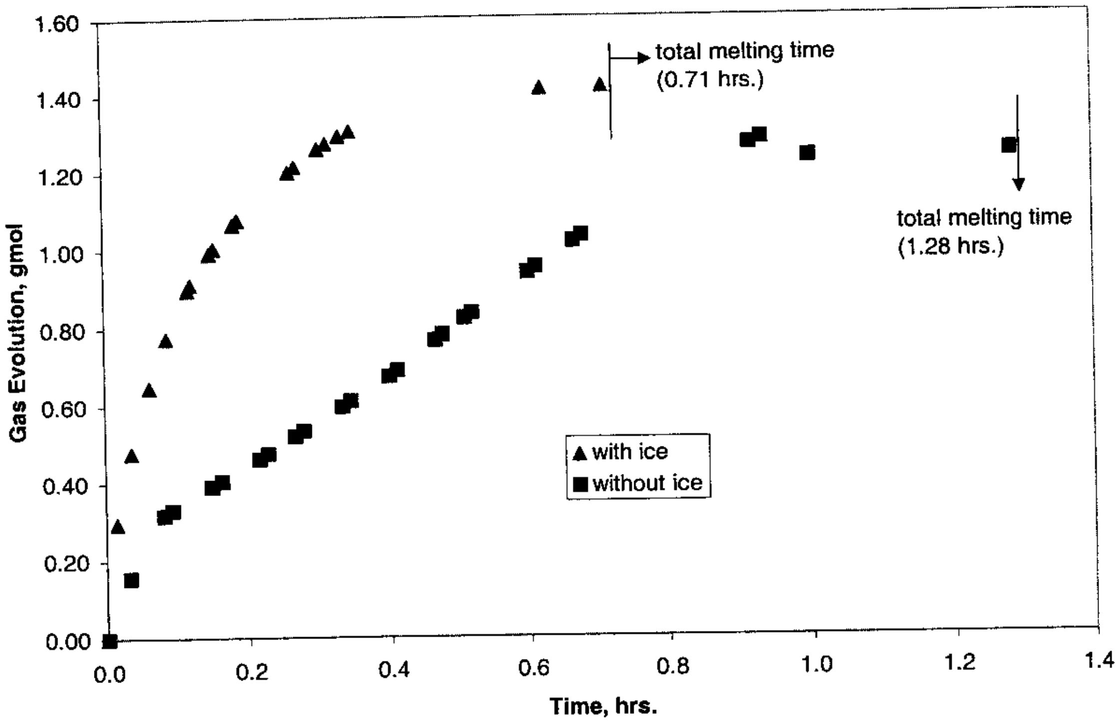

Figure 5.4: Ice Formation Reduces Time for Plug Melting

Two further tests were conducted by forming sII (plug 11) and sI (plug 16) hydrates in low and high pressure regions, subsequently dissociating the plugs by two sided depressurization. Table 5.2 summarizes the tests and lists the two different times for dissociation:

- hydrate dissociation time, represented by the time when gas evolution stopped
- total plug melting time, represented as the time when solids (both ice and hydrate) completely melted

It can be seen from Table 5.2 that total plug melting time for plug 14 was 0.75 hours, while for plug 16 was 0.93 hours indicating hydrate sI requires longer dissociation. The ambient temperature for plug 14 was 282.45 K, while plug 16 was 282.15 K. The dissociation temperature was 272.65 K in both the experiments. The driving force for dissociation for plug 14 was 282.95 K, while for plug 16 was 282.65 K. Hence with a lower driving force of 282.65 K, plug 14 might have dissociated slower. Further experiments are recommended to validate the actual difference in dissociation times. That is, there is no direct experimental confirmation of the predictions that sII requires longer dissociation time than sI.

Table 5.2: Summary of Two-sided Depressurization Experiments

Plug#	Type of hydrate	Porosity of hydrate	Time for hydrate dissociation (experiment) hrs.	Time for total plug melting (experiment) hrs.
11	SII	0.48	0.71	0.86
12	SII	0.7	0.51	0.57
13	SII	0.55	0.62	0.7
14	SII	0.51	0.61	0.75
15	SII	0.35	1.05	1.35
16	SI	0.5	0.72	0.93
17	SII	0.48	-	1.28

5.3 MODELING RESULTS

A double moving boundary radial heat conduction model was developed by Peters et al. (2000) for two-sided dissociation, and detailed in Chapter 3. This model was used to compare the results from the long cell data in Table 5.2 for structural transitions. In order to use the model, the following parameters are required as input: hydrate dissociation temperature, ambient temperature and porosity of the plug.

This section deals with dissociation time results from the two-sided model for seven plugs (11-17). The dissociation temperature was obtained experimentally by averaging the measured temperatures along the plug. The porosity of ice was known by measuring the amount of ice loaded in a known cell volume. It was assumed that the porosity of hydrate was equal to that of the original ice. The model gives the time for hydrate dissociation (end of gas evolution) and time for ice melting at T > 273.15 K (complete melting of the plug).

Figure 5.5 shows the comparison between model and data for plug 11. The model fits the data within the 12% error in the mass balance. The experimental time for hydrate dissociation was 0.71 hours, while the predicted time was 0.83 hours. The prediction was obtained for a dissociation temperature of 272.85 K, suggesting that ice formation was not avoided.

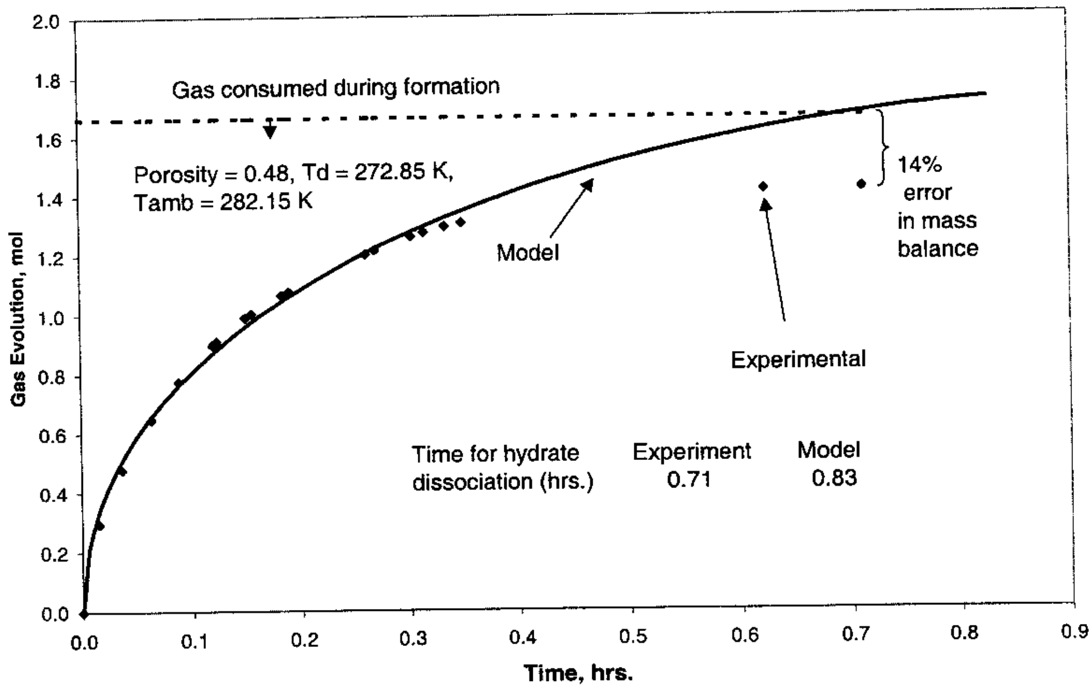

Figure 5.5: Predictions from Two-sided Radial Dissociation Model for Plug 11 (sII)

Figure 5.6 shows the predictions for plug 17 when ice formation was avoided. The experimental hydrate dissociation time was 1.28 hours, while the predicted time was 1.18 hours.

Figure 5.7 shows the results for sI hydrate plug 16. The radial model was used to predict the time for hydrate dissociation for two cases by changing sI and sII hydrate properties.

Predictions assuming sII were over predicted while sI fitted the gas evolution curve for plug 16. Both the predictions and spectra of Jager (2001) show sI as the stable structure at pressures above 12.41 MPa. Hence, the predicted time for hydrate dissociation was 0.8 hours, and experimental time for hydrate dissociation was 0.72 hours.

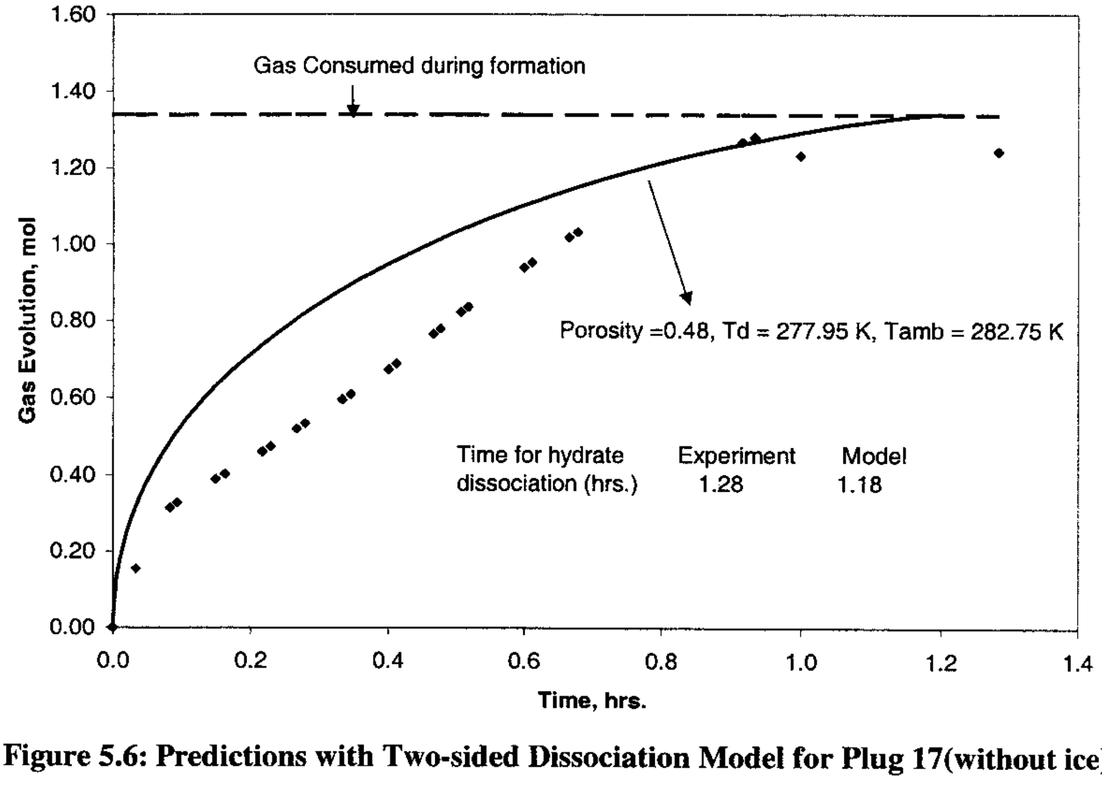

Figure 5.6: Predictions with Two-sided Dissociation Model for Plug 17(without ice)

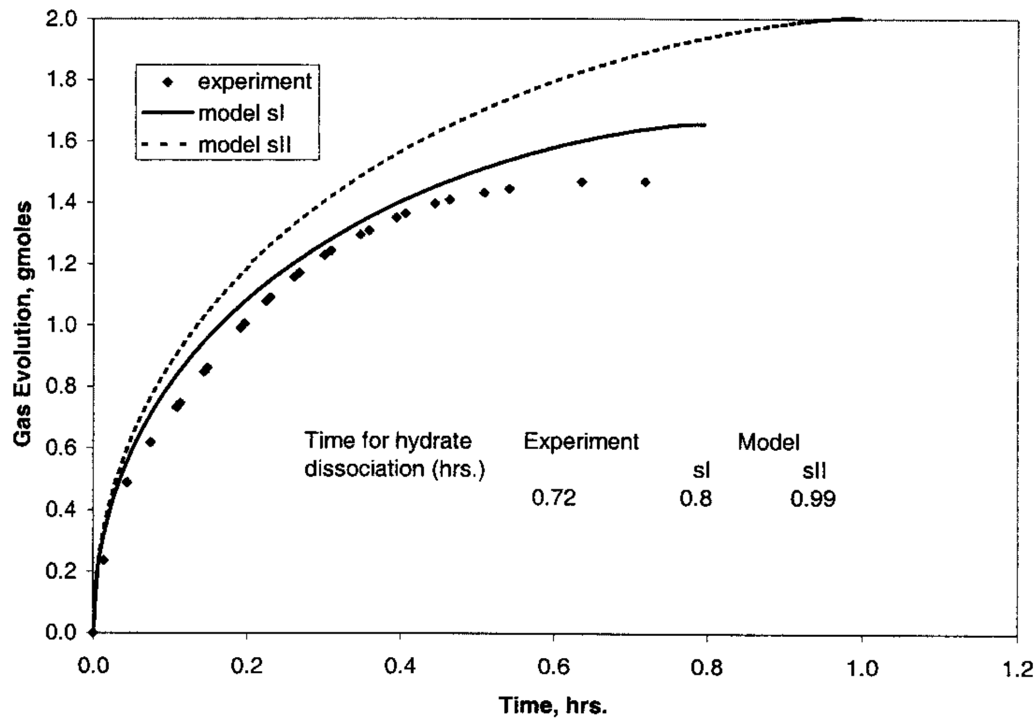

Figure 5.7: Predictions with Two-sided Dissociation Model for Plug 16 (sI)

A comparison of hydrate dissociation data and predictions is provided in Table 5.3. We purposely varied the porosities for plugs 11 through 15 with sII hydrates, all with complete depressurization, so that ice formed before complete plug melting. The low porosity of plug 15 was obtained by freezing cyclohexane, a heavy hydrocarbon that solidifies at 291.15 K, in the hydrate pores. Plug 16 contained sI hydrates and should be compared to plug 14, with similar porosity sII hydrates, but slightly different driving forces, to determine the effect of hydrate structure on dissociation time. Plug 17 is similar to plug 11, except that depressurization was done at high pressure so that ice did not form in plug 17; a comparison of plugs 11 and 17 show that complete depressurization of the pipe speeds the dissociation time of the hydrate/ice plug.

Table 5.3 Comparison of the Experiments and Predictions

Plug#	Type of hydrate	Porosity of hydrate	Time for hydrate dissociation, hrs.			Time to melt total plug, hrs.		
			experiment	model	% error	experiment	model	% error
11	SII	0.48	0.71	0.83	-16	0.86	0.91	-6
12	SII	0.7	0.51	0.47	7.8	0.57	0.51	10
13	SII	0.55	0.62	0.71	-14	0.7	0.76	-9
14	SII	0.51	0.61	0.76	-24	0.75	0.82	-9
15	SII	0.35	1.05	1.21	-15	1.35	1.21	10
16	SI	0.5	0.72	0.8	-11	0.93	0.82	11
17	SII	0.48	1.28	1.18	8	*		

* = no ice formation while dissociation, so total plug time = hydrate time

While hydrate dissociation times are of interest in Table 5.3, even more interesting are times for the total (hydrate plus ice) plug dissociation, indicated experimentally by the required time for the last pipe thermocouple to rise above 273.15 K. The experimental and calculated values of these times, together with the error are shown in the last three columns of Table 5.3. The model predicts the same time for plug melting for plugs 14 and 16. The different driving forces (described in Section 5.2), caused the prediction times to be equal. The predictions for the same driving force are described in Section 5.4.2. Both the hydrate and ice plug dissociation experiments and model predictions presented in Table 5.3 support the conclusion that the radial two-sided dissociation model acceptably predicts porous hydrate plug dissociation times in laboratory plugs.

5. 4 DISCUSSION

5.4.1 Evidence for sI – sII hydrate transition

In recent years, there have been significant advances in identifying hydrate structure by spectroscopic tools. Normally, produced natural gas and water form structure II hydrates, because structure II hydrates form more readily than structure I hydrates when significant amounts (>0.5 mole percent) of propane and/or butanes are present. While these larger components enter the large $5^{12}6^{4}$ cage of sII, propane, i-butane and n-butanes are too large to fit in structure I hydrate cages. (Note that still heavier components (pentanes^{+}) are too large to fit into any hydrate cage.)

With the processed natural gas, the total amount of propane and butanes was less than 0.18 mole percent. At higher temperatures and pressures small amounts of propane and butanes remain outside the hydrate phase and act as gas phase diluents, forming structure I hydrate at these conditions.

With the processed natural gas composition, two different structures are predicted by Multiflash® and were measured as a function of the pressure and temperature conditions of the pipeline. This transition phenomenon had not been measured before in gases with any amount of components heavier than ethane (e.g. propane, i- and n-butanes, etc.). Therefore the Multiflash® prediction prior to measurement represents a stringent test of the program's three-phase prediction ability.

Jager (2001) measured Raman spectra of such a hydrate phase transition from structure II at 274.25 K and 2.5 MPa to structure I at 292.6 K and 30.66 MPa, as shown in Figure 5.9. The spectra are for the C-H vibrations of the methane molecule in each hydrate cavity. The C-C signals were too weak to measure for ethane and higher components. Note that while the abscissa (frequency of vibration of methane) for each cavity is almost identical in the lower and upper spectra, the area ratios of the peaks are sufficient to distinguish structure in each spectra.

The lower spectra shows the frequency of methane in the structure II small cavity at the 2914 cm^{-1} peak and that of the large structure II cavity at 2904cm^{-1}. The peak areas are proportional to the occupation of the cavities by the methane molecule. Because there are twice as many small cavities as large cavities in structure II (small-to-large cavity ratio = 16:8), the peak at 2914 cm^{-1} is larger.

The upper spectra shows the occupation frequency of the structure I small cavity at the 2915 cm^{-1} peak and that of the large cavity at 2904.9 cm^{-1}. Because structure I has a small-to-large cavity ratio of 1:3, we see the 2915cm^{-1} peak has a lower area than that for the large structure I cavity (at 2904.9 cm^{-1}), in direct contrast to the peak area ratio results in the lower spectra for structure II.

These spectra are the first measured for such a natural gas hydrate structural transition with propane and higher components. The *a priori* prediction of the structural transition by Multiflash® lends confidence to that computer program in the three phase (L_W-V-H) region.

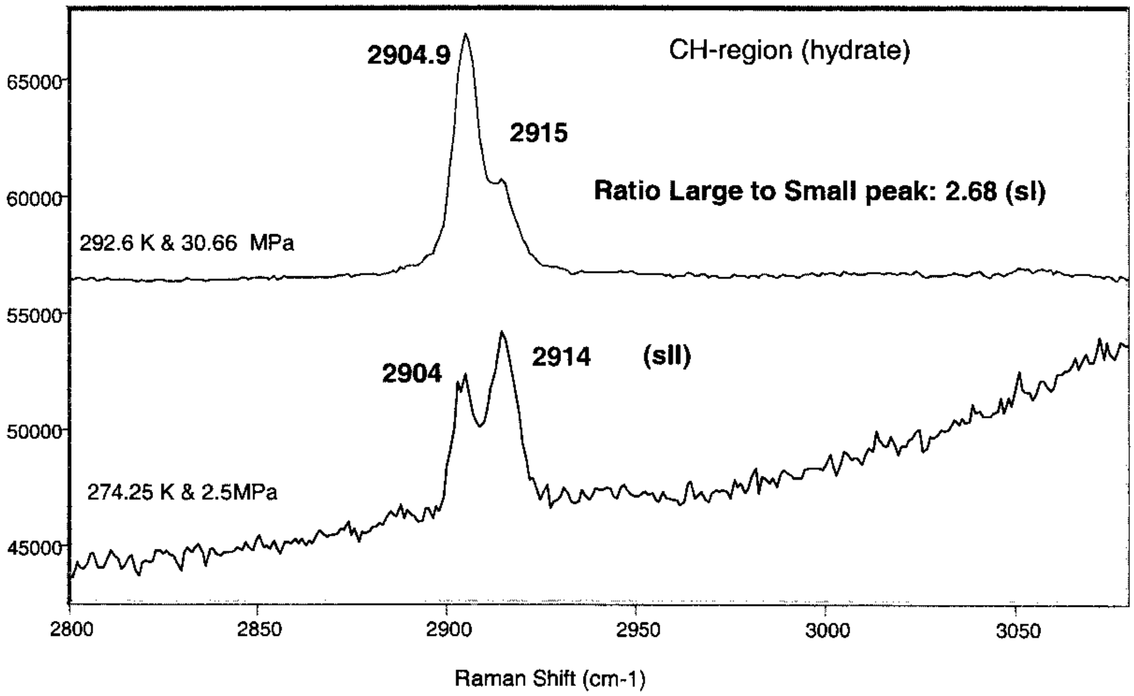

Figure 5.9: Raman Spectra for sI-sII Transitions for Processed Natural Gas (Jager, 2001)

As shown in Figure 5.10, this structural transition phenomenon is caused by a sharp decrease of the fugacity coefficients of the main sII formers (ethane, propane and the butanes) with pressure. The fugacity coefficients are in effect a measure of the driving force for hydrate formation. It appears that such high-pressure transitions may be a common (but unrecognized) occurrence for natural gases with very low concentrations of ethane, propane, n-butanes and i-butanes. The predictions were obtained from an in-house program (CSMChem) used at the Center for Hydrate Research to investigate water chemistry (Jager, 2001).

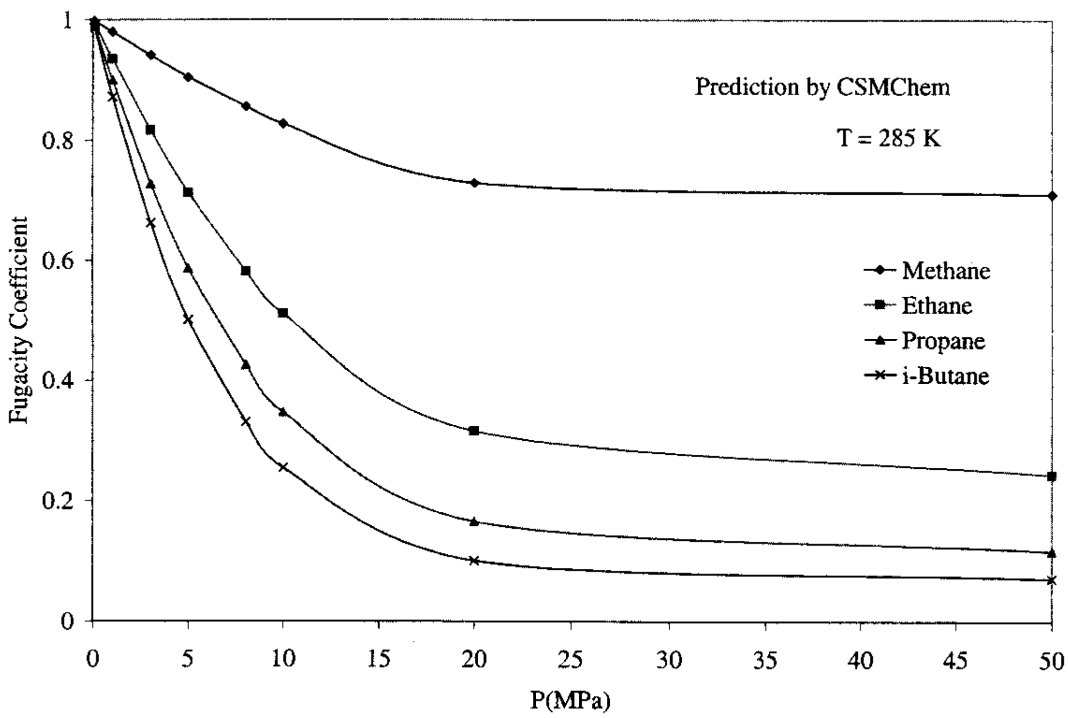

Figure 5.10: Fugacity Coefficient as a Function of Pressure (Jager, 2001)

5.4.2 The effect of sI - sII transition

The kinetics of hydrate dissociation depends on the type of hydrate structure present. Figure 5.11 shows that hydrate structure causes a difference in hydrate dissociation and plug melting time for the case when the dissociation temperature is below ice point. This figure was predicted for a 24-inch diameter pipeline using the two-sided radial dissociation model.

The time for sII hydrate dissociation is 1.3 times longer than for sI. Similarly, the time for complete plug removal for sII hydrate is 1.2 times longer than for sI. As shown in Figure 5.11, this time difference corresponds to about 4 days.

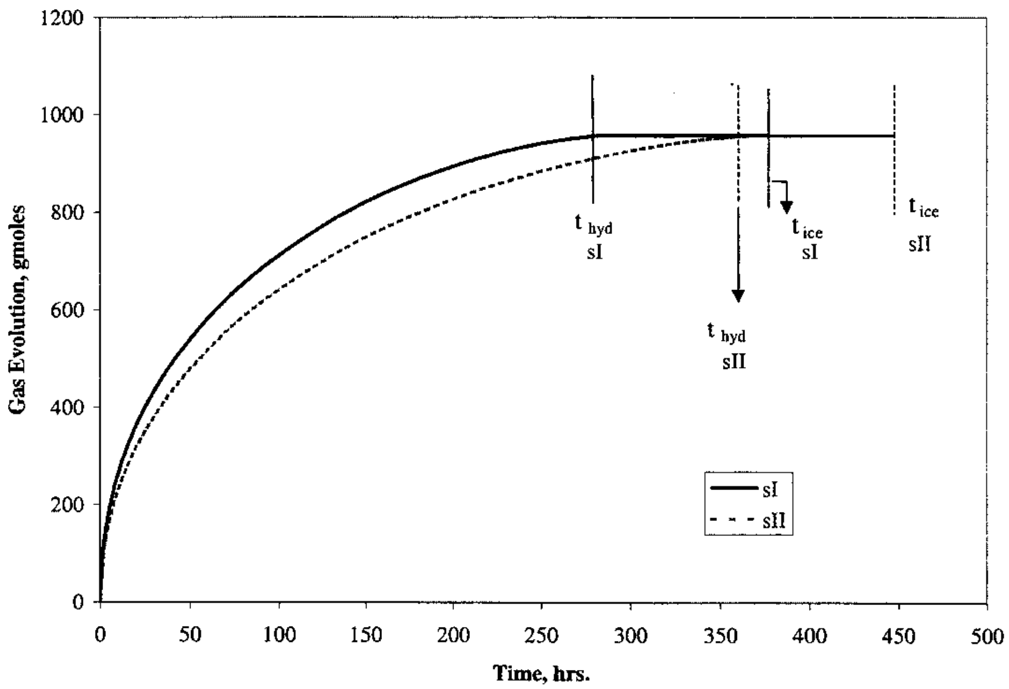

Figure 5.11: Effect of Hydrate Dissociation with Structure

5.5 Conclusions

Processed natural gas with low amounts of ethane, propane and butanes can cause structural transitions depending on the operating conditions in the pipeline. At low pressure sII hydrate is formed, while at high pressure sI hydrate. This structural transition phenomenon is caused by a sharp decrease of the fugacity coefficients of the main sII formers (ethane, propane and the butanes) with pressure.

The two-sided radial dissociation model was verified with the data obtained from the dissociation of the hydrate plugs. Good agreement was obtained for hydrate dissociation and ice melting times. It was showed that formation of ice during dissociation helped reduce the time for dissociation. It was predicted that the effect of structure on dissociation time indicated that hydrate plugs formed in the sII region required 1.3 times longer to dissociate than sI hydrate plugs. This additional time can translate into millions of dollars due to lost production.

CHAPTER 6

TWO-SIDED DEPRESSURIZATION OF FLOW LOOP PLUGS

This chapter details the hydrate plug formation and dissociation by two-sided depressurization in an industrial flow loop. During the dissociation of the flow loop plugs, the radial two-sided dissociation model was effectively used to recommend a safe operation. The comparisons of two-sided model are presented in this Chapter.

6.1 Introduction

Very few data are available for two-sided depressurization of hydrate plugs in flow loops. The goal behind these experiments was two fold. The first goal was to verify the two-sided dissociation model on flow loop. Chapter 4 and Chapter 5 showed that the radial dissociation model matched the laboratory data. Hence, the next logical step was to validate the model on a flow loop. The second goal was to exhibit a safe two-sided depressurization operation.

Two tests were conducted on the Marathon Oil Company's flow loop located in Littleton, Colorado. Both the tests were conducted by forming hydrate plugs from methane gas and water system, during the period November 8 – 16, 2000.

6.2 Description of the flow loop

Figure 6.1 shows the schematic of the flow loop. The flow loop had a 0.07366 m internal diameter and 50 meter-long flow path length. The maximum pressure rating of the flow loop was 15.17 MPa. The total flow loop volume was 58 gallons. The flow loop was mounted on a 3.65 m by 23.77 m platform, resting on a concrete base. The flow loop could be angled to simulate seafloor topography or set into rocking motion to move fluids without pump action. A Leistritz screw pump was used to circulate fluids in the loop. The maximum pump circulation rate was around 4.6 m/s.

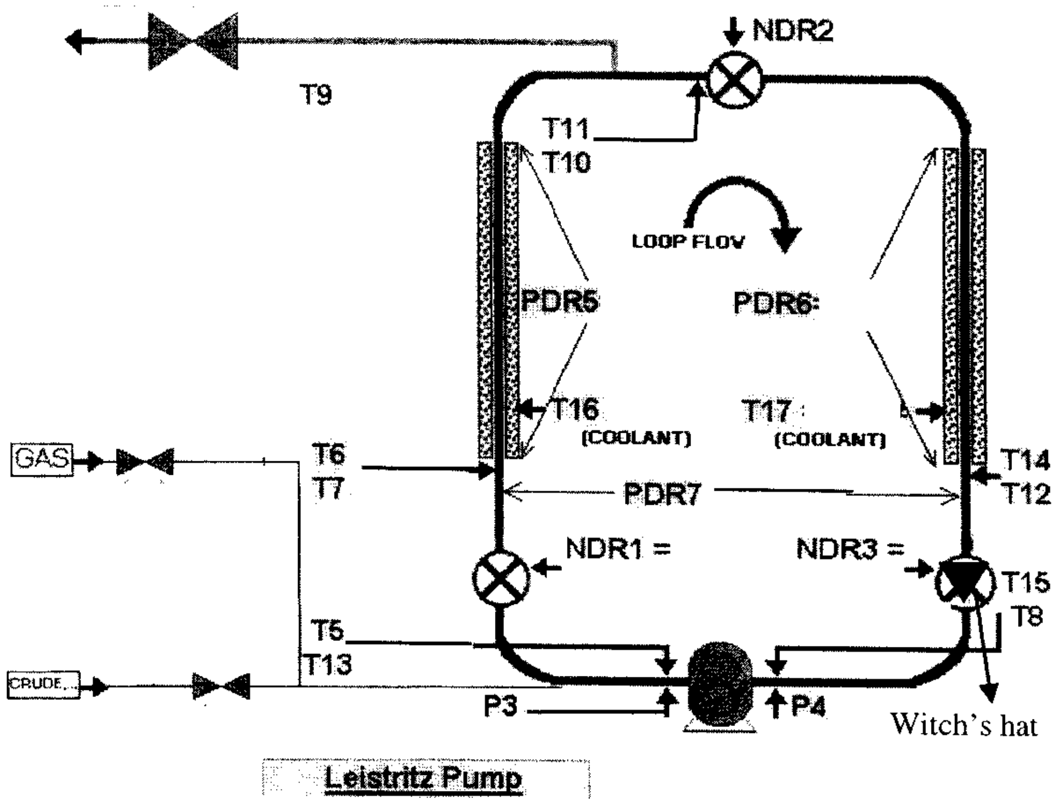

Figure 6.1: Schematic of Marathon Oil Flow Loop

Notations used in the schematic:
T# - RTD
P# - Pressure transducers
PDR# - Differential pressure transducers
NDR# - Nuclear density meters

The loop was equipped with four differential pressure transmitters, two pressure transmitters, ten RTD probes and three nuclear density gauges. The loop also had four sapphire 0.0381 m diameter view ports. The view ports were located at either end of the loop legs.

A witch's hat/screen was placed at one of flanges in the flow loop. The approximate location of the hat was at NDR3. This hat was used in order to form a hydrate plug at one end of the flow loop. Figure 6.2 shows a picture of the flow loop.

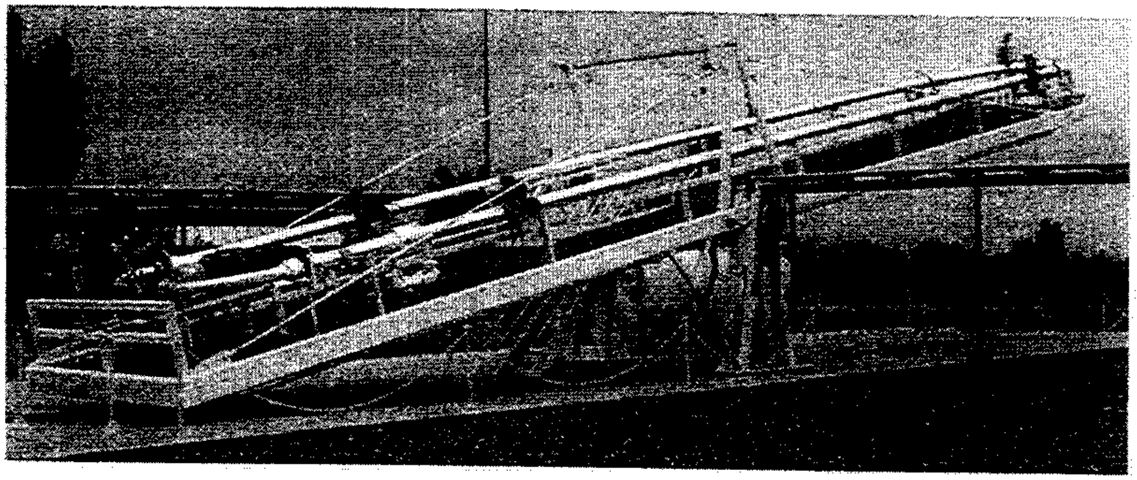

Figure 6.2: Picture of Flow Loop Used in Forming Hydrate Plugs

6.3 Hydrate Formation and Dissociation

Two tests were conducted by forming a hydrate plug in the flow loop with methane and water system. Table 6.1 shows the summary of methane, water and hydrate amount formed for Test 1. The volume of hydrate, water and gas after each charge was calculated by using Multiflash®.

Table 6.1: Summary of Hydrate Formation for Test 1

	Charge		Hydrate conditions				
	Water	Methane	Loop Temp	Loop Press	Hydrate	Gas	Water
Charge	Kg	Kg	K	MPa	vol%	vol %	vol%
1	187.7	2.5	280.37	5.46	2.9	16.1	81.0
2	187.7	4.98	280.37	5.46	10.3	16.1	73.6
3	187.7	7.48	280.37	5.46	17.7	16.1	66.2

Figure 6.3 shows the P-T curves during Test 1 as a function of time. Methane was added to the water, and temperature was decreased to allow hydrate formation. During this time, hydrate particles were observed at the sight glasses in the flow loop. After about 10 hours, most of the methane gas was used for hydrate formation. The loop was left at the equilibrium conditions of 280.37 K and 5.79 MPa. At this time, the circulation rate was decreased to form a hydrate plug.

Reducing the circulation rate, would prevent any shearing of the hydrate particles, and would increase the contact time required for particles to agglomerate and form a blockage. The circulation rate was maintained at 50 cm/s for about 15 hours. After 24 hours a hydrate plug was formed near the witch's hat. The differential pressure transmitter (PDR6) recorded 0.55 MPa across the plug.

The hydrate plug was dissociated by two-sided depressurization. Figure 6.4 shows the pressure profile during the dissociation process. Hydrate started dissociating when the pressure was below equilibrium dissociation pressure. The temperature of the flow loop was maintained at 277.6 K. The flow was resumed in the loop at 28 hours. As the loop was re-started hydrate particles were seen at the witch's hat (screen). Most of these hydrate particles disappeared within 10 minutes of re-start of the loop. The porosity of the hydrate plug was estimated by amount of hydrate formed during this time.

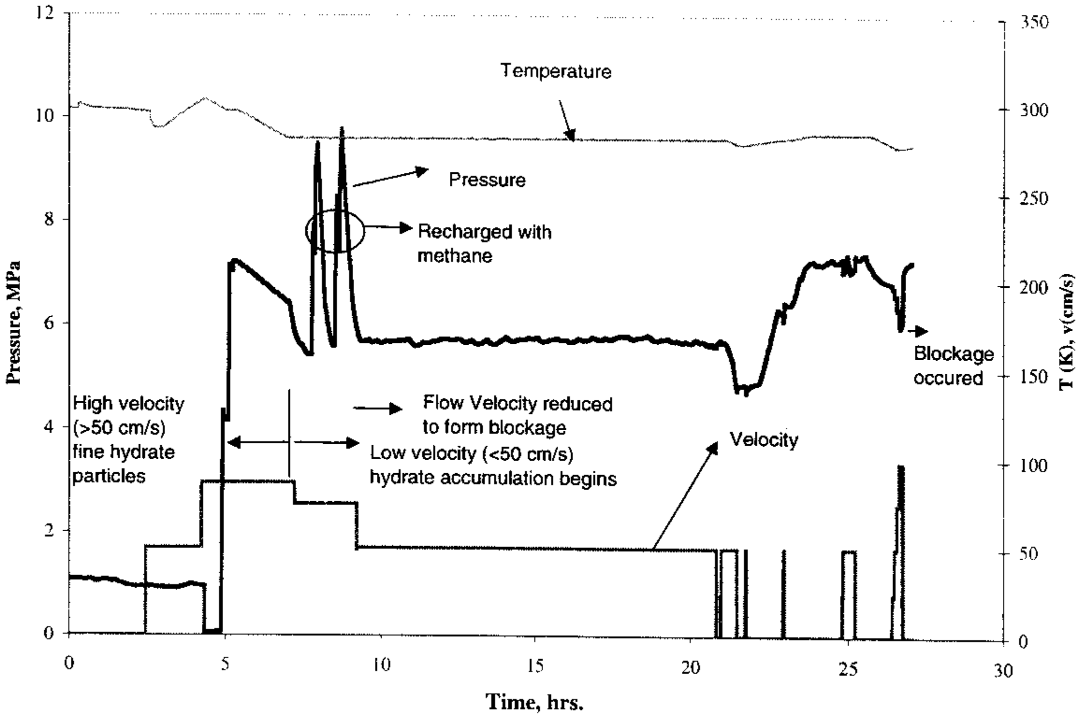

Figure 6.3: Hydrate Plug Formation for Test 1

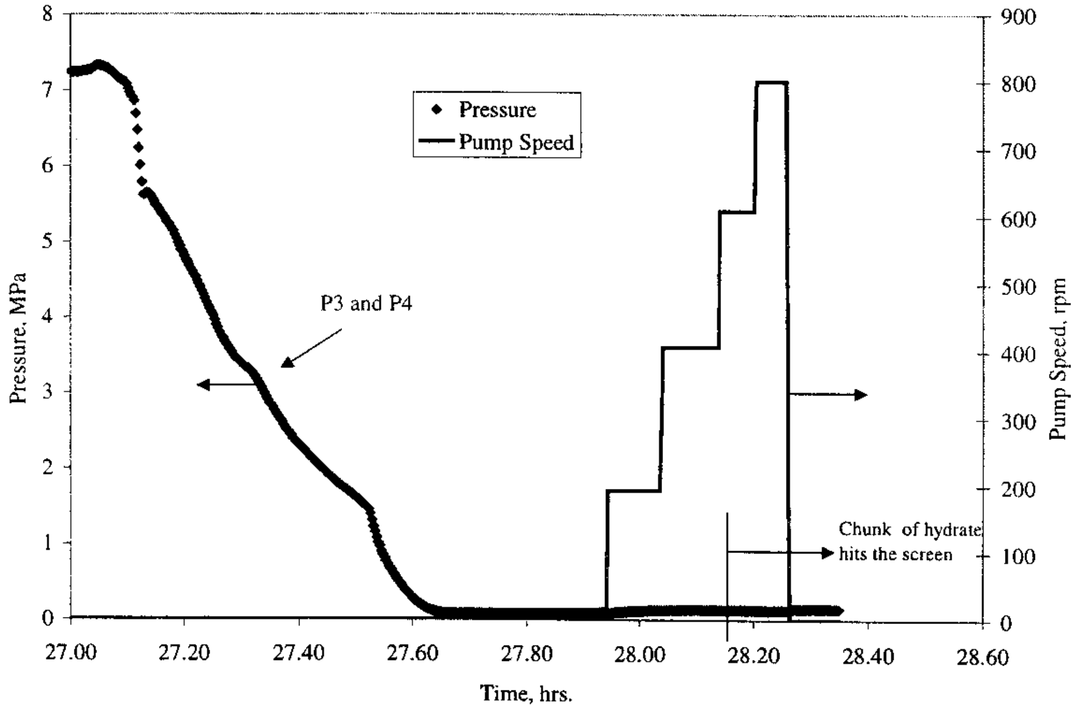

Figure 6.4: Two-sided Depressurization of Plug from Test 1

Figure 6.5 shows the P-T curves during the formation of hydrates in Test 2. The difference between Test 1 and 2 was the amount of hydrate formed. A less porous plug was formed in Test 2. After 7.5 hours the pump was clogged with hydrates, so that the loop had to be depressurized to 4.13 MPa. The loop was re-started at 8 hours and additional methane was injected into the system to form hydrates. After four additional charges of methane, a hydrate plug formed. Hydrate blockage occurred after 11 hours.

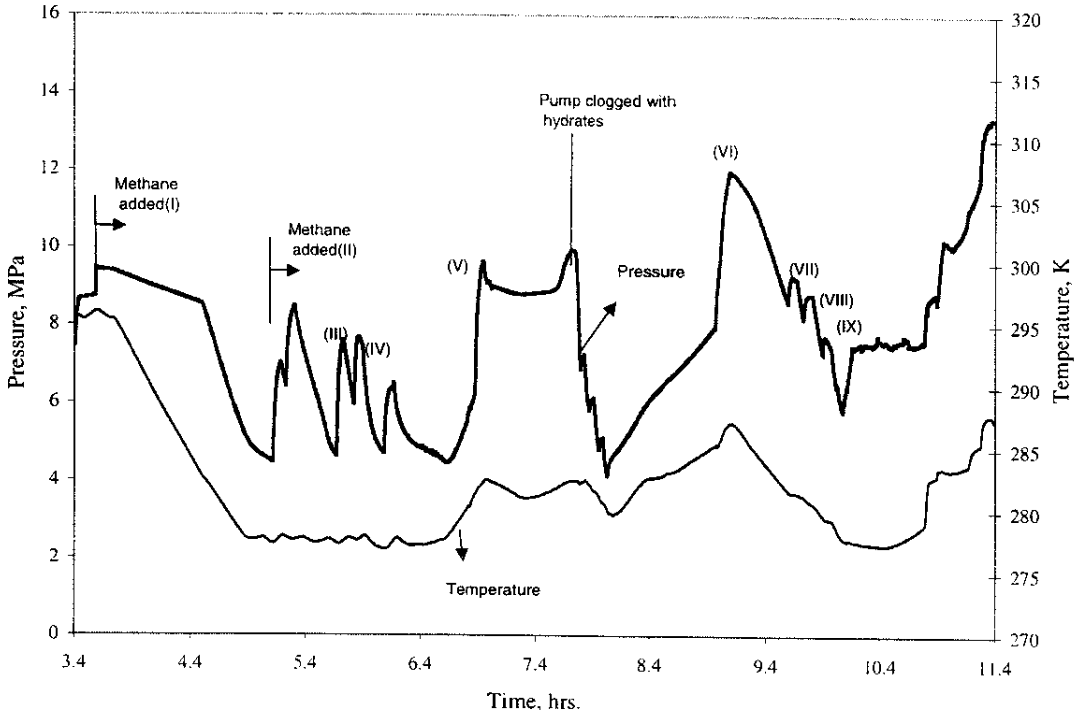

Figure 6.5: Hydrate Plug Formation for Test 2

One interesting phenomenon was observed during hydrate formation in both tests. Hydrate particles were formed, but no blockage was obtained immediately. This phenomenon is of significance in pipelines, where new technologies of hydrate prevention are being studied. For example, the slurry flow method consists of forming hydrates, but preventing them from agglomerating and forming blockages. In theory, these hydrate particles can then be transported in pipelines without forming blockages.

The hydrate plug from Test 2 was dissociated by two-sided depressurization. Figure 6.6 shows the pressure profile during the dissociation process. Hydrate started dissociating when the pressure fell below the equilibrium dissociation pressure. The temperature of the flow loop was maintained at 287.6 K. The flow resumed in the loop at 11.9 hours. Hydrate particles were seen at the witch's hat (screen). The porosity of the hydrate plug was estimated by amount of hydrate formed during this time.

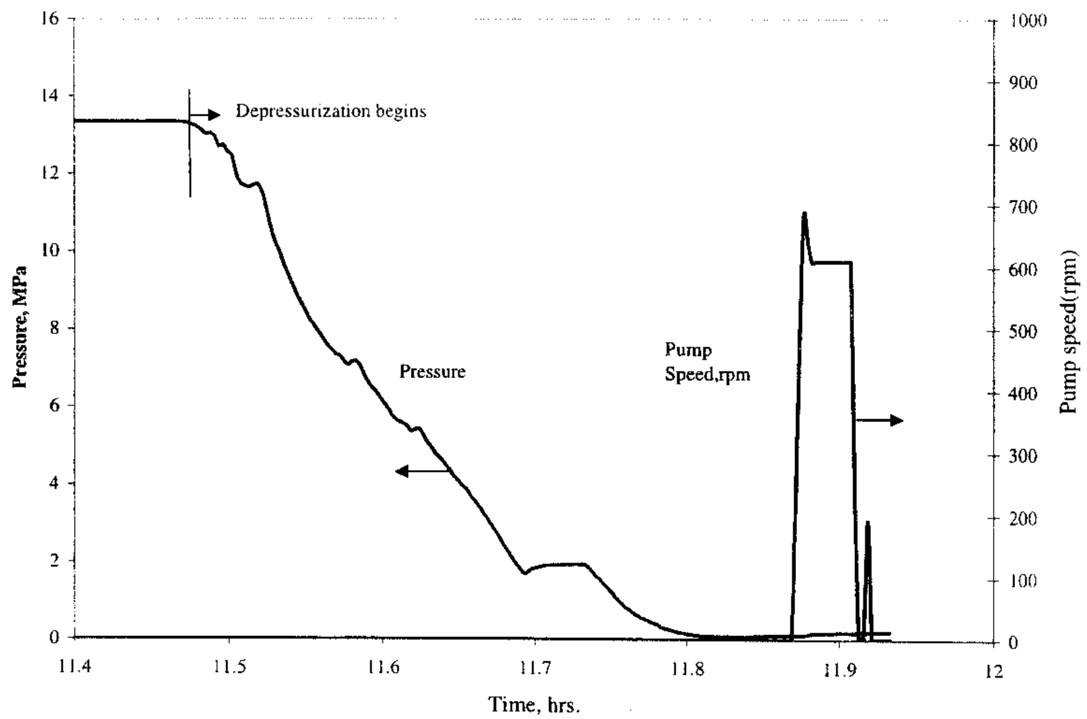

Figure 6.6: Two-sided Depressurization of Plug from Test 2

During the dissociation of Test 2, the inclination of the loop was changed. Changing the inclination led to flow of warm water at 287.6 K near the witch's hat, aiding the plug dissociation. Rapid gas evolution was observed near the witch's hat. Prior to changing the inclination of the flow loop, hydrate was observed to be dissociating radially from the pipe wall. The visual picture shows formation of ice when the pressure was dropped to atmospheric pressure. As the hydrate dissociated, ice was formed, and this ice melted to water.

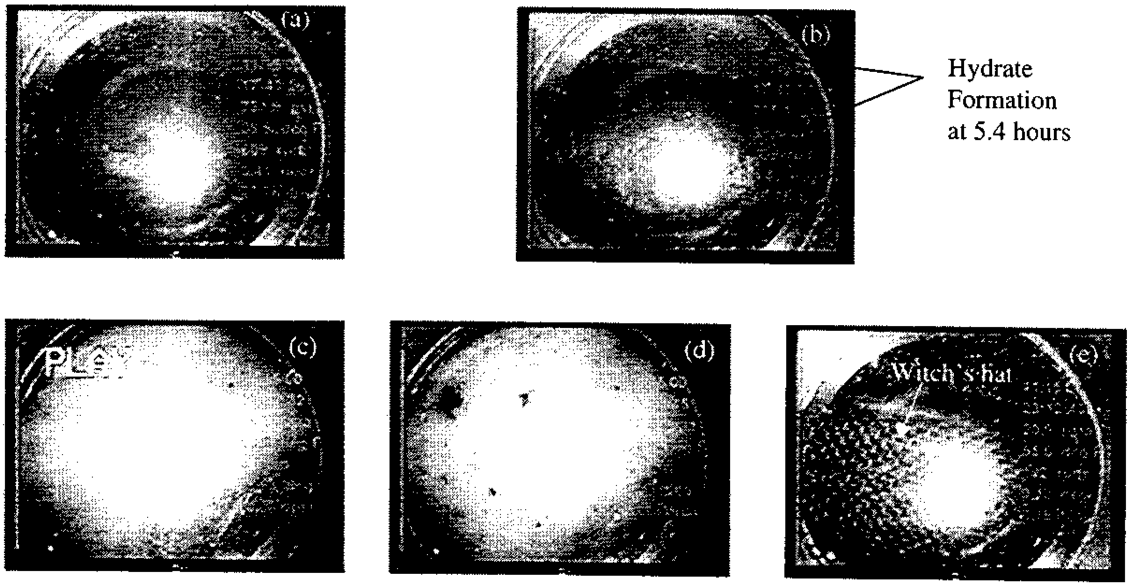

Hydrate Formation at 5.4 hours

Hydrate blockage at the witch's hat at 11 hours

Gas bubbles evolving due to hydrate dissociation at 11.7 hours

Flow resumed at 11.9 hours

Figure 6.7: Hydrate Plug Pictures from Test 2

Figure 6.7 shows the pictures of hydrate plug formation and dissociation for Test 2. Figure 6.7 (a) shows the initial loop when methane was injected with water. After 5.4 hours, hydrate particles formed and agglomerated to large particles as shown in Figure 6.7 (b). After about 11 hours, a complete blockage was formed at the witch's hat/screen as shown in Figure 6.7 (c). The pressure was reduced from both ends, and plug dissociated, with gas bubbles evolving from the hydrate plug as shown in Figure 6.7 (d). As plug dissociated, gas bubbles evolved from the outside, indicating that plug was melting radially. The ice formed at the pipe wall melted into water (no gas bubbles were seen after some time from the pipe wall and only from the interior of the plug). After about 11.9 hours, the loop was restarted (Figure 6.7 (e)) and only hydrate particles were observed, which melted in less than 5 minutes.

6.4 Comparison of Data with Two-sided Dissociation Model

The radial two-sided dissociation model was run to predict the dissociation for Tests 1 and 2. The porosities of hydrate plugs were calculated based on the amount of methane gas injected during the formation. The length of the plug was measured approximately by visual observation between the slight glasses located on the flow loop. Knowing the amount of hydrate formed and the volume of the plug, hydrate plug porosity was calculated. To run the two-sided dissociation model, the ambient temperature, dissociation temperature, plug porosity and radius of the pipeline were needed. The hydrate dissociation temperature was assumed to be at 272.15 K.

Table 6.2 shows the summary of the two-sided dissociation model and data from Tests 1 and 2. The predictions indicated that the flow loop was started at 25% annulus spacing for Test 1, and 28% annulus spacing for Test 2. The annulus spacing is defined as the percentage of the radius of the pipe that is not filled with any solids, i.e. either hydrate or ice.

Table 6.2: Two-sided Dissociation Predictions for Flow Loop Tests

Test	Plug Porosity	Ambient Temperature, K	Time when flow loop was re-started, hours	% annulus spacing predicted from two-sided model
1	0.83	277.6	0.67	25
2	0.72	287.6	0.41	28

Since the plug length could not be measured accurately, the plug porosity was varied by 10% to observe the effect on percent annulus spacing. Changing the porosity by 10% for both the runs resulted in changing the annulus spacing by 3%. Visual observations suggested that hydrate plug dissociation resulted in ice formation and the plug dissociated radially, indicating that heat transfer from the pipe wall to the hydrate is very important.

CHAPTER 7

RESULTS AND COMPARISON FOR ONE-SIDED DISSOCIATION

This chapter deals with results from one-sided depressurization experiments on the long cell for plugs 18 – 30. The goal behind these experiments was to conduct one-sided depressurization experiments in the lab, and obtain data to verify the one-sided model. The one-sided model was also verified by comparing the results from Tommeliten field trials.

7.1 One-sided depressurization for Plugs 18 - 30

The most important part of the one-sided depressurization experiments in the lab was to form impermeable plugs. The goal was to form plugs that would withstand a pressure drop below the hydrate equilibrium pressure. As described in Chapter 2, impermeable plugs were obtained by freezing the pore space of the hydrate plug with heavy hydrocarbons (tetradecane or cyclopentane) to reduce the flow channels. The selection of hydrocarbon greatly depended on the surrounding temperature. Tetradecane freezes at 279.15 K, hence was ideal for plugs dissociated at 277.15 K. While for plug #22, the surrounding temperature was 282.15 K, hence cyclopentane was used, as it's freezing point was 285.15 K.

Table 7.1 shows the summary for hydrate plugs 18 –30. The table lists the amount of ice used in each experiment to form the hydrate, and the amount of heavy hydrocarbon used to form the final hydrate plug. The porosity before and after adding the heavy hydrocarbon is also shown. The final porosity of the hydrate plug ranged from 0.15 - 0.28.

Table 7.1: Hydrate Formation Summary for Plugs 18 – 30

Plug #	Mass of ice (gm)	Porosity of plug before adding hydrocarbon	Volume of hydrocarbon added (ml)	Porosity of plug after adding hydrocarbon
18	216	0.49	100	0.28
19	239	0.44	115	0.19
20	256	0.40	80	0.23
21	246	0.42	120	0.17
22	196	0.54	150	0.22
23	210	0.51	120	0.25
24	236	0.45	65	0.31
25	223	0.47	116	0.23
26	218	0.49	145	0.18
27	253	0.41	120	0.15
28	248	0.42	98	0.21
29	237	0.44	87	0.26
30	258	0.39	83	0.22

Figure 7.1 shows the pressure response during one-sided depressurization for a typical plug 23 formed using methane gas. Upstream, downstream and differential pressures are plotted as a function of time. Initially during the pumping of heavy hydrocarbon, the line to the upstream pressure transducer was closed to prevent any flow of hydrocarbon in this line. This procedure was required to prevent any blockage due to the hydrocarbon in the upstream line, which would prevent safe one-sided depressurization. The line closure resulted in downstream pressure being greater

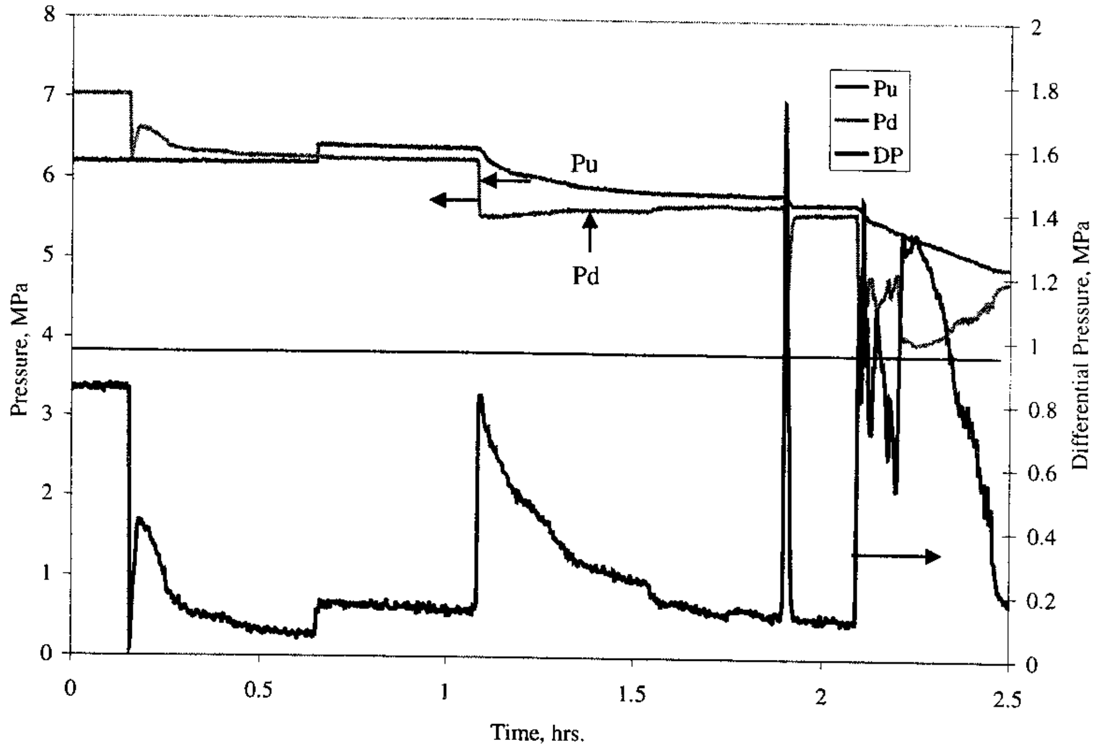

Figure 7.1: Pressure Response During One-Sided Depressurization for Plug 23

than upstream pressure at time t = 0 in Figure 7.1. The valve was opened later after 0.5 hours, when the upstream pressure increased above the downstream pressure. The pressure was slowly decreased in steps to prevent any large pressure drops across the cell. Reducing the pressure rapidly resulted in small hydrate particles clogging the tubing at the downstream end causing unwanted blockages.

As soon as the pressure downstream was reduced, large pressure differentials around 0.68 – 1.04 MPa were observed. As time progressed, the differential pressure reduced to about 0.17 MPa. The procedure of reducing the pressure was continued until the downstream pressure was below hydrate equilibrium pressure. The hydrate equilibrium pressure for sI methane hydrates at 277.15 K is 3.86 MPa.

Figure 7.2 shows the pressure response with time during one-sided depressurization for plug 23 after 2.5 hours. After about 3.5 hours, the downstream pressure was reduced below hydrate equilibrium pressure. During this time, the hydrate started dissociating and gas started evolving from the downstream end. Gas evolution from the hydrate plug was monitored using the inverted cylinder. It was rather difficult to maintain a constant downstream pressure without an automated pressure controller.

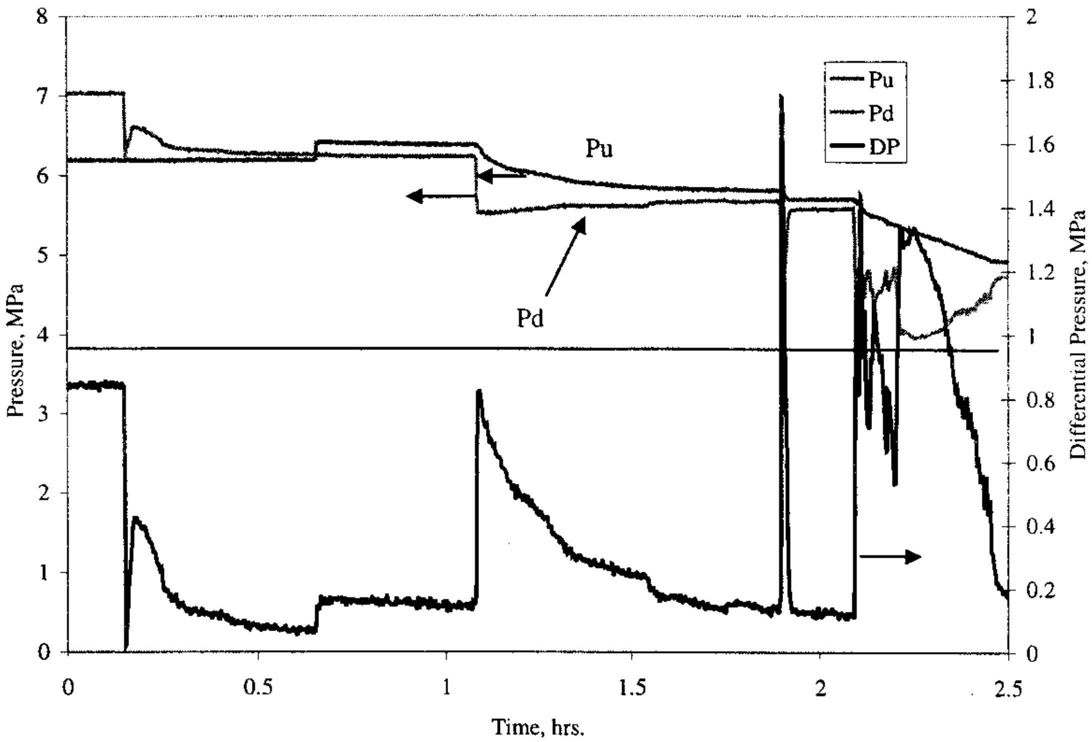

Figure 7.2: Pressure Response During One-sided Depressurization for Plug 23 after 2.5 hours

The idea behind the one-sided experiment was to obtain gas evolution data at different pressures, to verify the model presented in Chapter 3. As the hydrate dissociated radially from the pipe wall, the plug became permeable to flow. After 4.4 hours, the upstream and downstream pressures reacted to one another immediately, and the differential pressure reduced below 0.07 MPa. At this time, the plug may have been dissociating by two-sided depressurization.

Figure 7.3 shows the gas evolution data obtained from dissociating plug 23. Gas evolution from the hydrate dissociation was measured at several different pressures. Two different regimes for dissociation can be seen. One-sided depressurization occurred till about 4.3 hours, and two-sided depressurization after 4.3 hours. The downstream pressure was reduced to atmospheric pressure, and gas evolution monitored until no further gas evolved from the hydrate plug. During hydrate formation, 1.8 moles of gas was consumed, and 1.6 moles of gas evolved during dissociation. The discrepancy in mass balance is due to some lost gas (when the data was not collected) due to experimental difficulties.

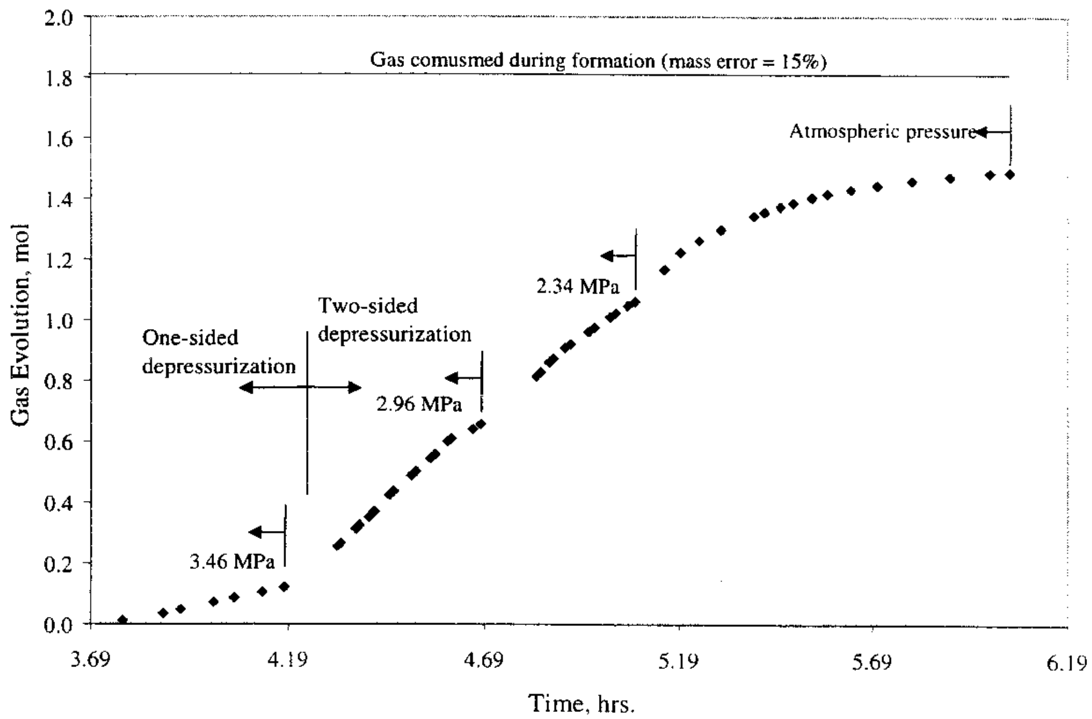

Figure 7.3: Experimental Gas Evolution by Dissociating Plug 23

Figure 7.4 shows another pressure and temperature response for plug 22. Plug 22 was formed using the processed natural gas described in Chapter 5. The plug was formed at low pressure; hence this resulted in sII hydrate. The surrounding temperature was maintained around 282.15 K. The downstream pressure was slowly reduced until the hydrate equilibrium pressure. The hydrate equilibrium pressure at 282.15 K is 5.65 MPa. The maximum and minimum differential pressure across the plug was 2.48 MPa and 0.248 MPa.

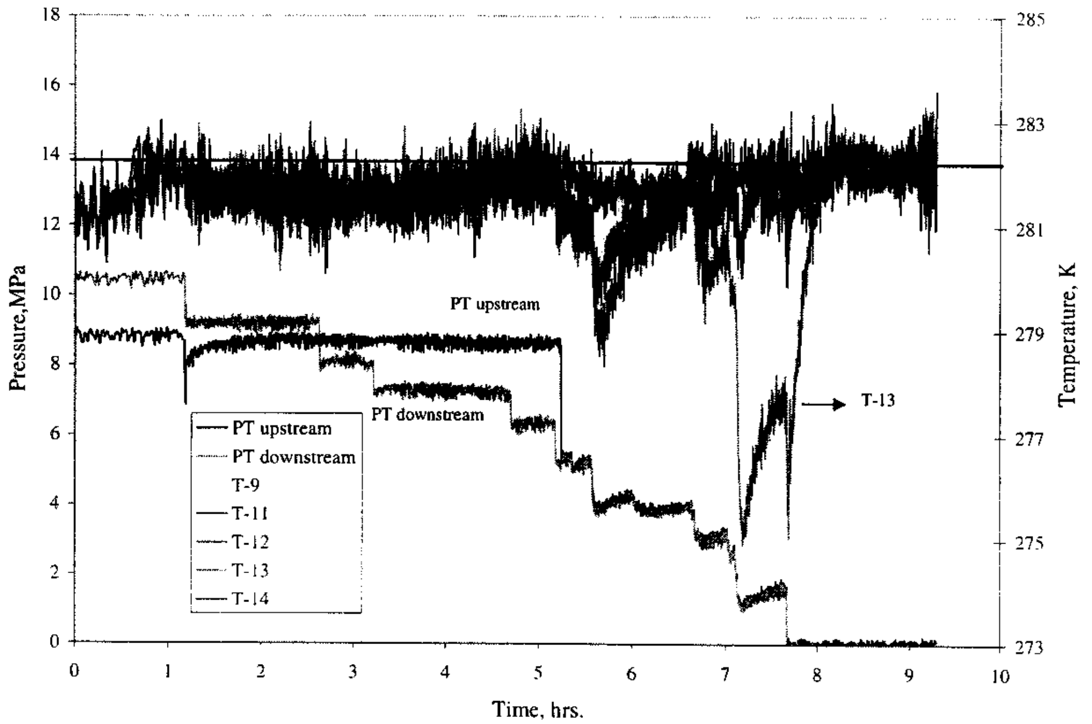

Figure 7.4: Pressure and Temperature Response for Plug 22

The downstream pressure was slowly reduced below the hydrate equilibrium pressure and gas evolution monitored as described in the previous discussion for plug 23. The same procedure for pressure reduction was followed as for plug 23. One-sided depressurization occurred until about 5.5 hours, and two-sided depressurization after 5.5 hours. After 5.5 hours, the pressure differential was recorded below 0.07 MPa.

Figure 7.5 shows the gas evolution data for plug 22 as a function of time. Gas evolution from the hydrate was measured at several different pressures. The downstream pressure was reduced to atmospheric pressure, and gas evolution monitored until no further gas evolved from the hydrate plug. During hydrate formation, 1.4 moles of gas was consumed, and 1.32 moles of gas evolved during dissociation.

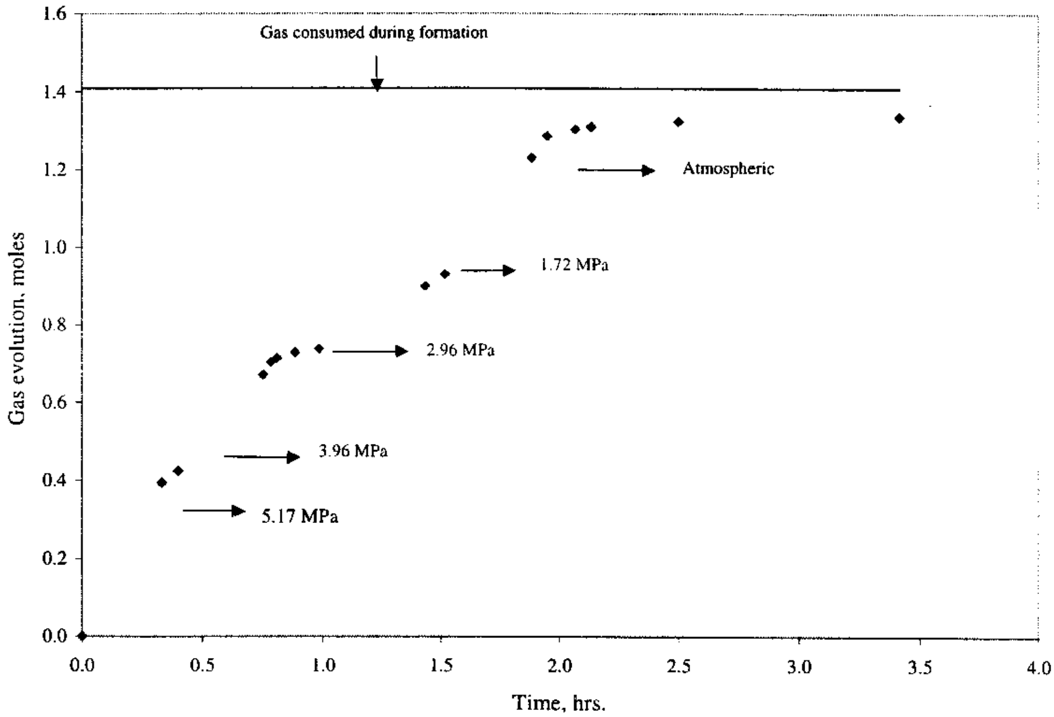

Figure 7.5: Gas Evolution During Depressurization for Plug 22

Table 7.2 shows the summary of dissociation for plugs 18 – 30. The table lists the amount of gas consumed, evolved during dissociation and error in mass balance for each plug. In most cases the gas evolved was less than the amount consumed during formation.

As stated earlier, the mismatch could be the result of experimental difficulties when measuring the gas evolution during the dissociation process.

Table 7.2: Summary of Hydrate Formation and Dissociation for Plugs 18 – 30

Plug #	Gas consumed during formation, mol	Gas evolved during dissociation, mol	Percentage Absolute error
18	1.9	1.96	3.15
19	2.1	1.98	5.71
20	2.2	2.15	2.27
21	2.18	2.33	6.88
22	1.4	1.32	5.71
23	1.8	1.6	11.11
24	2.09	1.91	8.61
25	1.97	2.16	9.64
26	1.93	1.77	8.29
27	2.24	2.08	7.14
28	2.2	2.1	4.54
29	2.1	1.87	10.95
30	2.28	1.79	21.49

7.2 Comparison of Plug Data with One-Sided Model

The true test of any model is how it fits the experimental data. The one-sided model was verified with the results from plugs 18 – 30. To run the model the input to the model is: 1. upstream and downstream pressure, 2. upstream and downstream temperature, 3. plug porosity, 4. plug permeability, 5. pipe radius, 6. plug length, and 7. hydrate structure. However, default values for many of these are already in the program. During the depressurization, upstream and downstream pressure, upstream temperature, radius and length of the plug were known. The downstream temperature was obtained by averaging the thermocouple readings from the experimental data. Hydrate porosity was obtained from the formation experiment. The only variable that was not known was the permeability of the hydrate plug.

The permeability of the hydrate plug was varied between 1 mD – 0.01 mD when verifying the model. Permeability did not change the results from the model for the long cell experiments. The pressure drops across the plug for the long cell experiments were small, typically in the range of 0.17 – 0.28 MPa. Hence, the effect of permeability was not noticed as shown in Figure 7.6. The figure shows the predictions for a case when the pressure drop is 0.2 MPa when the permeability of the plug is 1 mD and 0.01 mD. The temperature profiles are same for both cases, hence the same driving force for plug dissociation. Later, in Section 7.3, the effect of permeability will be shown on field plugs when the pressure drops are large.

Figure 7.7 shows the dissociation curve for plug 22 dissociation experiments. This figure shows a graph of total moles evolved versus time. Since, the pressure is changed with time, the one-sided model was run until 5.5 hours when the pressure differential was 0.25 MPa, and two-sided radial model after 5.5 hours. When running the two-sided model, the temperature downstream was changed in accordance with the experimental data. The model was able to track the dissociation boundary (converted to gas evolution) as a function of time. The prediction curve shows that the model and the experiment match reasonably well. The gas evolution from the model is under-predicted by 9.1% with respect to the data.

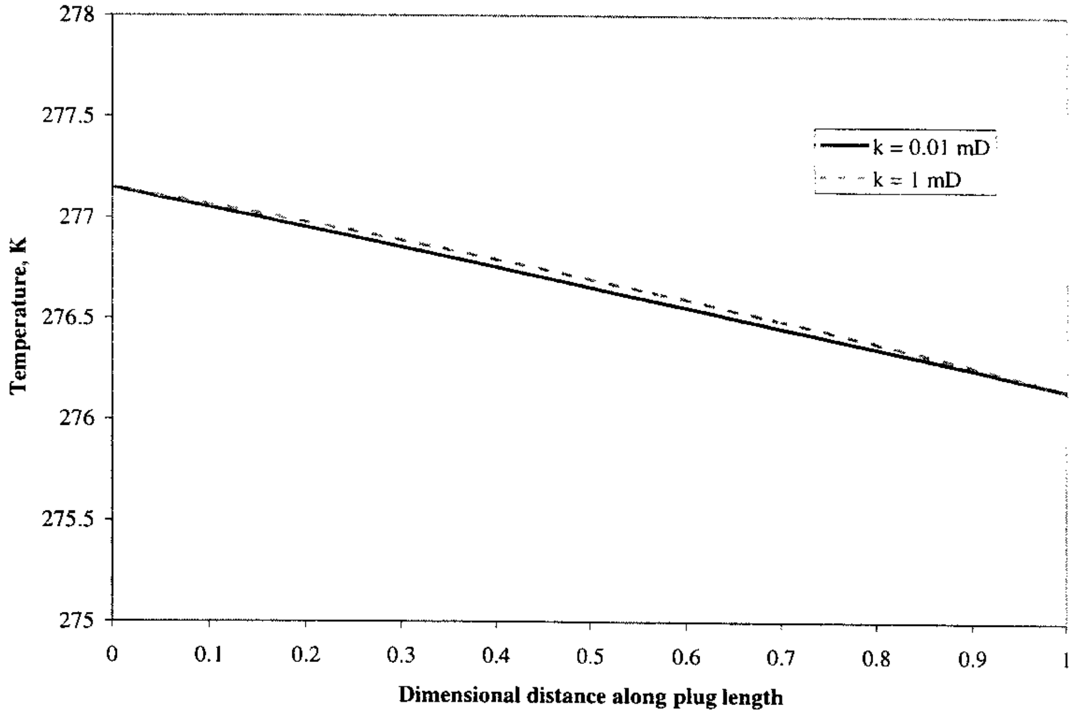

Figure 7.6: Permeability Effect on Temperature Distribution for Low Pressure Drops

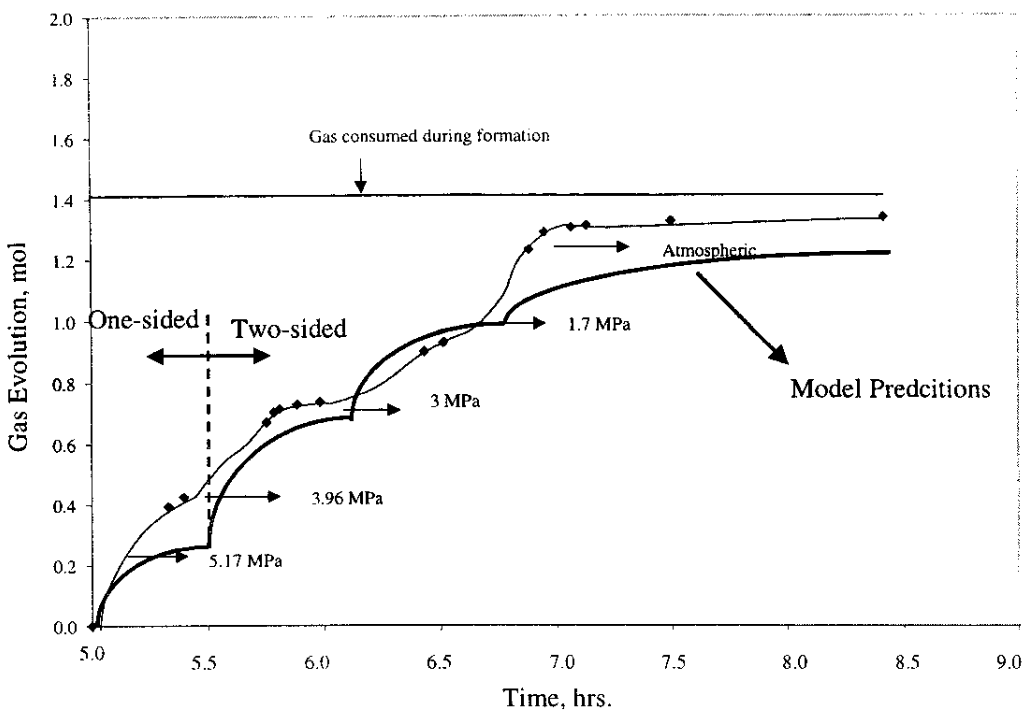

Figure 7.7: Comparison of Gas Evolved between Experiment and Model for Plug 22

Figure 7.8 shows a similar dissociation curve for plug 23 dissociation experiment. As described earlier, the pressure is changed as a function of time, and this information is input to the model. The one-sided model was run for 0.6 hours when the pressure differential was 0.17 MPa, and two-sided radial model after 0.6 hours. Again, the model matches the data well. Contrary to the prediction for plug 22, the model over predicts the gas evolution data by 2.5%.

Table 7.3 shows the results of the dissociation experiments along with the model predictions. The percent error between the model and the experiments, for the gas evolution varied for each plug. While running the model the thermal conductivity of the plug was based on the amount of hydrate and heavy hydrocarbon added to form the plug. The time for hydrate dissociation and ice melting are shown in the Table. The time for hydrate dissociation was obtained by the end of gas evolution, and the time for ice melting was obtained, when the last thermocouple measured a temperature greater than 273.15 K. Since, the pressure downstream is changed with time, the model was run at each time interval, to obtain the amount of gas evolved. The input to the model was changed in accordance with the pressure downstream. On an average the model matches the gas evolution data within an absolute error of 9.10%.

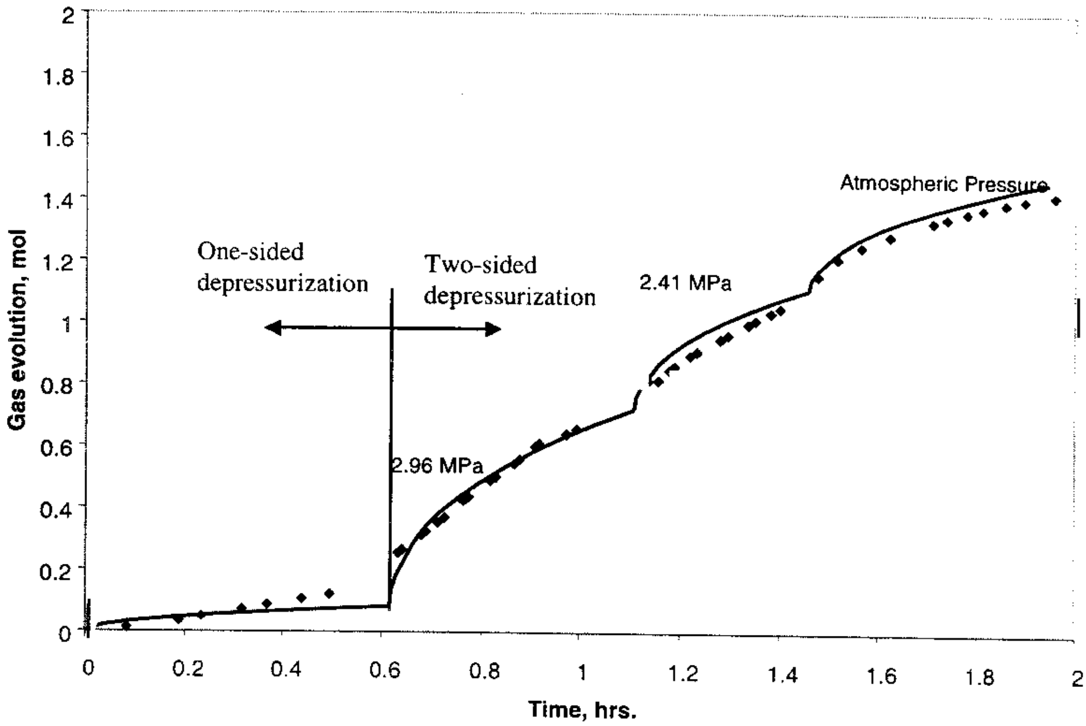

Figure 7.8: Comparison of Gas Evolved between Experiment and Model for Plug 23

During the initial part of depressurization, ice formation was not observed due to the set downstream pressure. For methane hydrates, as the downstream pressure is decreased below 1.37 MPa, ice forms during dissociation. As described in Chapter 4, ice formation helps in reducing the dissociation time due to two reasons: 1. ice has an order of magnitude higher thermal diffusivity relative to water, and 2. lower ice temperatures provide higher temperature difference for heat transfer between the pipe wall and the hydrate plug.

Table 7.3: Data Comparison with Model for Plugs 18 -30

Plug #	Porosity of plug before adding hydrocarbon	Porosity of plug after adding hydrocarbon	Time for dissociation, hrs.		Gas evolved during dissociation moles		
			Hydrate	Ice	Experiment	Model	% error
18	0.49	0.28	2.13	2.21	1.96	1.82	7.14
19	0.44	0.19	2.83	2.98	1.98	1.76	11.11
20	0.40	0.23	2.36	2.49	2.15	1.95	9.3
21	0.42	0.17	1.62	1.81	2.33	2.13	8.58
22	0.54	0.22	3.5	3.56	1.32	1.2	9.09
23	0.51	0.25	1.93	2.08	1.6	1.64	2.5
24	0.45	0.31	2.61	2.76	1.91	1.66	13.1
25	0.47	0.23	2.46	2.63	2.16	2.32	7.4
26	0.49	0.18	1.85	2.03	1.77	1.93	9.1
27	0.41	0.15	3.91	4.26	2.08	1.87	10.1
28	0.42	0.21	2.73	2.92	2.1	1.83	12.85
29	0.44	0.26	2.3	2.47	1.87	1.62	13.37
30	0.39	0.22	3.81	4.12	1.79	1.7	5.03

7.3 Comparison of Dissociation Model with Field Trials

The number of documented cases of hydrate plugs that have been dissociated by pressure reduction from one-sided depressurization is very limited. Statoil formed 17 hydrate plugs and dissociated them by pressure reduction in a 6 inch, 7 mile gas condensate pipeline. Only two plugs were dissociated by one-sided depressurization. These tests were conducted on the Tommeliten field in the North Sea in 1994. Berge et al. (1996) report the data from the two hydrate plugs that were dissociated by one-sided depressurization.

The first plug was located 2.5 miles from the platform. The relative volumes upstream and downstream of the plug were determined from measured changes in upstream and downstream pressure due to gas flow through the plug. Removal of the plug by pressure reduction from the downstream side of the plug was started. The upstream pressure was around 1300 psia (8.96 MPa) when the depressurization begun. The downstream pressure was slowly reduced below the hydrate equilibrium pressure. The hydrate equilibrium pressure was calculated to be around 200 psia (1.37 MPa). The final downstream pressure was maintained at 100 psia (0.68 MPa). Hydrates dissociated and the flow was re-started by injecting methanol after 60 hours of dissociation time.

The permeability and porosity of the hydrate plug was unknown in the Tommeliten field. Figure 7.9 shows the prediction from the one-sided model. This figure shows the effect of porosity on time when flow was re-started. The advantage of the one-sided model is that it gives the percentage annulus spacing as a function of time, defined as the percentage of the pipeline radius that is free of hydrates or ice. The model predicts that for a hydrate plug with porosity of 0.3, 5.5% annulus space is available for flow of methanol at 60 hours. If the hydrate porosity is 0.5, 6.5 % annulus space is available for flow of methanol at 60 hours.

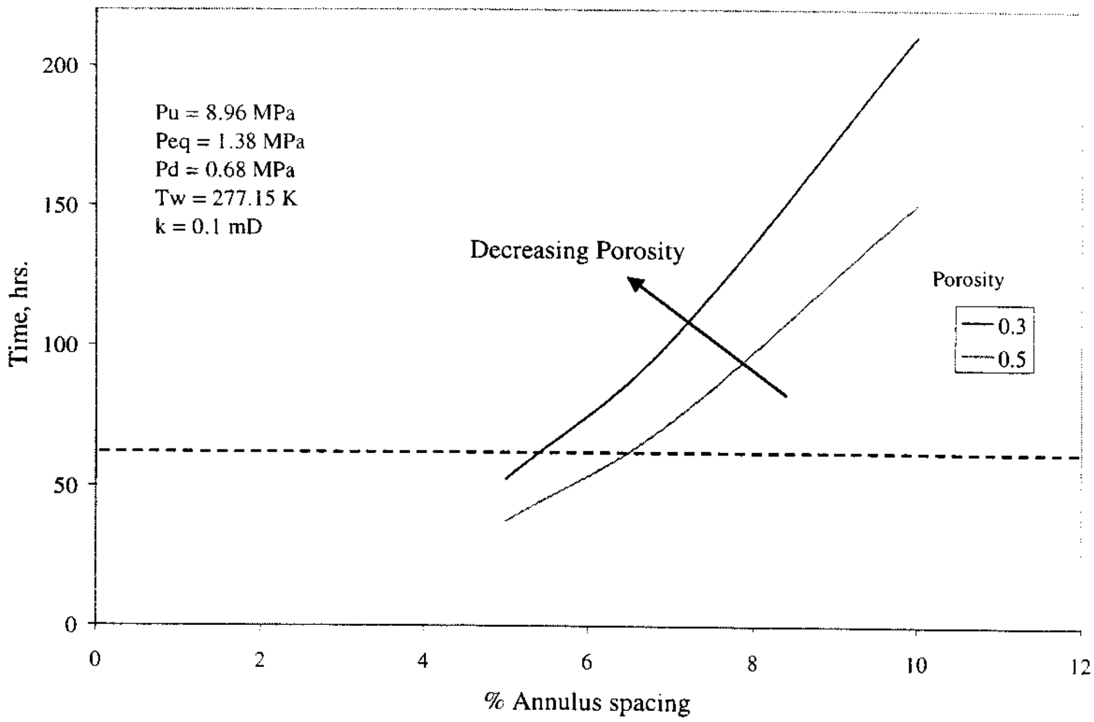

Figure 7.9: Comparison of Model and Data from Tommeliten Field Plug 1

The second plug was also located approximately 2.5 miles from the platform. Removal of the plug was by pressure reduction from the downstream side of the plug. The upstream pressure was around 780 psia (5.37 MPa) when the depressurization was begun. The downstream pressure was slowly reduced below the hydrate equilibrium pressure. The hydrate equilibrium pressure was calculated to be around 200 psia (1.37 MPa). The final downstream pressure was maintained at 180 psia (1.24 MPa). Hydrates dissociated and the flow was re-started by injecting methanol after 220 hours of dissociation time.

The permeability and porosity of the second hydrate plug was also unknown in the Tommeliten field. Figure 7.10 shows the prediction from the one-sided model. The model predicts that for a hydrate plug with porosity of 0.3, 7% annulus space is available for flow of methanol at 220 hours. If the hydrate porosity is 0.5, 8.5% annulus space is available for flow of methanol at 220 hours. If the hydrate porosity is 0.7, 11% annulus space is available for flow of methanol.

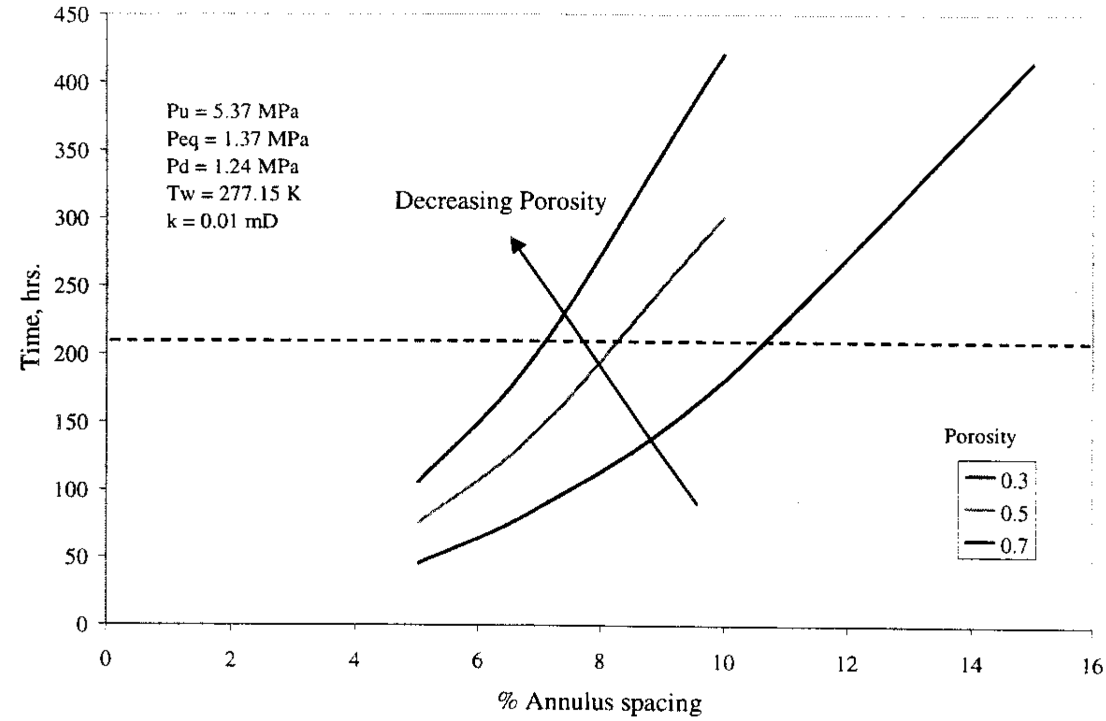

Figure 7.10:Comparison of Model and Data from Tommeliten Field Plug 2

Table 7.4 shows the summary of the comparison of model with field trials described above. The annulus spacing is converted into amount of methanol that can be injected for each plug when the flow was restarted. Sloan (2000, pg. 76) reported 21,000 gallons of methanol injection during the first 2 days of restart of a 16 inch pipeline. The numbers in Table 7.4 are comparable; hence these results suggest the dependability of the model for one-sided depressurization. The flow rate of methanol was calculated by calculating viscous flow through the calculated annulus in cylindrical coordinates. Bird et al. (1960, pg 51) describes the velocity profile through a pipe annulus.

Table 7.4: Data and Model Comparison for Tommeliten Plugs

Plug	Upstream pressure, MPa	Downstream pressure, MPa	Time when flow re-started, hrs.	Plug porosity	Percentage annulus spacing	Amount of methanol injection per day, Gallons
1	8.96	0.68	60	0.3	5.5	3735
1	8.96	0.68	60	0.5	6.5	6134
2	5.37	1.24	220	0.3	7.0	7641
2	5.37	1.24	220	0.5	8.5	13,576
2	5.37	1.24	220	0.7	11.0	29,042

The effect of J-T cooling can be observed in Figure 7.11 for the Tommeliten plug 2. Predictions for plug dissociation with out cooling were obtained at a downstream temperature of 276.15 K, while with cooling were obtained at 275.15 K. A 1 K drop in temperature increases the annulus spacing available to flow methanol at 220 hours. From Figure 7.11 it can be seen that with cooling the annulus spacing at 220 hours is 0.75 cm, and without cooling is 0.55 cm.

The effect of plug length on re-start time is shown in Figure 7.12. The Figure shows that re-start time is a strong function of the plug length. The predictions are for plug 1 of the Tommeliten field trial. As the plug becomes longer, the re-start time is really high, as much as 20 to 30 days. This high time can play a significant influence on the economics of oil and gas production.

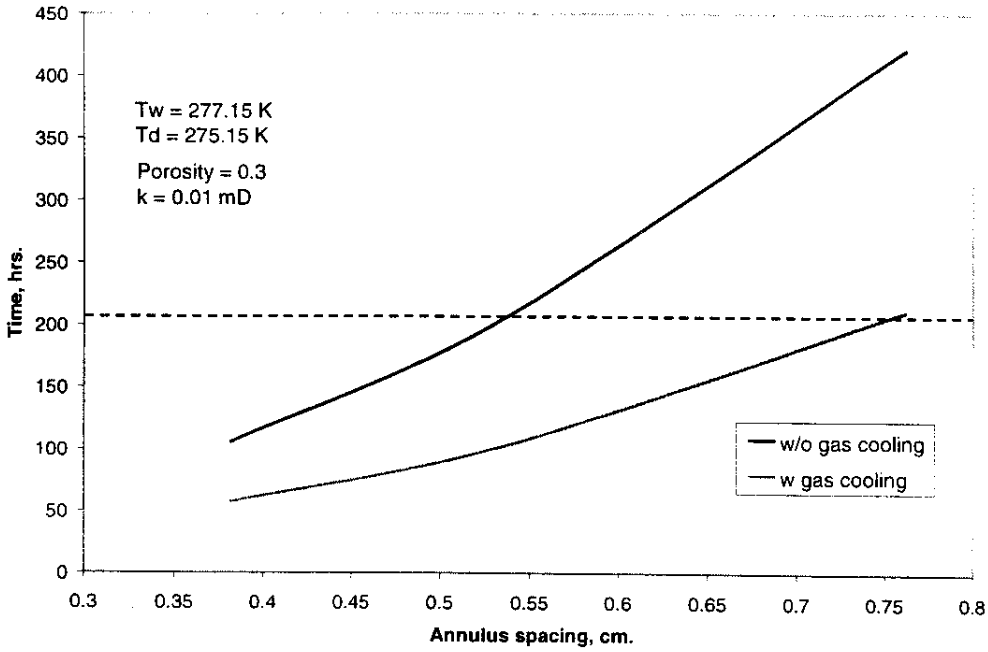

Figure 7.11: Prediction with and without Gas Cooling

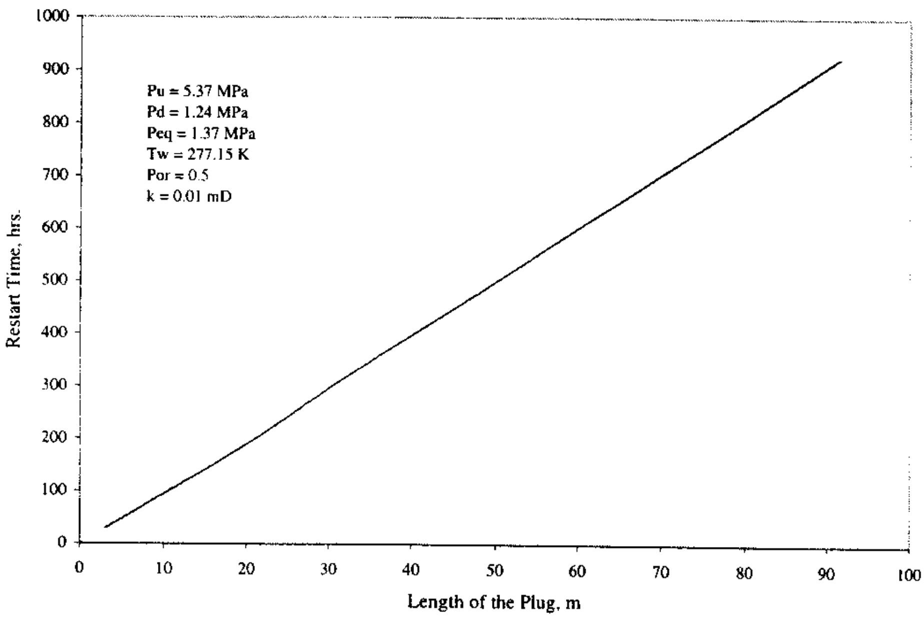

Figure 7.12: Effect of plug length on re-start time

7.4 Comparison of Safety Simulator with DeepStar Wyoming Field Trials

Xiao et al. (1998) report field trials on moving hydrate plugs in 4 inch, 4.5 mile gas-condensate pipeline in Wyoming. Xiao et al. used a multiphase flow simulator OLGA® to predict the velocities of hydrate plug subjected to pressure differentials. Plug velocities were measured for a number of plugs in the field trials. It was found that, except for the highest velocity case, the plug velocities measured in the field were consistent with the OLGA® predictions obtained prior to the field test.

The safety simulator developed in this work, described in Section 3.6, was run for the same cases described by Xiao et al. (1998). Two cases were considered in the simulations. Case one considers that a 30-foot-long (9.2 m) plug, lodged at a location 5660 ft (1725 m) from the pipeline inlet. The upstream pressure is 550 psig (3.79 MPa), and the downstream pressure is 50 psig (0.344 MPa). The same simulation was run for a shorter plug length of 15 ft (4.6 m). The second case considers that a hydrate plug is launched when the upstream pressure is 1050 psig (7.24 MPa), and the downstream pressure is 50 psig (0.344 MPa). The results from both the simulations are shown in Table 7.5.

Table 7.5: Comparison of Plug Movement between OLGA (Xiao, 1998) and Safety Model in this Work

Case & Plug Length	OLGA® Simulations		Safety Simulations (this work)	
	Maximum Velocity, m/s	Final Plug Position, m	Maximum Velocity, m/s	Final Plug Position, m
Case 1, 30 ft	106	4302	170	4078
Case 1, 15 ft	126	4302	242	4076
Case 2, 30 ft	136	-	292	3120

From Table 7.5 it can be seen that the velocities are over predicted in this work relative to OLGA® by 90%. The velocity of plug can also exceed the speed of sound (330 m/s) in the safety simulator. Figure 7.13 shows the predictions for maximum velocity as a function of mass of the plug. The pressure drop across the plug was 500 psia (3.44 MPa). The velocities exceed the speed of sound when the plug mass is less than 200 Kg. The reason for this is most likely in the assumption that interaction between plug and pipe wall are neglected. This model thus gives the worst-case scenario predictions. The addition of friction effects on plug movement is left as future work.

The most important outcome of the safety simulator is to provide a safe operating downstream pressure for a pipeline operator for one-sided depressurization. The safe operating pressure is defined as the optimal pressure that results in a minimum differential pressure for safe operation of the pipeline. This minimum differential pressure would not cause an increase in the downstream pressure above the bursting pressure of the pipeline.

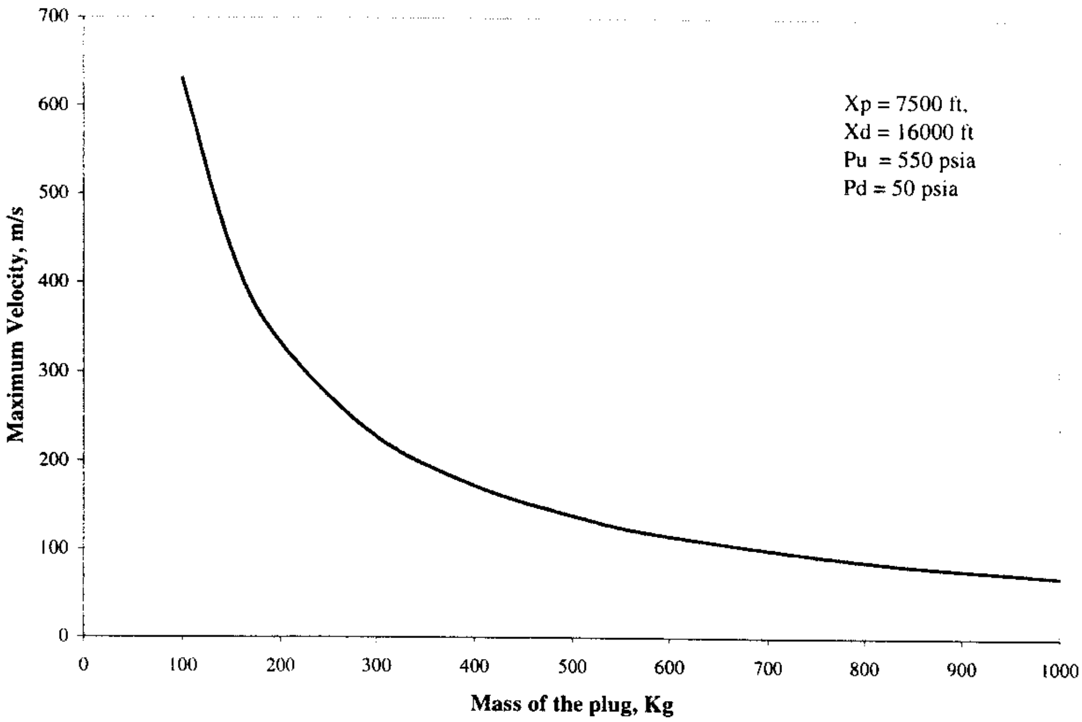

Figure 7.13: Maximum Velocity of the Plug as a Function of Plug Mass

Figure 7.14 shows the predictions from the safety model for a general case. The plug mass is 60 Kg, pressure drop across the plug is 10 MPa, the downstream pressure is 0.344 MPa, upstream pressure is 10.34 MPa, and length downstream of the plug is 4876 m. The pipe diameter is 0.1524 m. Figure 7.14 shows the effect of changing the volume of gas upstream to downstream by varying the volume upstream of the plug. As the plug moves, gas is compressed at the downstream end of the plug, thus increasing the pressure. The pressure increases immediately, typically within 5 – 6 seconds. As the ratio of volume downstream to upstream is increased, the maximum downstream pressure reduces dramatically as shown in Figure 7.14. This result is vital for a pipeline operator as he can determine the maximum pressure upon plug detachment for a given pressure drop. From Figure 7.14 the downstream pressure is below 69 MPa, when the ratio of volume downstream to upstream is around 21.

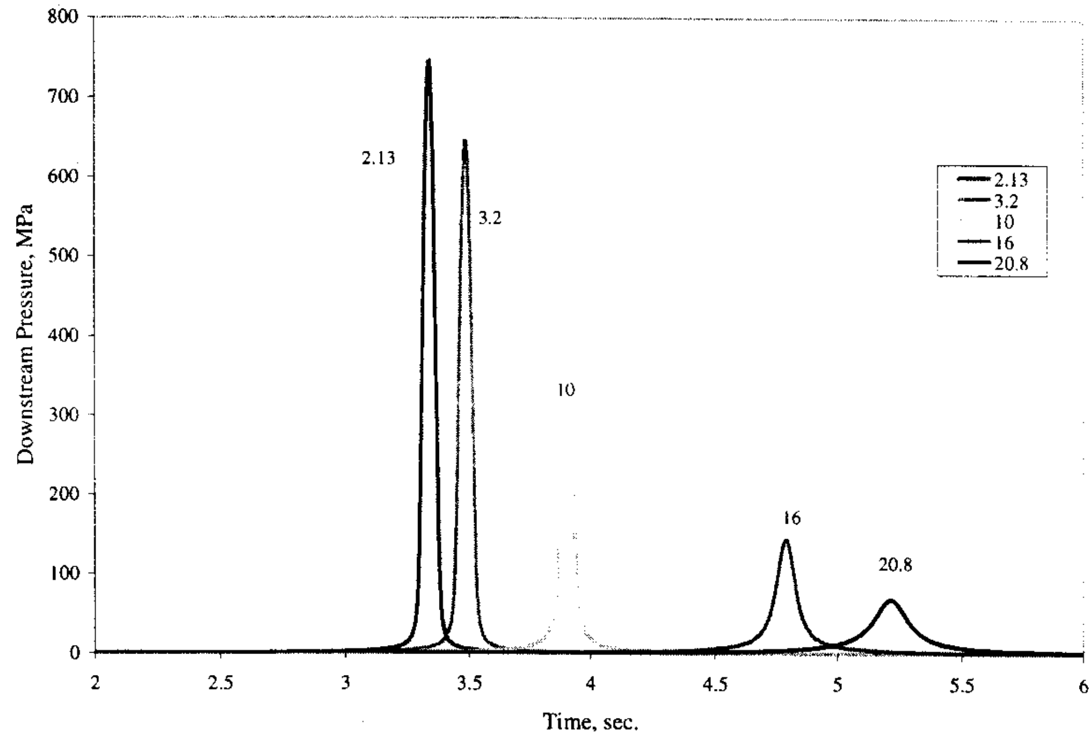

Figure 7.14 Effect of Volume Ratio on Downstream Pressure

Several cases were run to obtain Figure 7.15 by changing the volume ratio to obtain an optimal pressure ratio for safe one-sided depressurization. The graph is independent of plug mass and pipeline length, as friction effects are neglected. The graph shows the optimal pressure ratio as a function of volume ratio for two different cases when bursting pressure of the pipeline is 68.94 MPa (10,000 psia) and 103.42 MPa (15,000 psia). Optimal pressure ratio is defined as the ratio of upstream to downstream pressure, and volume ratio is defined as the ratio of downstream to upstream volume. The bursting pressure of the pipeline depends on the pipe radius, pipeline thickness and material of construction of pipe. The volume ratio is determined once a hydrate blockage is formed in the pipeline. So for instance with a pipeline bursting pressure of 103.42 MPa and a volume ratio of 4, the optimal pressure ratio is 0.1. If the upstream pressure is 6.89

MPa (known), the safe operating downstream pressure is around 0.689 MPa. To be more explicit, a pressure drop of 6.205 MPa will not result in damage to this pipeline.

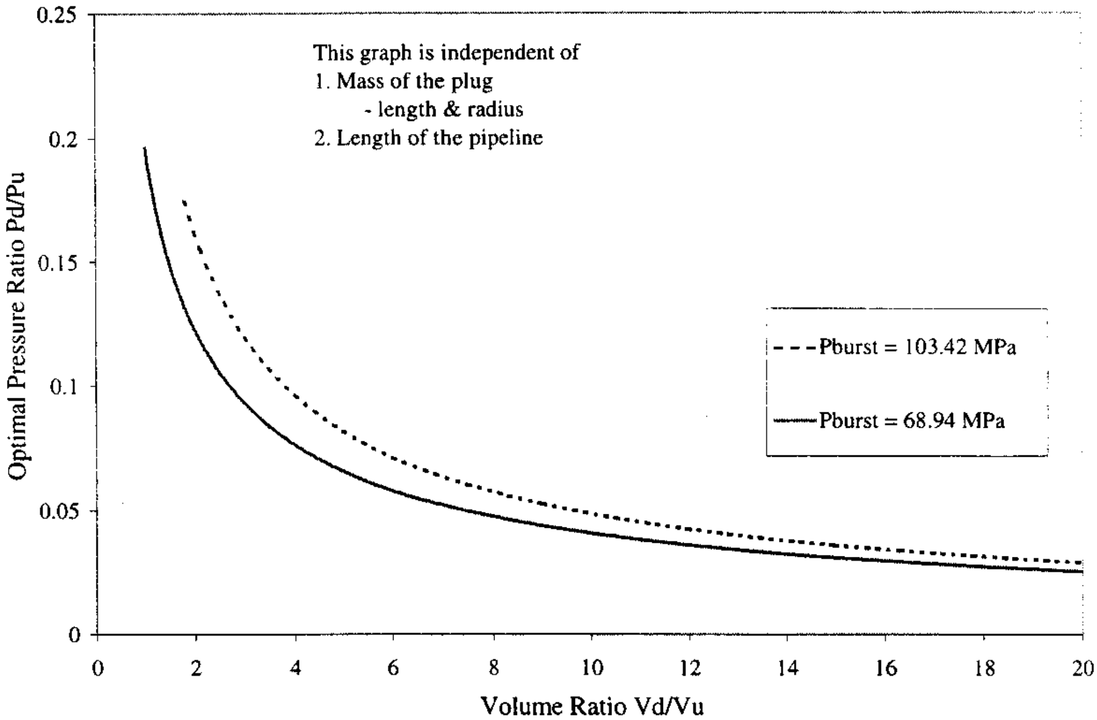

Figure 7.15 Optimal Pressure Ratio versus Volume Ratio

7.5 Conclusions

One-sided depressurization experiments were conducted on a long cell in the lab. A new method to form hydrate plugs that would withstand high pressure gradients was developed. This method uses heavy hydrocarbon to freeze the pore space in the hydrate. Pressure gradients as high as 2.41 MPa were observed before dissociating the plug, and on an average 0.17 – 0.21 MPa pressure drop was maintained during the one-sided depressurization procedure. These pressure drops translate to 6.89 MPa before dissociation and 0.76 – 1.93 MPa during dissociation for a 100 foot-long (30.48 m), 6 inch gas condensate pipeline.

The one-sided model was verified with the data from the long cell. Good agreement was obtained between the model and data. Permeability of the hydrate plug does not affect the results for these low-pressure drops. The predicted gas evolution curves matched the data within 10% absolute error. The model predicts data for plugs with a length to diameter ratio of 36. It is recommended that one-sided depressurization experiments be carried out for high pressure drops around 0.344 – 0.51 MPa for further verification of the model.

The one-sided model was also verified with the Tommeliten field plugs. Again, the model matched the data well. The effect of porosity, permeability and length of the hydrate plug was studied by using the one-sided model. The annulus spacing required for flowing methanol was established in this study as 8% of the radius of the pipe. The re-start time is a strong function of hydrate plug length. As the plug length increases (50 m), the re-start time can be as high 30 days. Users of this model are advised to run a sensitivity analysis for each system of study to determine design guidelines for pipeline remediation strategy.

Results from safety simulator were shown to match the OLGA® simulations. The worst-case scenario model provides a safe operating downstream pressure, given the downstream to upstream volume ratio and the upstream pressure. The downstream pressure may be used during the one-sided depressurization of hydrate plugs in field pipelines. The investigation of the effect of friction of wall and fluids is a recommendation to this work.

CHAPTER 8

CONCLUSIONS, GUIDELINES AND RECOMMENDATIONS

8.1 Conclusions

Several conclusions can be drawn from the separate entities of this research.

1. *One-sided depressurization model*

   In this work we developed a model for one-sided depressurization for porous and non-porous plugs. The previous models were applicable only to porous plugs, and most of these models assumed that pressure communication was important for dissociation. Introducing the porous medium concepts for modeling pressure, velocity and temperature distribution, eliminated this assumption. Solutions to temperature profiles were obtained by solving the convection-diffusion equation by using two finite difference schemes. The diffusion-dominant case was solved by using the standard second-order finite difference analysis, while the solution to convection dominant case was obtained by using the first-order upwinding finite difference scheme for accurate results.

   The safety aspects of pressure gradient across the plug were developed in the safety simulator model. The transient behavior of upstream, downstream pressures, velocity and position of the hydrate plug during movement were described. A safety plot (Figure 7.15) was provided for the effect of upstream and downstream gas volume.

2. *Two-sided radial dissociation*

The radial dissociation model was verified with hydrate plugs formed on a new long cell with a length to diameter ratio of 36. Hydrate plugs, when depressurized rapidly to atmospheric pressure were observed to be dissociating radially in the long cell. This indicates that for porous plugs, length of the plug does not effect the dissociation time. The two-sided model predicted the dissociation times for hydrate and ice melting in the long cell within 10% absolute error.

Hydrate plugs were formed on a flow loop with methane gas – water system. The plugs formed were very porous, and supported the conclusion by Austvik et al. (2000) that 77% of hydrate plugs formed in gas systems are porous in nature. The two-sided model was used to predict the annulus spacing during the depressurization of the loop plugs. The loop was re-started at 25% annulus spacing.

3. *Effect of Structural Transitions on Hydrate Dissociation*

Processed natural gas with low amounts of ethane, propane and butanes can cause structural transitions depending on the operating conditions in the pipeline. At low pressure sII hydrate is formed, while at high pressure sI hydrate is formed. This structural transition phenomenon is caused by a sharp decrease of the fugacity coefficients of the main sII formers (ethane, propane and the butanes) with pressure.

The two-sided radial dissociation model was verified with the data obtained from dissociation of the hydrate plugs. Good agreement was obtained for hydrate dissociation and ice melting times. It was shown that formation of ice during dissociation helps in reducing the time for dissociation. The effect of structure on dissociation time was also studied. Hydrate plugs formed in the sII region were predicted to require 30% longer time to dissociate than sI hydrate plugs. This has a serious implication on plug remediation costs due to production loss.

4. *Comparison of One-sided Model with Lab and Field Data*

The one-sided model was verified with the laboratory data. Permeability of the hydrate plug does not affect the results for the low-pressure drops obtained in this work. The predicted gas evolution curves matched the data within 10% absolute error. The model thus, predicts data for plugs with a length to diameter ratio of 36 and pressure drops ranging up to 0.35 MPa during the dissociation.

The one-sided model was also verified with the Tommeliten field plugs. Again, the model matched the data well. The effect of porosity, permeability and length of the hydrate plug was studied using the one-sided model. The annulus spacing required for flowing methanol was established in this study as 8% of pipeline radius. The re-start time is a strong function of hydrate plug length. As the plug length increases (50 m), the re-start time can be as high 30 days. Users of this model are advised to run a sensitivity analysis for each system of study to determine the design guidelines for pipeline remediation strategy.

Results from safety simulator were shown to match the OLGA® simulations. The worst-case scenario model provided a safe operating downstream pressure, given the downstream to upstream volume ratio and the upstream pressure. The downstream pressure may be used during the one-sided depressurization of hydrate plugs in field pipelines.

8.2 Guidelines for Plug Remediation

This section gives some guidelines for plug remediation by pressure reduction.

1. Careful observation of pressure drops is required during oil and gas production in pipeline, before really high-pressure drops such as 5 MPa are observed. High-pressure build up indicates formation of impermeable and/or long hydrate blockages.
2. Once, a hydrate blockage is formed, plug location is very vital for remediation strategy. The techniques that may be used are
    - downstream pressure reduction to locate the relative volumes of gas upstream and downstream of the plug.

- back-pressurization technique to determine the one end of the plug. The back-pressurization can lead to compacting of the hydrate plug, and decrease the plug permeability
- Other new technologies like coiled tubing, ROV deployment to measure the hoop strain of a pipeline as a function of line pressure blockage location, or Gamma-ray technique may be used. (See Sloan, 2000, Ch. 3)

3. If access points at both plug ends through dual production lines, or service lines are possible, then depressurization from both ends of the hydrate plug is preferred from standpoints of both safety and remediation time. Dissociation via depressurization from both ends takes far less time than from one side of the plug. The radial two-sided model of this work provides the annulus spacing between plug and wall as a function of time. As an approximation, the pipeline might be re-started by injecting methanol when the annulus spacing is 8% of the pipeline radius.

4. If two-sided depressurization is not possible, use the safety model (Figure 7.15) to calculate the optimum downstream pressure required to dissociate the plug without causing damage to the pipeline. The downstream pressure is dependent on the ratio of upstream to downstream volume, material, radius, thickness of the pipeline, and the upstream pressure.

5. A quick analysis of the time required for plug remediation by one-sided depressurization may be done with the default parameters. A more thorough analysis should be based on a sensitivity analysis of porosity, permeability and plug length based on each case of hydrate blockage. The pipeline may be re-started with methanol injection at 8% annulus spacing with respect to the pipeline radius.

6. Pressure downstream of the plug should be reduced slowly to prevent plug movement. The pressure must be reduced at least below the hydrate equilibrium pressure to dissociate the hydrates. Typically, the hydrate equilibrium pressure at ocean floor temperatures is around 1.38 MPa. Forming ice should be encouraged during dissociation for reducing the plug remediation time.

8.3 Recommendations

The following are the recommendations for future work, based on the experience from this research effort:

1. Hydrate Property Measurements

The models described in this work, one-sided model, two-sided depressurization model and the strength model all depend on the hydrate phase properties. Properties such as adhesive strength, latent heat of dissociation and thermal conductivity of hydrate play significant role in the final results. It is recommended that the adhesive strength of hydrates be obtained at temperatures greater than melting point of ice. The adhesion data will be very vital for plug dissociation and also address geohazard problems of hydrates. The structural transition results highlight the effect of hydrate structure on dissociation time.

2. Effect of Friction on Safety Simulator

The results from the safety simulator indicate that the plug velocity might reach sonic velocities. Hydrate plug velocities above speed of sound are not realistic. The results from the safety model predict higher velocities than the simulations from OLGA®, hence friction needs to be incorporated. The safety model results are independent of the plug mass, hence, it is recommended to model the plug-pipe, and plug-fluid interactions. The driving force for plug movement will reduced by adding these friction effects, and limiting the plug velocity below speed of sound. Studying this assumption will result in lower optimal downstream pressure for faster dissociation by one-sided depressurization.

3. One-sided Depressurization

All the one-sided depressurization plugs formed in the lab by freezing heavy hydrocarbons in the pore space, resulted in pressure gradients around 0.17 – 0.28 MPa. For a 6-inch (0.15 m) pipeline, these pressure gradients translate to 0.69 – 2.06 MPa. It is recommended that one-sided experiments be performed at higher-pressure drops, such as 0.55 MPa. The higher-pressure drops may be achieved in two ways: 1. uniform distribution of heavy hydrocarbon along the entire length of the plug, 2. increasing the diameter or length of the pipe. Uniform distribution of hydrocarbon reduces the channels available for gas flow. Increasing the diameter or length of the pipe will ensure more contact between the plug and pipe wall, to ensure hold up for high-pressure drops.

The next logical step for hydrate plug dissociation is to move to flow loops to simulate conditions in pipeline. It is recommended that the two-sided radial dissociation model be verified on black oil systems, to incorporate fluid characteristics in the model. We also recommend that the one-sided depressurization model be verified on flow loop plugs.

The future of hydrate dissociation modeling will be dependent on the data available to compare the predictions. The serious lack of data on hydrate plug dissociation needs to be addressed to test the limits of the model. This will lead us to develop better and reliable prediction models.

APPENDIX A

CALCULATION OF ICE CONVERSION TO HYDRATE

The calculation of ice converted to hydrate depends on the amount of ice loaded in to the cell, the pressure and temperature during the formation process, and volume of the cell including the pipe volume. The mass of ice used in the experiment was measured from the amount of ice loaded prior to the formation process. The volume of the ice is calculated using the density of the ice.

$$V_I = \frac{m_I}{\rho_I} \tag{A.1}$$

where V_I is the volume of ice, m_I is the mass of ice, and ρ_I is the density of ice. The volume of gas in the cell is obtained by the following relation

$$V_g = V_C - V_H - V_I \tag{A.2}$$

where V_g, V_H, and V_C are the volume of gas, hydrate and cell. The initial number of moles of gas injected during formation is obtained from Peng-Robinson equation of state.

$$P = \frac{RT}{v-b} - \frac{a(\omega,T)}{v(v+b)+b(v-b)} \tag{A.3}$$

where v is the molar volume of gas, R is the gas constant, P and T are the system pressure and temperature. The coefficients a, and b depend on the eccentricity factor (ω), system pressure, temperature and critical properties of the gas.

The number of moles of gas is calculated by obtaining the molar volume of gas,

$$N_g = \frac{V_g}{v} \tag{A.4}$$

To calculate the amount of hydrate formed, an iterative procedure is required as the hydrate forming gas is being consumed. As gas is incorporated into the hydrate, the hydrate volume increases, and the ice volume decreases. The mass of hydrate formed is calculated by the following equation

$$V_H = \frac{N_g(MW_g + \theta MW_w)}{\rho_H} \tag{A.5}$$

where MW_g and $MW_w$are the molecular weight of gas and water, and θ is the cage occupancy, obtained from a thermodynamic prediction program CSMHYD.

To solve for the amount of gas incorporated into the hydrate, a guess for initial amount of hydrate is made. A new gas volume is obtained from Equation A.2, moles of gas is obtained from Equation A.4, and finally the volume of hydrate calculated from Equation A.5. This volume is compared to the initial guess until final agreement is obtained.

APPENDIX B

CALCULATION OF PECLET NUMBER

Peclet number is expressed as the ratio of convection to conduction. The relation is expressed as

$$Pe_D = \Pr \mathrm{Re}_D = \frac{v_z D \rho C_P}{k} \tag{B.1}$$

where v_z is the velocity of gas, D is the diameter of pipe, ρ is the density of gas, C_P is the specific heat at constant pressure of gas, and k is the thermal conductivity of gas. The velocity can be expressed as the volumetric flow rate (Q)

$$Q = v_z(\frac{\pi D^2}{4}) = -\frac{\kappa \Delta P}{\mu L}(\frac{\pi D^2}{4}) \tag{B.2}$$

where κ is the permeability of the medium, μ is the viscosity of the gas, ΔP is the pressure gradient, and L is the length of the pipe. Substituting Equation B.2 into B.1 gives the Peclet Number in the radial direction as

$$Pe_D = \frac{4Q}{\pi D}\frac{\rho C_P}{k} \tag{B.3}$$

Changing the characteristic dimension from D to L, in Equation B.1, Peclet number with characteristic length is

$$Pe_L = \frac{4QL}{\pi D^2}\frac{\rho C_P}{k} \tag{B.4}$$

Knowing the pressure drop across the pipe, pipe radius and length, permeability, viscosity, specific heat at constant pressure, and density of the fluid, Peclet number can be estimated.

APPENDIX C

PRESSURE DISTRIBUTION FOR REAL AND IDEAL GAS

Equation 3.10 can be modified for a real gas using the compressibility factor (Z) for the gas to give:

$$P = \rho ZRT \tag{C.1}$$

Using this Equation, the steady state pressure distribution along the plug length results in

$$\frac{d}{dz}\left(\frac{P}{1+aP}\frac{dP}{dz}\right) = 0 \tag{C.2}$$

where the compressibility factor is expressed as a linear function of pressure using second virial coefficient. The coefficient a is given as B/RT, where B is the second virial coefficient, R is the gas constant, and T is the absolute temperature (277.15 K, ocean temperature).

The solution to Equation C.2 using the same boundary conditions described by Equations 3.12 and 3.13 is:

$$e^{aP}(aP-1) = (C_1 z + C_2)a^2 \tag{C.3}$$

where

$$C_1 = \frac{1}{L}\{f(P_d) - f(P_u)\} \tag{C.4}$$

$$C_2 = f(P_u) \tag{C.5}$$

$$f(P) = \frac{e^{aP}(aP-1)}{a^2} \tag{C.6}$$

Figure C.1 shows the comparison of pressure distribution along dimensionless plug length for three different cases. The ideal gas solution to pressure distribution was obtained by using Equation 3.28. The three cases provided are for N (P_u/P_d)= 2.2, 4 and 20. As shown in Figure C.1, the pressure distribution is similar in both cases at 277.15 K for methane gas. The average absolute difference in pressure calculation was around 0.14 MPa (2% of the average pressure). During the calculations for hydrate dissociation, the pressures that are used significantly are when the downstream pressure is below hydrate equilibrium pressure. In pipelines, this pressure is around 1.37 MPa, hence, in this region the pressure distribution between a real and perfect gas is almost negligible. Thus, it can be concluded that the compressibility factor plays a minor role in hydrate dissociation calculations.

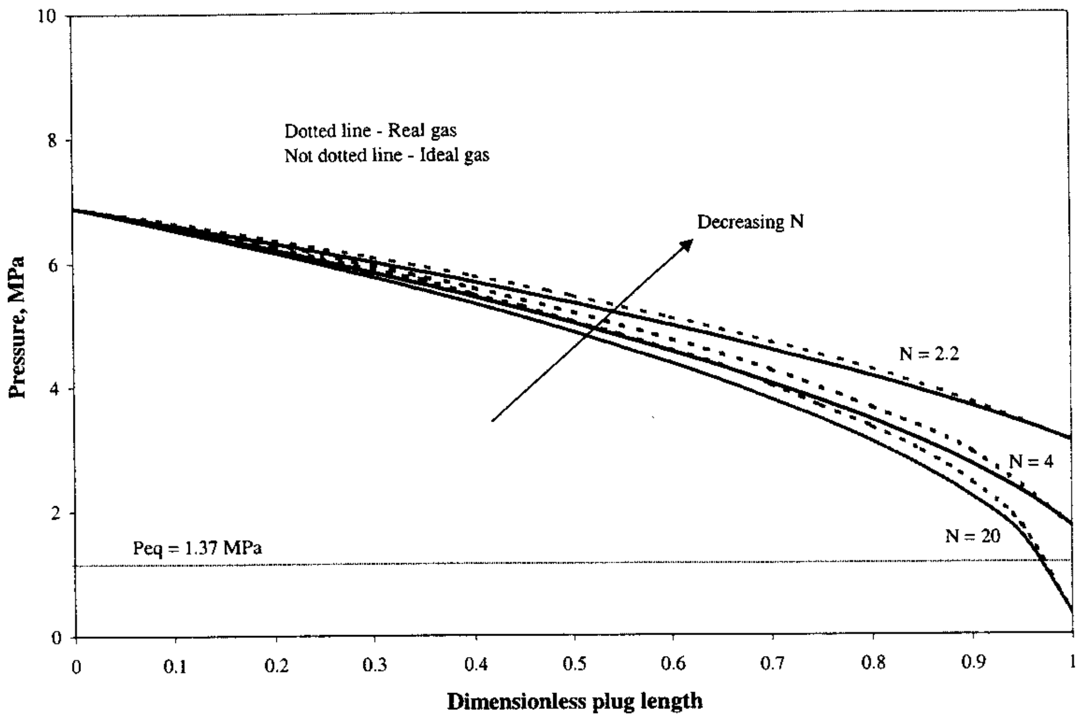

Figure C.1: Comparison of Pressure Distribution for Real and Perfect Gas

APPENDIX D

CALCULATION OF VOLUMETRIC COEFFECIENT OF EXPANSION

The coefficient of volumetric expansion of gas (β) is obtained by the following relation,

$$\beta = \frac{-1}{\rho}\left(\frac{\partial \rho}{\partial T}\right)_P = \frac{1}{v}\left(\frac{\partial v}{\partial T}\right)_P \qquad \text{(D.1)}$$

where ρ is the density of gas, v is the molar volume of gas, T is the system temperature and P is the system temperature. Equation D.1 can be simplified by using Maxwell's relationships as

$$\beta = \frac{1}{v}\left[\frac{-\left(\frac{\partial P}{\partial T}\right)_v}{\left(\frac{\partial P}{\partial v}\right)_T}\right] \qquad \text{(D.2)}$$

The derivatives in Equation D.2 can be obtained by using Redlich-Kwong cubic equation of state

$$P = \frac{RT}{v-b} - \frac{a}{v(v+b)T^{0.5}} \qquad \text{(D.3)}$$

where a, and b are the coefficients that depend on critical temperature and pressure of the gas and R is the gas constant. The derivatives calculated using Equation D.3 are

$$\left(\frac{\partial P}{\partial T}\right)_v = \frac{R}{v-b} + \frac{a}{2v(v+b)T^{1.5}} \qquad \text{(D.4)}$$

$$\left(\frac{\partial P}{\partial v}\right)_T = -\frac{RT}{(b-v)^2} + \frac{a}{bv^2T^{0.5}} - \frac{a}{bT^{0.5}(b+v)^2} \qquad \text{(D.5)}$$

Substituting Equations D.4 and D.5 into Equation D.2, the coefficient of volumetric expansion of gas can be obtained at a specified temperature and pressure.

APPENDIX E

ANALYTICAL SOLUTION TO THE TEMPERATURE DISTRIBUTION

As described in Section 3.4.3, analytical solution to Equation 3.47 was obtained to verify the finite difference solution for temperature distribution. Equation 3.47 described the temperature distribution when work done by pressure is neglected.

$$\frac{d^2\theta}{d\eta^2} = F_t\, f(\eta)\, \frac{d\theta}{d\eta} \tag{E.1}$$

where the variables F_t and $f(\eta)$ are given by

$$F_t = \frac{\kappa\, P_d}{\mu\, \alpha_m} \tag{E.2}$$

$$f(\eta) = \frac{N^2 - 1}{\sqrt{N^2 - (N^2 - 1)\eta}} \tag{E.3}$$

Equation E.1 may be simplified further to

$$\frac{d^2\theta}{d\eta^2} = \frac{F_t'}{\sqrt{1 - a\eta}} \frac{d\theta}{d\eta} \tag{E.4}$$

where the variables F_t' and a are given by

$$a = \frac{(N^2 - 1)}{N^2}, \quad F_t' = F_t\left(\frac{N^2 - 1}{N}\right) \tag{E.5}$$

Using the transformation $d\theta/d\eta = \beta$, the second-order ordinary differential Equation E.4 simplifies to a first-order ordinary differential equation

$$\frac{d\beta}{d\eta} - \frac{F_t'}{\sqrt{1 - a\eta}}\, \beta = 0 \tag{E.6}$$

The solution to Equation E.6 is given by

$$\beta = C_1 e^{\left(\frac{-2F_t' \sqrt{1-a\eta}}{a}\right)} \quad \text{(E.7)}$$

where C_1 is a constant of integration. Resubstituting the transformation for β into Equation E.7 and re-integrating provides the solution

$$\theta = \frac{C_2}{a} + \frac{C_1}{F_t'} A(a,\eta,F_t') \quad \text{(E.8)}$$

where $A(a,\eta, F_t')$ is given by

$$A(a,\eta,F_t') = e^{-\frac{2F_t'}{a}\sqrt{1-a\eta}} \left(\sqrt{1-a\eta} + \frac{a}{2F_t'}\right) \quad \text{(E.9)}$$

The constants of integration can be found by using the following boundary conditions

$$\theta = 1 \qquad \eta = 0 \quad \text{(E.10)}$$

$$\theta = 0 \qquad \eta = 1 \quad \text{(E.11)}$$

The solution to Equation E.8 will be

$$\theta = \frac{A(a,\eta = 1,F_t') - A(a,\eta,F_t')}{A(a,\eta = 1,F_t') - A(a,\eta = 0,F_t')} \quad \text{(E.12)}$$

as given in Section 3.4.3 as Equation 3.48.

APPENDIX F

CSMPlug USER'S MANUAL

The program has capabilities to do hydrate plug remediation by two-sided and one-sided depressurization. The plug dissociation program was written in Visual Fortran code, and interfaced with Visual Basic to get the windows front-end for CSMPlug.

This appendix will guide the user through some sample problems to familiarize the features of CSMPlug . The following sample problems will be illustrated:

1. Two-sided dissociation
2. One-sided dissociation
3. Safety Simulator

Example Problem 1: Two-Sided Dissociation:

We are required to determine the time required for hydrate and ice melting when a hydrate blockage occurs in a 12-inch uninsulated pipeline. Default values will be used to run the program

Figure F.1 shows the layout of CSMPlug. The problem is set up by selecting the method of pressure reduction – two-sided depressurization in this case. Inputs to the model are: Ambient and dissociation temperature, hydrate structure, plug porosity, radius of the pipeline.

The default values are given by placing the mouse at each input box. The default values for the variables are determined by previous experience.

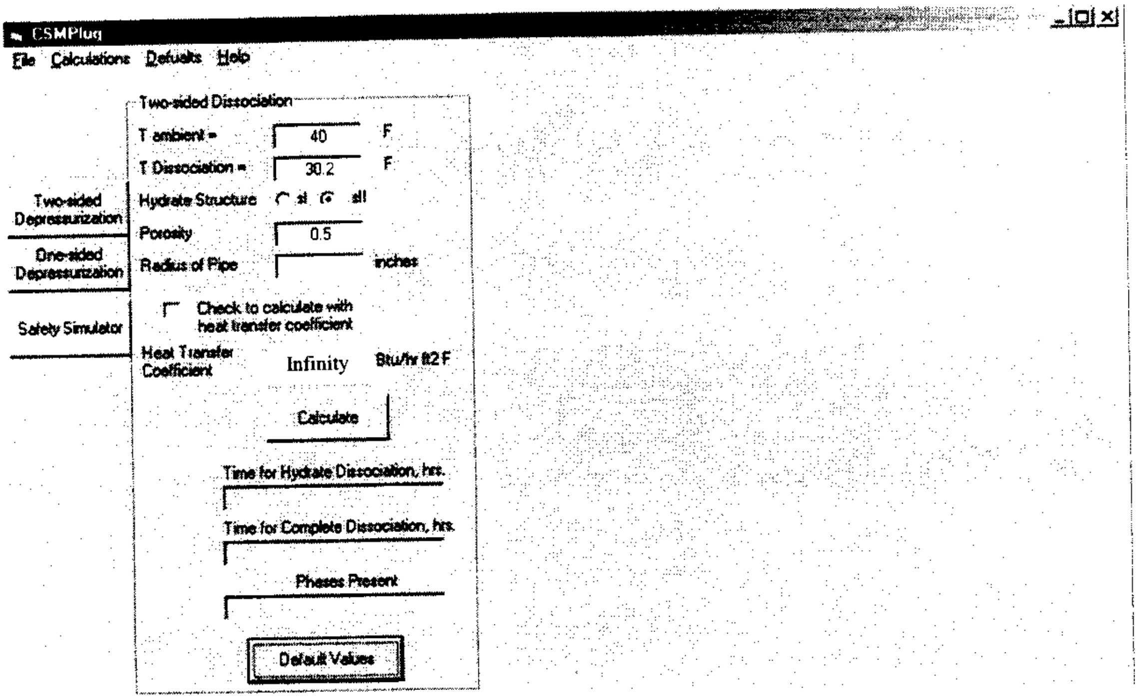

Figure F.1: Layout of the CSMPLUG program

1. Ambient temperature : $40^{0}F$
2. Dissociation temperature: $30.2^{0}F$
3. Hydrate structure: sII
4. Porosity: 0.5
5. Heat Transfer Coefficient: Infinity Btu/hr ft^{2} ^{0}F

The other variable required for running the model is for the individual case at hand:

6. Radius of the pipe: 6 inch

Input of the above values into the respective text boxes, and clicking the "Calculate" button, gives the result for two-sided dissociation. The results are shown in the output box labeled: Time for Hydrate Dissociation, Hrs. (132), Time for

Complete Plug Dissociation, Hrs. (208) and Phases Present (W-H-I) during dissociation.

The Figure F.2 output is obtained after the values are displayed in the text boxes. The figure shows the water/ice and ice/hydrate interface positions as a function of time. This graph can be used to determine the time when pipeline can be re-started when the 50% solids have dissociated. For this case, the time when 50% solids dissociated (3 inch interface position of ice/hydrate) is 130 hours.

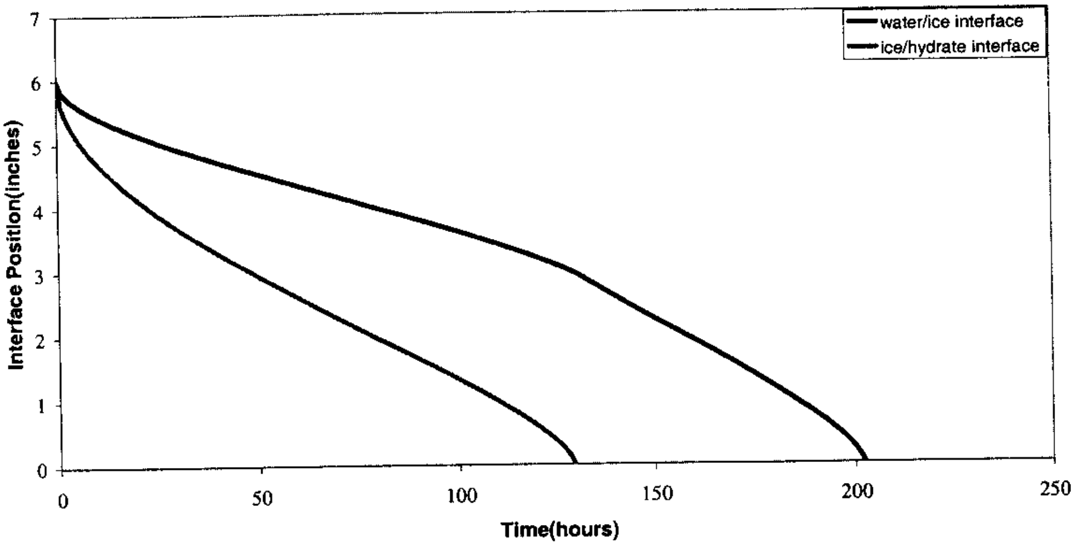

Figure F.2: Interface Position as a Function of Time

Example Problem 2: One-Sided Dissociation

We are required to calculate the time when pipeline can be re-started when a 30 ft hydrate blockage occurs in a 6-inch uninsulated pipeline. The upstream and downstream pressures are 780 psia and 180 psia. The equilibrium pressure is 200 psia. Default values will be used to run the program.

Figure F.3 shows the layout of CSMPLUG by selecting the method of pressure reduction – one-sided depressurization in this case.

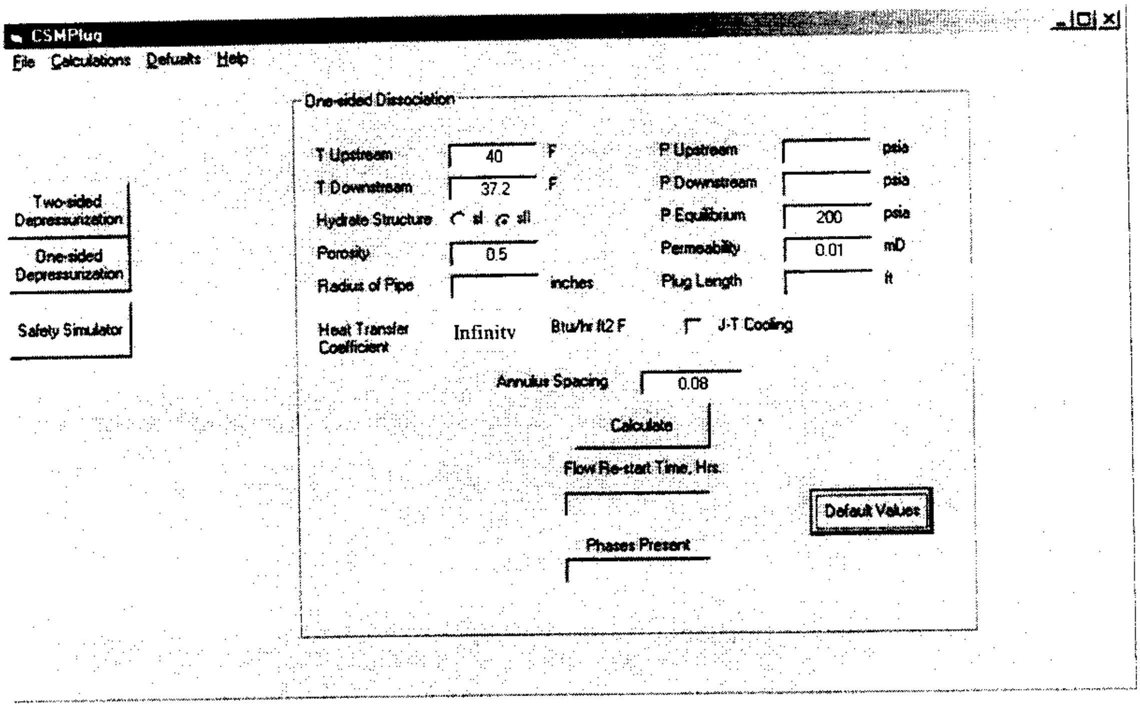

Figure F.3: Layout of CSMPlug for One-Sided Dissociation

Inputs to the model are: Upstream and downstream temperature and pressure, equilibrium pressure, hydrate structure, plugporosity, permeability, radius of the pipeline, and length of the plug.

The default values are given by placing the mouse at each input box. The default values for the variables are:

1. Upstream temperature : 40^0F
2. Hydrate structure: sII
3. Porosity: 0.5
4. Permeability: 0.01mD
5. Heat Transfer Coefficient: 0 Btu/hr ft^2 ^{0}F

The other variable required for running the model are individual to each case:

6. Radius of the pipe: 6 inch
7. Plug length: 30 ft
8. Upstream Pressure: 780 psia
9. Downstream Pressure: 180 psia
10. Equilibrium Pressure: 200 psia
11. Downstream Temperature: 37.2^0F
12. Annulus Spacing: 0.08

Input of the above values and then clicking the "Calculate" button gives the results in text boxes: Flow Restart Time, Hrs. as 220, Phases Present as W-H during dissociation. The user should do a sensitivity analysis for the effect of all parameters (particularly porosity and permeability) on the results.

Example Problem 3: Safety Simulator

A hydrate plug is formed in a 4-inch gas condensate pipeline. The mass of the plug is 60 Kg (determined by length, radius and density of hydrate 957 Kg/m^3), and the plug is located at 5660 ft from the pipeline inlet. The downstream length is 16000 ft. The upstream pressure is 550 psia, and the downstream pressure is 50 psia. It is required to find what is the maximum plug velocity and final position of the plug.

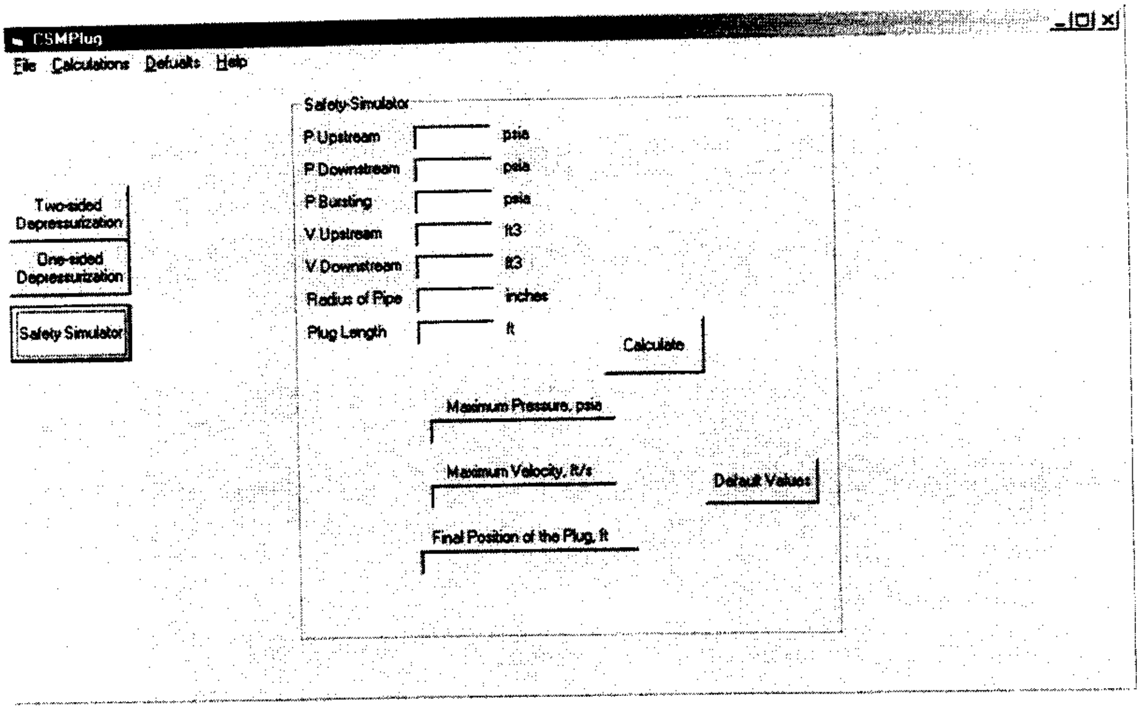

Figure F.4: Layout of Safety Model in CSMPlug

Figure F.4 shows the layout of CSMPLUG for safety model. The inputs to the model are:

1. P upstream: 550 psia
2. P downstream: 50 psia
3. P bursting: 10,000 psia
4. V upstream: 1975.13 ft^3
5. V downstream: 5585 ft^3
6. Radius of pipe: 4 inch
7. Plug length: 30 ft

Input of the above values and clicking the "Calculate" button, gives the result in the text boxes – Maximum Velocity, ft/s as 347, and Final Position of the plug, ft as 14114.

REFERENCES

1. Austvik, T., Ph. D. Thesis, "Hydrate Formation and Behavior in Pipes," Norwegian Institute of Technology, University of Trondheim, 1992
2. Austvik, T., Hustvedt, E., Gjertsen, L.H., Urdahl, O., "Formation and Removal of Hydrate Plugs, Field Trial at Tommeliten," Proc. Gas Processors Association Conference, San Antonio, Texas, March 1997
3. Austvik, T., Li, X., Gjertsen, L. H., "Hydrate Plug Properties Formation and Removal of Plugs," Proceedings 3rd. International Conference on Natural Gas Hydrates, p. 294, Salt Lake City, June 2000
4. Ballard, A., Ph.D. Thesis, " A Non-ideal Hydrate Solution Model for a Multi-phase Equilibria Program," Colorado School of Mines, Golden, CO, 2002
5. Bear, J., "Dynamics of Fluids in Porous Media," Dover Publications, Inc., 1972
6. Berge, L., Gjersten, L., Lysne, D., "The importance of porosity and permeability for dissociation of hydrate plugs in pipes," Proceedings 2nd. International Conference on Natural Gas Hydrates, p. 533, Toulouse, 2-6 June 1996
7. Bird, B. R., Stewart, E. W., Lightfoot, E. N., "Transport Phenomena," John Wiley and Sons, pg. 51, 1960.
8. Bondarev, E. A., Groisman, A. G., Savvin, A. Z., "Adhesive properties of gas hydrates and ice," Proceedings 2nd. International Conference on Natural Gas Hydrates, p. 95, Toulouse, 2-6 June 1996
9. Campbell, K. J., Offshore, 46, October 1991
10. Corrigan, A., *et al.* "Trials of Threshold Hydrate Inhibitors in the Revenspurn to Cleeton Line," SPEPF, 250, 1996
11. Davy, H., Phil. Trans. Roy. Soc. London, 101, 1, 1811
12. De Boer, R. B., Houbolt, J. J. H. C., Lagrand, J., "Formation of Gas Hydrates in Permeable Medium", Geologie en Mijnbouw, 1985, 64, 245-249
13. Davalath, J., "Methods to Clear Blocked Flowlines," Mentor Subsea, DeepStar IIA CTR A208-1, 157 pages and a appendix, January 1996

14. Fidel-Dufour, A., Nguyen, H., D., Herri, J. M., "Formation and Dissociation of Hydrate Plugs in a Water in Oil Emulsion," Proceedings of The Fourth International Conference on Gas Hydrates, Vol. 2, 938, 2002

15. Fulton, J., "Personal Communication", 2001.

16. Gjersten, L. H. *et al.*, "Removal of a Gas Hydrate Plug from a Subsea Multiphase Pipeline in the North Sea," *Proc.*, BHR Group 1997 Multiphase Conference, Cannes, France, 1997

17. Gudmundsson, J., Borrehaug, A., "Frozen Hydrate for Transport of Natural Gas", Proceedings 2nd. International Conference on Natural Gas Hydrates, p. 415, Toulouse, 2-6 June 1996

18. Hammerschmidt, E.G., "Formation of Gas Hydrates in Natural Gas Transmission Lines, Industrial and Engineering Chemistry, 26, 851, August 1934

19. Hatton, G.J., Barajas, A.M., Kuhl, C.A., Hydrate Plug Decomposition Test Program, Final Report, SwRI Project 04-8217, October 1997, Prepared for DeepStar 3204 Subcommittee

20. Hwang, M. J., Wright, D. A., Kapur, A., Holder, G. D., "An Experimental Study of Crystallization and Crystal Growth of Methane Hydrates from Melting Ice," Journal of Inclusion Phenomena and Molecular Recognition in Chemistry, 1990, 8, 103

21. Hoffman, J. D., "Numerical Methods for Engineers and Scientists," Marcel Dekker, New York, 2001

22. Jager, M. D., Ph. D. Thesis, "High Pressure Studies of Hydrate Phase Inhibition Using Raman Spectroscopy," Colorado School of Mines, Golden, CO, USA, 2001

23. Kelkar, S.K., Selim, M.S., Sloan, E.D., "Hydrate dissociation rates in pipelines," Fluid Phase Equilibria 1998, 150-151, 371

24. Kofoed, E. E., "Dissociation of Hydrates in Pipelines," Masters Thesis, Technical University of Denmark, 2001

25. Kvenvolden, K.A., "Gas Hydrate-Geologic Perspective and Global Change," Reviews of Geophysics, 31, 173 1993

26. Larsen, R., Wessel-Berg, D., Borthne, G., Nakamura, A., "Simple Modeling of Hydrate Dissociation in Reservoirs Caused by Pressure Drawdown," Proceedings of

The International Symposium on Methane Hydrates Resources in the Near Future?, JNOC, 175 – 182, 1998

27. Leonard, B. P., "A Stable and Accurate Convective Modelling Procedure Based on Quadratic Upstream Interpolation," Computer Methods in Applied Mechanics and Engineering, 19, 59-98 1979
28. Lingelem, M. N., Majeed, A. I., Stange, E., "Industrial Experience in Evaluation of Hydrate Formation, Inhibition, and Dissociation in Pipeline Design Operation," Proc., First Intl. Conference on Natural Gas Hydrates, New York Academy of Sciences, 715, 75, 1994
29. Lynch,P., "Orwell Field Pipeline Blockage Report, April-June 1996, " ARCO British Ltd. Report, 23 pages, November 1996
30. Lysne, D., Saeter, G., Lund, A., Evaluation of Potential Hydrate Problems for Tordis Field Development, NPF Conference Multiphase Transportation III-Present Application and Future Trends, Roros, Norway, September 1992
31. Lysne, D., "An Experimental Study of Hydrate Plug Dissociation by Pressure Reduction," Ph.D. Thesis, Norwegian Institute of Technology, University of Trondhiem, 1995
32. Mak, T. C. W., McMullan, R. K., Jeffrey, G.A., "Polyhedral Clathrate Hydrates. X. Structure of the Double Hydrate of Tetrahydrofuran and Hydrogen Sulfide," J. of Chem. Phys., 42, 2732, 1965
33. McMullan, R. K., Jeffrey, G.A., "Polyhedral Clathrate Hydrates. IX. Structure of Ethylene Hydroxide," J. of Chem. Phys., 42, 2725, 1965
34. Morrison, F. A., "Transient Gas Flow in a Porous Column," Ind. Eng. Chem. Fundam., Vol.11, No. 2, 191, 1972
35. Muskat, M., "The Flow of Homogeneous Fluids Through Porous Media," McGraw-Hill Book Company, Inc., 1937
36. Neild, D. A., "Convection in Porous Media," Springer- Verlag, New York, 1992
37. Notz, P.K., Technical Memorandum TM 94-0145 on Relative Inhibitor Costs, Texaco, 26 July 1994
38. Peter, L. J., "Peter's Quotations: Ideas from our Times," Quill, 1993

39. Peters, D.J., "A Study of Hydrate Dissociation in Pipelines by the Method of Two-Sided Depressurization: Experiment and Model," Master's Thesis, Colorado School of Mines, May 1999

40. Peters, D.J., Selim, M.S., Sloan, E.D. "Hydrate Dissociation in Pipelines by Two – Sided Depressurization: Experiment and Model," DeepStar final report, 1999

41. Peters, D. J., Mehta, A., Walsh, J., "The Physics of Hydrate Plug Dissociation: A Comprehensive Model Based upon Facts, Conjecture, and Field Experience," Proceedings 4th. International Conference on Natural Gas Hydrates, p. 952, Yokohama, May 2002

42. Pozrikidis, C., "Numerical Computation in Science and Engineering," Oxford University Press, 1998

43. Ripmeester, J. A., Tse, J. A., Ratcliffe, C. I., Powll, B. M., Nature, 325, 135, 1987

44. Shirota, H. Aya, I., Namie, S., Bollavaram, P., Turner, D., Sloan, E. D., "Measurement of Methane Hydrate Dissociation for Application of Natural Gas Storage and Transportation," Proceedings 4th. International Conference on Natural Gas Hydrates, p. 972, Yokohama, May 2002

45. Sloan, E.D. "Hydrate Engineering," SPE, Richardson, TX, 2000

46. Sloan, E.D., "Clathrate Hydrates of Natural Gases 2nd Edition," Marcel Dekker, New York, 1998

47. Stern, L.A., Kirby, S.H., Durham, W.B., "Peculiarities of Methane Clathrate Hydrate Formation and Solid-State Deformation, Including Possible Superheating of Water Ice," Science, 273, 1843, 1996

48. Stern, L.A., Circone, S., Kirby, S., Durham, W., "Anomalous Preservation of Pure Methane Hydrate at 1 atm," Journal of Physical Chemistry, 105, pg 1756-1762, 2001

49. Xiao, J. J., George Shoup, Greg Hatton, Veet Kruka,"Predicting Hydrate Plug Movement Druing Subsea Flowline Depressurization", Offshore Technology Conference 8728, 1998, 161

50. Yakushev, V., Istomin, V., "Gas Hydrate Self Preservation Effect," Physics and Chemistry of Ice, Hokkaido University Press, Sapporro, pp 136 – 139, 1992